Niklas Jantunen

DEVELOPMENT OF LIQUID–LIQUID EXTRACTION PROCESSES FOR CONCENTRATED HYDROMETALLURGICAL SOLUTIONS

ACTA UNIVERSITATIS LAPPEENRANTAENSIS 1066

Niklas Jantunen

DEVELOPMENT OF LIQUID–LIQUID EXTRACTION PROCESSES FOR CONCENTRATED HYDROMETALLURGICAL SOLUTIONS

Dissertation for the degree of Doctor of Science (Technology) to be presented with due permission for public examination and criticism in the Auditorium 2 at Lappeenranta-Lahti University of Technology LUT, Lahti, Finland on the 20th of January 2023, at 10:00.

Acta Universitatis
Lappeenrantaensis 1066

Supervisors Docent Sami Virolainen
LUT School of Engineering Science
Lappeenranta-Lahti University of Technology LUT
Finland

Professor Tuomo Sainio
LUT School of Engineering Science
Lappeenranta-Lahti University of Technology LUT
Finland

Reviewers Associate Professor Martina Petranikova
Department of Chemistry and Chemical Engineering
Chalmers University of Technology
Sweden

Professor Kathryn Sole
Department of Materials Science and Metallurgical Engineering
University of Pretoria
South Africa

Opponents Professor Kathryn Sole
Department of Materials Science and Metallurgical Engineering
University of Pretoria
South Africa

Professor Mark Hlawitschka
Institute of Process Engineering
Johannes Kepler University
Austria

ISBN 978-952-335-913-0
ISBN 978-952-335-914-7 (PDF)
ISSN 1456-4491 (Print)
ISSN 2814-5518 (Online)

Lappeenranta-Lahti University of Technology LUT
LUT University Press 2023

Abstract

Niklas Jantunen
Development of liquid–liquid extraction processes for concentrated hydrometallurgical solutions
Lappeenranta 2023
78 pages
Acta Universitatis Lappeenrantaensis 1066
Diss. Lappeenranta-Lahti University of Technology LUT
ISBN 978-952-335-913-0, ISBN 978-952-335-914-7 (PDF), ISSN 1456-4491 (Print), ISSN 2814-5518 (Online)

Hydrometallurgical liquid–liquid extraction is a separation and purification method used for the recovery of metals from aqueous solutions. In this thesis, process design methods were studied and evaluated for the development of liquid–liquid extraction processes for concentrated sulfate solutions. The conceptual process design was based on batch equilibrium experiments, theoretical equilibrium calculations, McCabe–Thiele analyses, pseudo-countercurrent extractions, and continuous experiments in industrial-type laboratory-scale mixer-settlers. Three different separation processes were studied: I) separation of arsenic from concentrated H_2SO_4, II) purification of a concentrated $MnSO_4$ solution, and III) separation of cathode metals from lithium-ion battery (LIB) leachates.

Extraction of arsenic from concentrated (10.4 M) H_2SO_4 by undiluted tri-*n*-butyl phosphate (TBP) is accompanied by significant changes in phase densities and volumes, which were quantified. TBP extracted 83.7 % arsenic and 31.4 % H_2SO_4 from the H_2SO_4 solution in three countercurrent extraction stages.

Bis(2-ethylhexyl) hydrogen phosphate (D2EHPA) and bis(2,4,4-trimethylpentyl)phosphinic acid (BTMPPA) were used to purify concentrated $MnSO_4$ leachate that contained over 150 g L^{-1} manganese. More than 99 % of the zinc and 98 % of the iron were removed by both extractants in two countercurrent extraction stages. However, BTMPPA co-extracted less manganese than D2EHPA. Calcium was not extracted due to the high manganese-to-calcium ratio of the leachate.

A liquid–liquid extraction flowsheet was developed for producing nickel-rich sulfate mixtures from cobalt-rich LIB leachates. The nickel-rich solutions can be re-used in the synthesis of new cathode precursors. Additionally, purified Li_2SO_4, $CoSO_4$, and $MnSO_4$ are obtained simultaneously from the process. The benefit of the process is that no additional inputs of lithium, nickel, cobalt, or manganese are required. None of the developed processes are optimized. The future research could focus on process optimization through numerical flowsheet simulations based on mechanistic equilibrium models in which non-ideality and organic phase speciation are considered.

Keywords: solvent extraction, liquid–liquid extraction, flowsheet development, arsenic, sulfuric acid, lithium, cobalt, nickel, manganese, zinc, hydrometallurgy, recycling

Acknowledgements

This work was carried out at LUT University in Lappeenranta, between 2018 and 2022. It has been a privilege to do research at LUT and enjoy the company of many inspiring people, who I want to thank for cherishing strong work ethic and humour. Special thanks to Fedor Vasilyev, Harri Nieminen, Hoang S. H. Nguyen, Jari Heinonen, Jussi Tamminen, Pavel Maksimov, Santeri Kurkinen, Tobias Wesselborg, Tommi Huhtanen, and Tuomas Sihvonen for sharing many great ideas and moments both in academia and elsewhere.

Associate Professor Martina Petranikova, Professor Kathryn Sole, and Professor Mark Hlawitschka have my humble gratitude for examining this dissertation.

Business Finland and the industrial partners of Circular Metal Ecosystems, Symbiosis of metals production and nature, and Finland-Based Circular Ecosystem of Battery Metals, BATCircle2.0 project consortia are gratefully acknowledged for research funding. I thank Technology Industries of Finland Centennial Foundation (Teknologiateollisuus ry:n 100-vuotissäätiö) and LUT Research Foundation for personal grants.

I'm deeply grateful for all guidance, support, and wisdom that I have received from my supervisors, Docent Sami Virolainen and Professor Tuomo Sainio. I highly appreciate the patience Sami and Tuomo had while supervising my work. Additionally, I want to thank my co-authors, our support team at Lappeenranta campus (Liisa Puro, Mari Raitavuo, Markku Rahikainen, and Mikko Huhtanen), and LUT Voima.

In eternal debt of gratitude to my friends, relatives, and family

Niklas Jantunen
January 2023
Lappeenranta, Finland

Contents

List of publications

This dissertation is based on the following papers. The rights have been granted by the publishers to include the papers in the dissertation.

I. Jantunen, N., Virolainen, S., Latostenmaa, P., Salminen, J., Haapalainen, M. Sainio, T., Removal and recovery of arsenic from concentrated sulfuric acid by solvent extraction, *Hydrometallurgy*, 187 (2019), pp. 101–112.

II. Jantunen, N., Kauppinen, T., Salminen, J., Virolainen, S., Lassi, U., Sainio, T., Separation of zinc and iron from secondary manganese sulfate leachate by solvent extraction, *Minerals Engineering*, 173 (2021), 107200.

III. Jantunen, N., Virolainen, S., Sainio, T., Direct production of Ni–Co–Mn mixtures for cathode precursors from cobalt-rich lithium-ion battery leachates by solvent extraction, *Metals*, 12(9) (2022), 1445.

Author's contribution

Publication I: Niklas Jantunen (the author) planned the experimental work with the co-authors, conducted major part of the experimental work and analyses, performed all theoretical calculations and post processing of the experimental data. The author wrote the original draft of the manuscript.

Publication II: The author planned the experimental work with the co-authors, conducted major part of the experimental work and analyses, performed most of the theoretical calculations and post processing of the experimental data. The author wrote the original draft of the manuscript.

Publication III: The author planned the experimental work with the co-authors, conducted minor part of the experimental work and analyses, performed all theoretical calculations, and had major contribution in post processing of the experimental data. The author wrote the original draft of the manuscript.

Nomenclature

Latin alphabet

A	Debye–Hückel parameter	$kg^{0.5}\ mol^{-0.5}$
a	activity	–
B	Debye–Hückel parameter	$kg^{0.5}\ mol^{-0.5}\ cm^{-1}$
$\dot{B}$	empirical parameter in the extended Debye–Hückel equation	$kg\ mol^{-1}$
b	stoichiometric coefficient	–
c	concentration	$mol\ L^{-1}$
D	distribution ratio	–
D_0	distribution ratio without adduct formers	–
E	volumetric flow rate of the extract	$L\ s^{-1}$
E_M	percentages of M extracted	%
E_h	redox potential vs. standard hydrogen electrode	mV
E/R	extract-to-raffinate volumetric flow ratio	–
F	volumetric flow rate of the aqueous feed	$L\ s^{-1}$
F_E	enrichment factor	–
f^*	formal mole fraction	–
f_E	fraction extracted	–
I	ionic strength	$mol\ kg^{-1}$
k_B	Boltzmann constant	$erg\ K^{-1}$
K	equilibrium constant	–
K_a	acid dissociation constant	–
$K_{ad,b}$	adduct formation constant for adducts with b adduct formers	–
$K´$	apparent extraction constant	–
K_{EX}	extraction constant	–
M_E	Murphree extract efficiency	–
M_R	Murphree raffinate efficiency	–
m	molality	$mol\ kg^{-1}$
N	Avogadro’s constant	mol^{-1}
n	amount of substance; indexing variable when dimensionless	mol
O/A	organic-to-aqueous volumetric ratio	–
P	partition ratio	–
P_R	relative purity	%
p	stoichiometric coefficient	–
q	stoichiometric coefficient	–
q_e	elemental charge	statC
R	volumetric flow rate of the raffinate	$L\ s^{-1}$
S	volumetric flow rate of the solvent	$L\ s^{-1}$
S/F	solvent-to-feed volumetric flow ratio	–
T	temperature	K
t_{eq}	equilibration time	min
V	volume	L

w	stoichiometric coefficient	–
x	concentration in the heavy liquid phase	mol L^{-1}
y	concentration in the light liquid phase	mol L^{-1}
z	valence	–
$å$	ion size parameter	cm

Greek alphabet

α	separation factor	–
β	complex formation constant	–
γ	activity coefficient	–
ε	relative permittivity	–
ρ	density	g cm^{-3}
τ_{mix}	the mean residence time in mixer	min

Superscripts

0	standard or reference state
*	equilibrium

Subscripts

0	initial
aq	aqueous phase
avg	average
eq	equilibrium
i	indexing variable
org	organic phase
n	indexing variable
tot	total

Abbreviations

BTMPPA	bis(2,4,4-trimethylpentyl)phosphinic acid
D2EHPA	bis(2-ethylhexyl) hydrogen phosphate
CoSX	cobalt solvent extraction
DL	detection limit
IUPAC	International Union of Pure and Applied Chemistry
LIB	lithium-ion battery
LLE	liquid–liquid extraction
MnSX	manganese solvent extraction
NiSX	nickel solvent extraction
NCM	nickel–cobalt–manganese
PC88-A	2-ethylhexoxy(2-ethylhexyl)phosphinic acid
PLS	pregnant leach solution

pH_{50}	the pH value where 50 % of the target solute is extracted
SX	solvent extraction
TBP	tri-*n*-butyl phosphate
TOPO	trioctylphosphine oxide
UNIQUAC	universal quasichemical
ZnEW	zinc electrowinning

1 Introduction

Technological development and high living standards are heavily dependent on the intelligent utilization of metals and metalloids. Metals have high electric and thermal conductivity, a tendency to donate electrons, high melting points (mercury being an exception), and are malleable. Alloying and special metalworking techniques enable the production of materials with properties tailored to various applications. This explains the widespread use of metallic materials, for example, in steel structures, the generation and delivery of electricity, energy storage, catalysis, electronics, and utensils.

Extraction of metals from metal-bearing raw materials and refining of the metals are referred to as extractive metallurgy, which can be further divided into hydrometallurgy, pyrometallurgy, and electrometallurgy. In general, pyrometallurgy covers the conversion and refining operations in high-temperature (around 1000 °C or higher) furnaces. Pyrometallurgy is the primary route in the processing of primary high-grade ores, but it is not feasible for the processing of low-grade and complex raw materials because a large amount of energy is wasted for heating gangue material and separation of the metals becomes difficult. However, hydrometallurgical methods are known for high separation efficiencies that allow the utilization of both complex and low-grade raw materials in metal production (Habashi, 1999). Indeed, hydrometallurgy is particularly useful for the valorisation of various secondary raw materials, including by-products (*e.g.*, slag and flue dusts) from the pyrometallurgical industry.

Hydrometallurgy involves the liberation of metals from solid raw materials by leaching them with an aqueous solution, followed by concentration and purification of the metal-bearing solution, and precipitation or electrodeposition of the purified metal compound or metal. Besides selective leaching, high separation efficiencies are enabled by chemical separation methods: liquid–liquid extraction (LLE), ion exchange, adsorption, and precipitation. Hydrometallurgical processes—especially separations—are mostly operated at relatively low temperatures, typically below 80 °C. However, certain leaching applications require temperatures higher than 100 °C. Often both hydro- and pyrometallurgical steps are required. A famous example is the heat-intensive Bayer process, where bauxite ore is digested with NaOH at 140–250 °C and up to 3.45 MPa to liberate the aluminium from the ore. In the end, $Al(OH)_3$ is obtained after several hydrometallurgical steps. Then, almost all of it is converted to alumina (Al_2O_3) by calcination at above 1100 °C (Sleppy, 2002).

High energy and resource consumption together with major environmental impact are widely recognized challenges in the mining and metallurgical industry. Research into low-temperature hydrometallurgical processes is important because the technological development in these processes improves material and energy efficiency. This thesis is focused on the development of hydrometallurgical liquid–liquid extraction processes for concentrated sulfate solutions.

1.1 Liquid–liquid extraction (solvent extraction)

Liquid–liquid extraction—also known as solvent extraction (SX) and liquid–liquid distribution—is a separation and purification method based on the uneven distribution of chemical species between two immiscible or partially miscible liquid phases with different densities. The technique is referred to as solvent extraction in this thesis. When the distribution of a solute is completely determined by its solubilities between the two liquid phases, the extraction is non-reactive and can also be referred to as partitioning. In reactive solvent extraction, the target specimen (solute) reacts with another chemical specimen (extractant) to form a compound with different distribution characteristics than the solute in its original form. Figure 1.1 summarizes the basic principles of non-reactive and reactive solvent extraction. Mass transfer of the solute is accelerated by mixing or shaking the liquids. Once mixing or shaking is stopped, the phases separate because of the density difference.

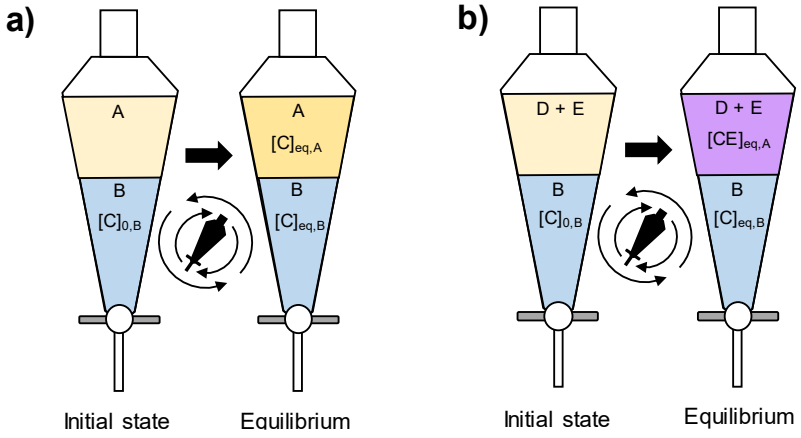

Figure 1.1 Classification of solvent extraction processes: a) The non-reactive solvent extraction of C from liquid B to liquid A; and b) the reactive solvent extraction of C from liquid B to liquid D. E denotes an extractant, CE is the complex or adduct formed by the target specimen, C, and the extractant, E.

Hydrometallurgical solvent extractions are mostly reactive extractions in which the heavy liquid phase is an aqueous solution with dissolved metals and the light liquid phase is a hydrocarbon mixture containing an extractant, a diluent, and, often, a modifier. Extractant formulations with high metal loading capacity, high selectivity, good chemical stability under process conditions, and fast extraction kinetics are preferred. Additionally, regeneration (stripping) of the extractant must be possible and straightforward, phase separation must be reasonably fast, and the extractant solution should have minimum solubility to the aqueous phase. Recycling the expensive extractant solution within the process—thus using it repeatedly for the separation—is the essence of industrial solvent extraction.

Figure 1.2 shows a general flowsheet of an industrial solvent extraction process. The minimum configuration includes extraction and stripping steps. In addition, an intermediate purification step (scrubbing) is often required before stripping. The extraction mechanism determines whether a pre-conditioning step is required, or how useful it will be if it is optional. A more detailed discussion of the extraction mechanisms is given in Chapter 2.3. The individual steps (extraction, scrubbing, stripping) in a solvent extraction process may require several extraction stages to achieve satisfactory separation efficiencies and purity targets. Moreover, multicomponent separations may require the use of different extractants in several extraction–scrubbing–stripping circuits.

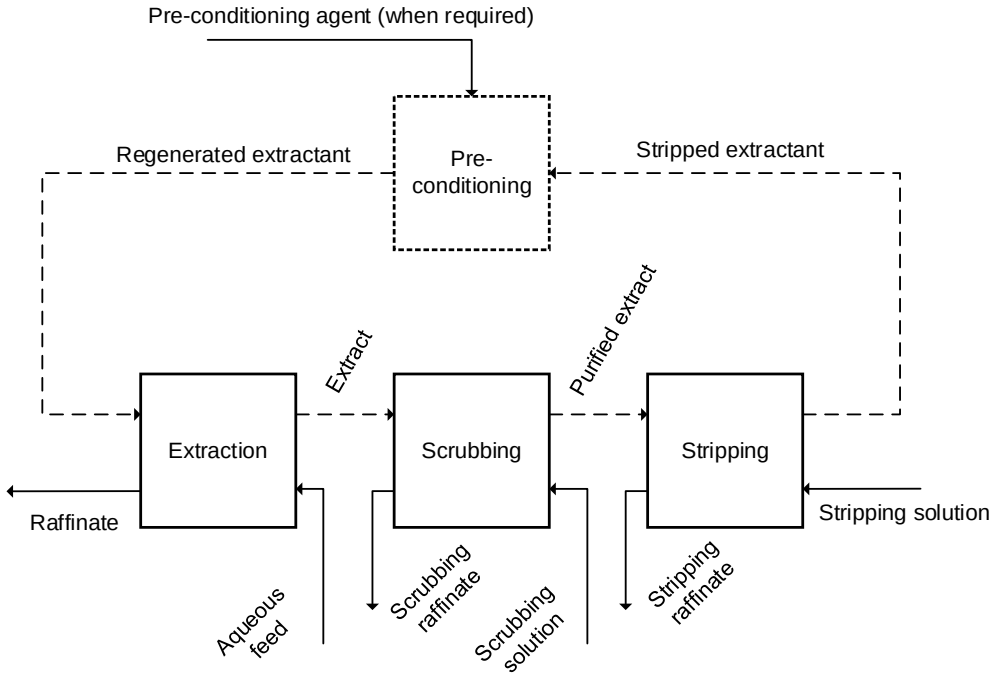

Figure 1.2 Block diagram of a generic industrial solvent extraction flowsheet. Dashed line: organic flow; solid line: aqueous flow.

Mixer-settlers (Figure 1.3 a) and extraction columns (Figure 1.3 b) are the most common solvent extraction equipment in the industry. A mixer-settler consists of a mixing chamber in which dispersion is created by agitation and a settler where the phases are separated. The extraction performance of a single mixer-settler approximates that of a single batch extraction. Therefore, mixer-settlers are stagewise contactors. The overall extraction performance is significantly increased when multiple mixer-settlers are connected into a countercurrent cascade (see Chapter 3.1). Then again, extraction columns are differential mass-transfer units in which a countercurrent flow is created by gravity. Extraction columns can perform equal to several stagewise contactors operating

in a countercurrent mode. The overall extraction performance in a column can be affected by increasing column height or by using internals that modify the hydrodynamic environment.

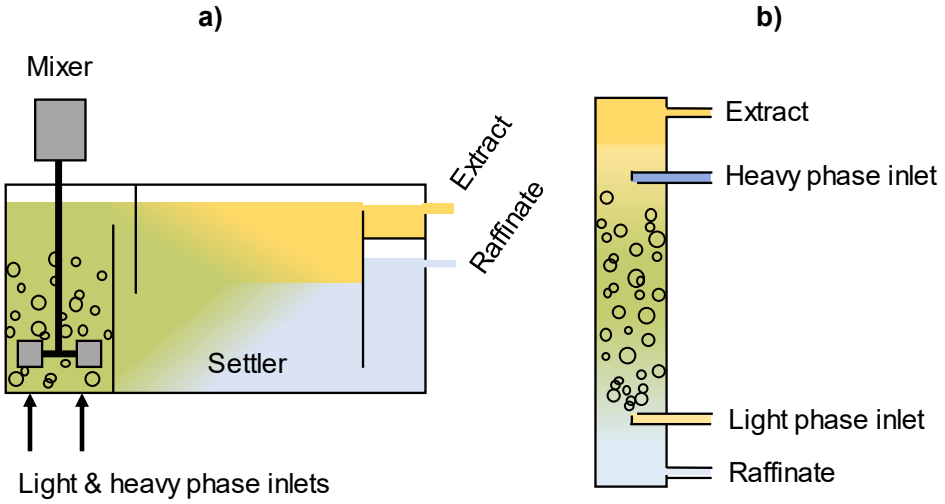

Figure 1.3 Schematic diagrams of a) a mixer-settler and b) a solvent extraction column with heavy liquid as the continuous phase.

1.2 Objectives and challenges in the design of solvent extraction processes

The goal in process design is to enable industrial scale solvent extraction separations to run safely, economically, and sustainably. The development of a hydrometallurgical solvent extraction process for a given feed solution involves the determination of the following:

- Compositions of the extractant, stripping, and scrubbing solutions
- Required number of extraction stages in each process step (*e.g.*, extraction, scrubbing, stripping)
- Operating parameters (temperature, pH, solvent-to-feed ratio, total flowrate, phase continuity) in each process step
- Extraction order of the metals
- Reflux streams and their flow rates (between different process steps)

Entrainment and solvent losses are part of the evaluation when choosing the extractant formulation. The operating parameters are interdependent; a change in one parameter may affect the whole process in such a way that the adjustment of the other parameters becomes necessary as well. Different chemical systems and processes are not equally

sensitive to changes in the operating parameters and, usually, several parameter combinations exist that enable the target yield, separation efficiency, and product purity to be achieved (Grinbaum, 2002).

A common approach in developing an SX flowsheet is to, first, find the most promising extractants based on the available literature and speciation analyses. The chemical and physical performances of the most promising extractant solutions are then experimentally studied with the authentic feed solution and the best one is chosen. From this point forward, the process design is continued by flowsheet development to narrow down the flowsheet alternatives and operating parameters that must be tested in the piloting stage of process development. The development of flowsheets relies on both computational and experimental methods. A brief overview of these is given in this chapter but the methods used in this thesis are presented in Chapter 3.

The well-known McCabe–Thiele method (Chapter 3.2) can be used to estimate the required number of extraction stages for individual solvent extraction cascades. Application of the method is relatively easy and fast. However, accurate optimization of individual operating parameters by the McCabe–Thiele method is laborious because, in principle, a new distribution curve (a plot of $c(\text{solute})_{\text{org}}$ vs. $c(\text{solute})_{\text{aq}}$) should be measured each time the composition of the extractant solution, temperature, or pH is changed (Bourget *et al*., 2011; Grinbaum, 2002). The method is inaccurate in predicting the solution compositions in cases where multiple metals are extracted simultaneously, the stages operate at different pH values, or changes in chemical speciation or volumetric phase ratio occur during the extraction (Bourget *et al.*, 2011; Kislik, 2012).

Steady-state mass-balance calculations, parameter optimization, and sensitivity analyses can be done for multiple flowsheets through computer simulations. It is common to solve the flowsheets with the assumption that equilibrium is reached in each extraction stage (Chagnes, 2020; Vasilyev *et al*., 2019; Yun *et al*., 2016), although this assumption is invalid in continuous extractors. Non-ideal mass transfer can be considered in flowsheet simulations by implementing kinetic and hydrodynamic models, but the required parameters and physical properties of the chemical system must be available (Chen *et al.*, 2018a). However, the assumption of ideal extraction stages is often reasonable because the hydrodynamic models can significantly increase the complexity and computational load. It is also possible to account for the difference from ideal performance by single empirical parameters (Chapter 3.2). Nevertheless, there must be a mathematical description for calculating the equilibrium compositions.

Equilibrium descriptions in the solvent extraction of metals are based on empirical equations, response surface methodology (Vieceli *et al*., 2021), artificial neural networks (Acharya & Mishra, 2017; Anitha & Singh, 2008), or mechanistic equilibrium models (Chen *et al*., 2018a; Omelchuk & Chagnes, 2018; Sorel *et al*., 2011; Vasilyev *et al*., 2017, 2018, 2019; S. Wang *et al*., 2021; Yun *et al*., 2016). Considerable accuracy can be achieved with these models (Acharya & Mishra, 2017; Anitha & Singh, 2008; Bourget *et al.*, 2011; Chen *et al*., 2018a;

Omelchuk & Chagnes, 2018; Sorel *et al*., 2011; Vasilyev *et al*., 2017, 2018, 2019; Vieceli *et al*., 2021; Wang *et al*., 2021a; Yun *et al*., 2016), but plenty of experimental work is still involved with the simulation approach because experimental data are required for fitting the model parameters and validating the simulation results. To the best of the author's knowledge, the currently available experimental data for multi-metal extraction systems do not cover the entire concentration range. Therefore, many of the published models have not been validated against equilibrium data from highly concentrated multi-metal solutions. Besides, so far, simulation work requires manual complementation of the existing equilibrium models when the chemical system to be simulated differs from the systems that the models were originally built to describe. Hence, the use of numerical simulation in the design of reactive solvent extraction processes requires a thorough understanding of equilibrium chemistry, speciation, chemical thermodynamics, and numerical methods (Vasilyev, 2018).

Extraction performance in continuous multi-stage extractions can be experimentally evaluated by carrying out batch extractions with a suitable contact pattern (Chapter 3.3; Publication I) or through pilot-studies in mixer-settler cascades (Publications II & III) or extraction columns. Experimental simulation of multistage extraction cascades by batch extractions is a useful approach when the studied chemical system contains hazardous or expensive substances; the procedure can be performed in small scale using separation funnels. However, this method is practical only for testing a single cascade at once. Furthermore, many repetitive extractions are required for testing a single set of operating parameters. In addition, the requisite delicate pH adjustment is cumbersome. Eventually, pilot testing of the whole flowsheet is—or at least should be—performed using mixer-settlers and columns, regardless of the applied design methods. Piloting requires time, physical resources, and economic resources—testing several flowsheets or carrying out parameter optimization by piloting becomes expensive. Major advantages of the experimental methods include that physical phase behaviour can be assessed and the results are correct for the given extraction system, provided that the experimental and analytical work are executed carefully.

1.3 Research contribution

This thesis contributes to the research on hydrometallurgical solvent extraction with an emphasis on flowsheet development for concentrated solutions. The speciation of electrolyte solutions varies with ionic strength, which makes the solution environments of concentrated and dilute electrolyte solutions different (see Chapter 2.1). Saturation phenomena are more likely to be encountered with concentrated solutions, and the hydrodynamic behaviours of the concentrated and dilute solutions are different due to different physical properties.

Extraction of arsenic from concentrated H_2SO_4 was studied in Publication I. New liquid–liquid distribution data were measured and reported for arsenic and H_2SO_4 with two extractant solutions: undiluted tri-*n*-butyl phosphate (TBP) and a mixture of 1,2-

octanediol (6 mass %) in 2-ethylhexanol. Co-extraction of H_2SO_4 and water cause significant changes in phase densities and volumes; these changes were quantified. The McCabe–Thiele method and experimental pseudo-countercurrent extractions were used to estimate the extraction and stripping performance in countercurrent cascades. The McCabe–Thiele analysis of the countercurrent stripping cascade deviated from the experimental pseudo-countercurrent results.

Purification of an industrial H_2SO_4 leachate containing over 150 g L^{-1} manganese was studied in Publication II. Bis(2-ethylhexyl) hydrogen phosphate (D2EHPA) and bis(2,4,4-trimethylpentyl)phosphinic acid (BTMPPA, CYANEX 272®) were used for the extraction of low levels of zinc and iron from the leachate. Over 99 % of the zinc and over 98 % of the iron were extracted by both extractants. The countercurrent separation performance was studied in continuous industrial-type laboratory-scale mixer-settlers. The rejection of calcium by D2EHPA was an anomalous observation with respect to the published literature. Numerical analysis suggested that calcium is rejected by D2EHPA when the Mn:Ca ratio in the sulfate solution is very high. This observation highlights the necessity of experimental data over various concentration ranges. The removal of zinc and iron from the leachate enabled the use of $MnSO_4$ solution in the hydroxide co-precipitation synthesis of nickel–cobalt–manganese (NCM) cathode precursors.

Publication III presents the development of a non-optimized solvent extraction flowsheet for the treatment of cobalt-rich lithium-ion battery (LIB) leachates. The flowsheet utilizes partial separations to produce, for example, nickel-rich ternary sulfate mixtures with the desired stoichiometric ratios of nickel, cobalt, and manganese. The excess metals (lithium, cobalt, and manganese, in this case) are simultaneously obtained in their own purified fractions from the same process. The proposed flowsheet does not involve the use of additional transition metal salts for compositional adjustments. The key steps of the proposed process were studied in continuous industrial-type laboratory-scale mixer-settlers. New liquid–liquid distribution data were measured and reported in Publications II and III for the studied extraction systems.

1.4 Overview and limitations

This dissertation consists of the summary and three articles that have been published in international scientific journals. The summary is divided into five main chapters. Chapter 1 introduces the background of solvent extraction and the objectives of solvent extraction process development. Chapter 2 includes the basic theories and quantitative descriptions used to characterize distribution and process performance in hydrometallurgical solvent extraction. Chapter 3 explains the process development methods that were used in this thesis. Publications I–III present detailed descriptions of the experimental methods, equipment, chemicals, and analytical procedures. Chapter 4 contains the results and discussion. Conclusions and recommendations for future research are given in Chapter 5.

This dissertation is focused on process development via the knowledge of equilibrium distributions. Extraction kinetics and hydrodynamic effects were not studied *per se*, but their effects on the studied extraction processes (Publications II and III) were introduced during the experimental demonstrations in continuous countercurrent mixer-settler equipment.

2 Equilibrium in hydrometallurgical solvent extraction

All chemical systems drift spontaneously towards chemical and thermal equilibrium. In equilibrium, the concentrations in each phase remain constant over time and no changes in the properties of the system can be observed. Additionally, the chemical reactions proceed both forward and backward at equal rates. Likewise, mass transfer is continued in both directions through the phase interface with equal rates—there is no net mass transfer. Net transfer of mass between two distinct phases requires that the chemical system is in a non-equilibrated state. The extent of mass transfer can be calculated for a contact of non-equilibrated phases with known compositions when there is *a priori* knowledge of the distribution in equilibrium and the process conditions are known. The equilibrium compositions are, with certain limitations, determined experimentally.

Hydrometallurgical solvent extraction most often involves the transfer of metals from aqueous electrolyte solutions to water-immiscible organic solvents, and vice versa. The extraction process is controlled by several inter-dependent equilibrium reactions (see Chapter 2.3). Some of the equilibrium reactions occur only between the organic or the aqueous species, but the overall extraction reactions are affected by both organic and aqueous species. This chapter gives a superficial description of these equilibrium reactions and factors that determine the equilibrium compositions.

2.1 Solution chemistry

Metals exist as different types of charged or uncharged species in aqueous solutions. The charged ionic species form upon electrolyte dissociation. The relative amounts of different species (speciation) in an aqueous solution are determined by temperature, pH, ionic strength, redox potential, and the chemical elements within the solution. In contrast, electrolyte dissociation is unfavourable in non-polar organic solvents with low relative permittivity ($\varepsilon < 10$) because the intensity of ion association is inversely proportional to the relative permittivity of the solvent, the temperature, and the distance between oppositely charged ions (Marcus, 2004; Ritcey, 2006). Rigorous treatment of solution thermodynamics is beyond the scope of this thesis, but a superficial description of non-ideality is given to explain *why* changes in the phase compositions have significant effects on solvent extraction process performance.

In liquid–liquid equilibrium, the chemical potentials of the independent components must be equal in both phases. Formal concentrations can be used to calculate the chemical potentials only for ideal solutions, whereas activities (*i.e.*, "effective concentrations") must be used for non-ideal solutions. A non-ideal solution is a solution in which solvent–solvent interactions are not identical with solvent-solute interactions and the vapor pressures of the solution components do not obey Raoult's law ($p_i = x_i p_i^*$, where p_i is the vapor pressure of component i in the mixture, p_i^* is the vapor pressure of pure i, and x_i is the mole fraction of i in the mixture) (Rumble, 2021). The electrolyte solutions

encountered in practice are non-ideal. Consequently, the concentrations should be multiplied by the activity coefficients to account for this non-ideality:

$$a_i = \gamma_i \frac{m_i}{m^0}, \tag{2.1}$$

where a_i is the activity of specimen i, γ_i is the activity coefficient of i, m_i is the molality of i [mol kg^{-1}], and m^0 is the standard state (1 mol kg^{-1}). Activities should be used also in the mass-action law expressions of the equilibrium constants (Chapter 2.3).

Activity coefficients of the aqueous species can be calculated using mathematical models, many of which are extended versions of the Debye–Hückel equation. Casas *et al*. (2003), and Vasilyev *et al*. (2018, 2019) applied the B-dot equation (Equation 2.2) to speciation calculations. The B-dot equation as given by Casas *et al*. (2003) is

$$\log(\gamma_i) = -\frac{Az_i^2\sqrt{I}}{1 + B\text{å}_i\sqrt{I}} + \dot{B}I, \tag{2.2}$$

where γ_i is the activity coefficient of specimen i, A and B are constants of the Debye–Hückel term, $\dot{B}$ is an empirical parameter [kg mol^{-1}], I is ionic strength [mol kg^{-1}], å_i is an ion-specific size parameter (hard core diameter) [cm], and z_i is the charge of specimen i. The Debye–Hückel parameters A and B can be calculated from (Helgeson & Kirkham, 1974):

$$A = \frac{\sqrt{2\pi N}q_e^3\sqrt{\rho}}{\ln(10)\sqrt{1000}\sqrt{\varepsilon^3 k_B^3 T^3}} \tag{2.3}$$

and

$$B = \sqrt{\frac{8\pi N\rho q_e^2}{1000\varepsilon k_B T}}, \tag{2.4}$$

where q_e is the elemental charge ($4.80320425 \cdot 10^{-10}$ statC), k_B is the Boltzmann constant ($1.380649 \cdot 10^{-23}$ erg K^{-1}), N is Avogadro's number ($6.02214076 \cdot 10^{23}$ mol^{-1}), T is absolute temperature [K], ε is the relative permittivity of the solvent, and ρ is the density of the solvent [g cm^{-3}]. The values of A and B at 25 °C are approximately 0.51 kg$^{1/2}$ mol$^{-1/2}$ and $3.285 \cdot 10^7$ kg$^{1/2}$ mol$^{-1/2}$ cm^{-1}, respectively.

Equation (2.2) may be valid at ionic strengths up to 3 mol kg^{-1}, depending on the composition of the solution (Hörbrand *et al*., 2018); it simplifies to $\log(\gamma_i) = \dot{B}I$ for neutral species. For example, Pitzer equations (Pitzer, 1991) or the extended universal quasichemical (UNIQUAC) model (Thomsen, 2005) are more suitable for the calculation of activity coefficients in solutions with $I > 1$ mol kg^{-1}. However, the Pitzer model and

extended UNIQUAC model require a high number of interaction parameters that are not readily available. Additionally, their determination is experimentally laborious.

The molal ionic strength required in Equation (2.2) is defined by

$$I = \frac{1}{2}\sum_i z_i^2 m_i, \tag{2.5}$$

where I is the ionic strength [mol kg^{-1}]. The ionic strength in [mol L^{-1}] is calculated by replacing molalities m_i with concentrations in Equation (2.5).

Because the composition (ionic strength) of the aqueous phase affects the activities of the aqueous species, all equilibria involving aqueous species in a solvent extraction system depend on ionic strength in addition to the solvent medium and temperature. Therefore, the extraction performance may change significantly with a change in concentrations even if the system components remain the same. For example, the extraction order of metals by acidic extractants may change due to variations in ionic strength or the extraction of a metal may be inhibited by the formation of ion–associate complexes or non-extractable ion pairs (Ritcey, 2006).

Speciation in the organic phase is affected by molecular aggregation and hydration, which increase the difficulty of calculating the activity coefficients for the organic species. Furthermore, speciation in the organic phase depends on the metal (*i.e.*, the aggregation and hydration characteristics are different for different organometallic complexes). Therefore, as in the calculation of aqueous activity coefficients, the difficulty arises from the necessity to evaluate a high number of empirical interaction or solubility parameters for the models.

2.2 Quantification of mass transfer and separation in solvent extraction

Physical distribution of a solute S between immiscible organic and aqueous liquids can be described by Equation (2.6)

$$\mathrm{S_{aq}} \rightleftarrows \mathrm{S_{org}} \tag{2.6}$$

and the Nernst distribution law

$$P_\mathrm{S} = \frac{[\mathrm{S}]_\mathrm{org}}{[\mathrm{S}]_\mathrm{aq}}, \tag{2.7}$$

where P_S is the *partition ratio* (distribution constant) of S and [S] is the concentration of S. Subscripts ‘org’ and ‘aq’ denote the organic and the aqueous phases, respectively. Equation (2.7) describes only the distribution of a single chemical specimen, such as an

uncharged metal compound. P_S is related to the thermodynamic *partition constant* via Equation (2.8)

$$P_S^0 = \frac{\gamma_{S,org}[S]_{org}}{\gamma_{S,aq}[S]_{aq}} = \frac{y_{S,org}}{\gamma_{S,aq}} P_S, \tag{2.8}$$

where P_S^0 is the thermodynamic partition constant of S at infinite dilution, $\gamma_{S,org}$ is the activity coefficient of S in the organic phase, and $\gamma_{S,aq}$ is the activity coefficient of S in the aqueous phase (Marcus & Kertes, 1969; Rydberg *et al*., 2004).

Metals are typically found in several different chemical forms (species) in solutions. The concentrations of all individual metal species—and hence their partition ratios—cannot be independently determined. Therefore, the distribution of metals in solvent extraction is often described by using the *distribution ratio*, which is defined by Equation (2.9)

$$D_M = \frac{[M]_{tot,org}}{[M]_{tot,aq}}, \tag{2.9}$$

where D_M is the distribution ratio of M, $[M]_{tot,org}$ is the total (analytical) concentration of M in the organic phase, and $[M]_{tot,aq}$ is the total concentration of M in the aqueous phase (Habashi, 1999; Marcus & Kertes, 1969; Ritcey, 2006; Rydberg *et al.*, 2004). Despite the similarity of Equations (2.7) and (2.9), the distribution and partition ratios quantify different things and are rarely equal.

The percentage of solute transferred during extraction is described by Equation (2.10)

$$E_M = \frac{100 D_M}{D_M + \frac{V_{aq}}{V_{org}}}, \tag{2.10}$$

where E_M is the percentage of M extracted, V_{aq} is the volume of the aqueous phase, and V_{org} is the volume of the organic phase (Habashi, 1999; Marcus & Kertes, 1969; Ritcey, 2006; Rydberg *et al*., 2004). When two solutes, A and B, have different distribution ratios, the metal with higher distribution ratio will be enriched to the organic phase and separation occurs. The separation efficiency between the solutes is characterized by the ratio of their *D* values

$$\alpha(A/B) = \frac{D_A}{D_B}, \tag{2.11}$$

where α(A/B) is the separation factor between A and B. The solutes can be separated from each other only if $\alpha \neq 1$. The enrichment factor is

$$F_{\mathrm{E}} = \frac{E_{\mathrm{A}}}{E_{\mathrm{B}}}, \tag{2.12}$$

where F_{E} is the enrichment factor (Habashi, 1999; Ritcey, 2006).

The distribution ratio, percentage of extraction, separation factor, and enrichment factor (Equations 2.9–2.12) are the key quantities used to describe the extent of mass transfer and separation in solvent extraction.

2.3 Extraction mechanisms

The most relevant extraction mechanisms are included here as they are described in the fundamental literature on solvent extraction (Marcus & Kertes, 1969; Ritcey, 2006; Rydberg *et al.*, 2004). The chapter follows the classification by Rydberg *et al*. (2004). Because of the reasons given in Chapter 2.1, determining the equilibrium constants and stoichiometries for the equilibrium reactions is not straightforward. The simplified equilibrium descriptions in this chapter offer useful qualitative information about the extraction systems despite losing their predictive accuracy for extraction systems involving concentrated solutions.

2.3.1 Extraction of coordinatively saturated metal complexes

Extraction of a metal cation of charge z^+ by a monobasic chelating extractant is formally described by Equations (2.13–2.16) (Marcus & Kertes, 1969)

- Distribution of the extractant, HA, between the organic and the aqueous phase

$$\mathrm{HA} \rightleftarrows \overline{\mathrm{HA}} \tag{2.13}$$

- Dissociation of the extractant

$$\mathrm{HA} \rightleftarrows \mathrm{H^+} + \mathrm{A^-} \tag{2.14}$$

- Overall formation of the coordinatively saturated metal complex

$$\mathrm{M^{z+}} + z\mathrm{A^-} \rightleftarrows \mathrm{MA}_z \tag{2.15}$$

- Distribution of the metal chelate, MA_z, between the organic and the aqueous phases

$$\mathrm{MA}_z \rightleftarrows \overline{\mathrm{MA}_z} \tag{2.16}$$

The equilibria in Equations (2.13–2.16) are depicted in Figure 2.1. The equilibrium constants for these formal reactions are defined by Equations (2.17–2.20)

$$P_{\mathrm{HA}} = \frac{\overline{[\mathrm{HA}]}}{[\mathrm{HA}]} \tag{2.17}$$

$$K_{a,\mathrm{HA}} = \frac{[\mathrm{H}^+][\mathrm{A}^-]}{[\mathrm{HA}]} \tag{2.18}$$

$$\beta_{\mathrm{MA}_z} = \frac{[\mathrm{MA}_z]}{[\mathrm{M}^{z+}][\mathrm{A}^-]^z} \tag{2.19}$$

$$P_{\mathrm{MA}_z} = \frac{\overline{[\mathrm{MA}_z]}}{[\mathrm{MA}_z]}, \tag{2.20}$$

where P_{HA} is the partition ratio of the extractant, $K_{\mathrm{a,HA}}$ is the dissociation constant of the extractant, β_{MA_z} is the overall formation constant of the coordinatively saturated metal chelate, and P_{MA_z} is the partition ratio of the coordinatively saturated metal complex.

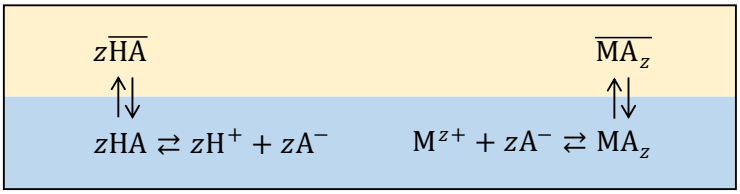

Figure 2.1 Simplified representation of the equilibria involved in extraction of a coordinatively saturated metal complex (MA_z) by an acidic extractant (HA).

The balanced overall reaction of Equations (2.13–2.16) is

$$\mathrm{M}^{z+} + z\overline{\mathrm{HA}} \rightleftarrows \overline{\mathrm{MA}_z} + z\mathrm{H}^+ \tag{2.21}$$

and the equilibrium constant for the extraction reaction (Equation 2.21) is

$$K_{\mathrm{EX}} = P_{\mathrm{MA}_z} K_{a,\mathrm{HA}}^z \beta_{\mathrm{MA}_z} P_{\mathrm{HA}}^{-z} \tag{2.22}$$

where K_{EX} is the extraction constant. If MA_z and M^{z+} are the only metal species in the system, substituting concentrations into Equation (2.22) yields

$$K_{\mathrm{EX}} = \frac{\overline{[\mathrm{MA}_z]}[\mathrm{H}^+]^z}{[\mathrm{M}^{z+}]\overline{[\mathrm{HA}]}^z} = D_{\mathrm{M}} \frac{[\mathrm{H}^+]^z}{\overline{[\mathrm{HA}]}^z}. \tag{2.23}$$

Extending Equation (2.23) with activity coefficients gives

$$D_{\mathrm{M}} = K_{\mathrm{EX}} \frac{\gamma_{\mathrm{M}^{z+}} \bar{\gamma}_{\mathrm{HA}}^{z}}{\bar{\gamma}_{\mathrm{MA}_z} \gamma_{\mathrm{H}^+}^{z}} \frac{[\overline{\mathrm{HA}}]^z}{[\mathrm{H}^+]^z}, \tag{2.24}$$

where $\gamma_{\mathrm{M}^{z+}}$ is the activity coefficient of M^{z+}, γ_{H^+} is the activity coefficient of a proton, $\bar{\gamma}_{\mathrm{HA}}$ is the activity coefficient of HA in the organic phase, and $\bar{\gamma}_{\mathrm{MA}_z}$ is the activity coefficient of MA_z in the organic phase. If the quotient of the activity coefficients is constant, K_{EX} and the activity quotient can be lumped together into an *apparent extraction constant*, K'. Combining Equation (2.10) with Equation (2.24) and substituting the apparent extraction constant yields

$$E = \frac{100}{1 + (K')^{-1}[\overline{\mathrm{HA}}]^{-z}[\mathrm{H}^+]^z \frac{V_{\mathrm{aq}}}{V_{\mathrm{org}}}}. \tag{2.25}$$

Equation (2.25) qualitatively shows that extraction by acidic extractants is increased when: I) the apparent extraction constant is increased, II) the extractant concentration is increased, III) the proton concentration is lowered (*i.e.*, the pH is increased), and IV) the O/A ratio is increased. The value of K' is affected by temperature, pressure, and the quotient of the activity coefficients for a given extractant.

2.3.2 Extraction of metal complex adducts

A coordinatively unsaturated metal complex is hydrated by water molecules to form $\mathrm{MA}_z(\mathrm{H_2O})_w$ complexes, which become more extractable to the organic phase when the water molecules are replaced by suitable organic molecules (adduct formers). Rydberg *et al*. (2004) present three types of adducts: I) metal–organic complexes with organic adduct formers, II) metal–inorganic complexes with organic adduct formers, and III) self-adducts. Extraction of these adducts can be described in a stepwise manner similar to Equations (2.13–2.16) that were shown for the extraction of metal chelates.

Metal-organic complexes with organic adduct formers

Extraction of a metal–organic complex, MA_z, with an organic adduct former, B, can be described by an overall reaction

$$\mathrm{M}^{z+} + z\overline{\mathrm{HA}} + b\overline{\mathrm{B}} \rightleftarrows \overline{\mathrm{MA}_z\mathrm{B}_b} + z\mathrm{H}^+. \tag{2.26}$$

The apparent equilibrium constant of Equation (2.26) is

$$K' = \frac{\overline{[\mathrm{MA}_z\mathrm{B}_b]}[\mathrm{H}^+]^z}{[\mathrm{M}^{z+}][\overline{\mathrm{HA}}]^z[\overline{\mathrm{B}}]^b}, \tag{2.27}$$

where b is the number of associated B molecules in the adduct. Because adducts with different numbers of B molecules can simultaneously exist, the distribution ratio of the metal is written as

$$D_{\mathrm{M}} = \frac{[\overline{\mathrm{MA}_z}] + [\overline{\mathrm{MA}_z\mathrm{B}}] + [\overline{\mathrm{MA}_z\mathrm{B}_2}] + \cdots}{[\mathrm{M}] + [\mathrm{MA}^{z-1}] + [\mathrm{MA}_2^{z-2}] + \cdots}. \tag{2.28}$$

If the fraction of charged complexes formed by M^{z+} and A^- is negligible, derivation from the formal stepwise reactions gives

$$D_{\mathrm{M}} = \frac{P_{\mathrm{MA}z}\beta_{\mathrm{MA}z}[\mathrm{A}^-]^z(1 + K_{\mathrm{ad},1}[\overline{\mathrm{B}}] + K_{\mathrm{ad},2}[\overline{\mathrm{B}}]^2 + \cdots)}{\sum_0^n \beta_n[\mathrm{A}^-]^n}, \tag{2.29}$$

where $P_{\mathrm{MA}z}$ is the partition ratio of the uncharged metal complex, β_{MA_z} is the overall formation constant of the uncharged metal complex, $K_{\mathrm{ad},1}$ is the adduct formation constant for adducts with $b = 1$, $K_{\mathrm{ad},2}$ is the adduct formation constant for adducts with $b = 2$ and so on (Equation 2.32). β_n is the overall formation constant of the nth complex of the form MA_n^{z-n}, and n is the number of A^- ions complexed with the metal cation. The summation includes all metal species in the aqueous phase. Alternatively, Equation (2.29) can be written as

$$D_{\mathrm{M}} = D_{0,\mathrm{M}}\left(1 + K_{\mathrm{ad},1}[\overline{\mathrm{B}}] + K_{\mathrm{ad},2}[\overline{\mathrm{B}}]^2 + \cdots\right), \tag{2.30}$$

where $D_{0,\mathrm{M}}$ is the distribution ratio of M in a system without an adduct former and defined by

$$D_{0,\mathrm{M}} = \frac{[\overline{\mathrm{MA}_z}]}{\sum[\mathrm{MA}_n^{z-n}]} = \frac{P_{\mathrm{MA}z}\beta_{\mathrm{MA}z}[\mathrm{A}^-]^z}{\sum \beta_n[\mathrm{A}^-]^n}. \tag{2.31}$$

The adduct formation constants are defined by

$$K_{\mathrm{ad},b} = \frac{[\overline{\mathrm{MA}_z\mathrm{B}_b}]}{[\overline{\mathrm{MA}_z}][\overline{\mathrm{B}}]^b}. \tag{2.32}$$

Extraction of inorganic metal salts as adducts

Strongly basic extractants, such as TBP or trioctylphosphine oxide (TOPO), can replace the hydrate water molecules around an inorganic metal salt to form an adduct that is soluble in the organic phase. Alternatively, solvating solvents (ethers, ketones, alcohols, and esters) can be used as adduct formers (Rydberg *et al.*, 2004). Organophosphorus compounds usually completely displace the water from the metal complex, whereas the complexes formed by carbon-bonded oxygen-donor extractants contain hydrate water. These solvating extractants also extract acids (see Chapter 2.3.4). Extraction of a metal

cation M^{z+} as an adduct with an inorganic monovalent anion, X^-, and an organic solvating molecule, B, is described by the overall reaction (Marcus & Kertes, 1969)

$$M^{z+} + zX^- + b\overline{B} \rightleftarrows \overline{MX_zB_b}. \tag{2.33}$$

The apparent extraction constant for Equation (2.33) can be written

$$K' = \frac{\overline{[MX_zB_b]}}{[M^{z+}][X^-]^z[\overline{B}]^b}. \tag{2.34}$$

The derivation of the distribution ratio is analogous to the extraction of MA_zB_b. However, now the amount of the metal salt, MX_z, in the organic phase is negligible. Hence the distribution ratio can be written in the form

$$D_M = \frac{\beta_{MX_z}[X^-]^z \sum K_{ad,b}[\overline{B}]^b}{1 + \sum \beta_n [X^-]^n}, \tag{2.35}$$

where the summations begin from 1 and $K_{ad,b}$ is defined as in Equation (2.32).

Self-adducts

Water molecules in the hydrated $MA_z(H_2O)_w$ complexes can be replaced by undissociated acidic extractant molecules. The formal stepwise analysis is similar to the extraction of coordinatively saturated metal complexes (Equations (2.13–2.16)), but hydrate water is present in Equations (2.15–2.16). Formation of the self-adduct is then described by

$$\overline{MA_z(H_2O)_w} + b\overline{HA} \rightleftarrows \overline{MA_z(HA)_b} + wH_2O, \tag{2.36}$$

where w is the number of replaced hydrate water molecules (Rydberg *et al.*, 2004). Equation (2.36) assumes complete replacement of the hydrated water molecules and $w = b$. In this case, the extraction can be described formally by the overall equation (Marcus & Kertes, 1969)

$$M^{z+} + (z + b)\overline{HA} \rightleftarrows \overline{MA_z(HA)_b} + zH^+. \tag{2.37}$$

Acidic extractants can be considered liquid cation exchangers and the extraction can proceed via several mechanisms (Equations 2.21, 2.26, and 2.37).

2.3.3 Liquid anion exchange

Organic amines form stable cations via protonation, then the protonated amines form ion pairs (*i.e.*, ammonium salts) with the anions of the extraction system. Tertiary amines and quaternary ammonium salts are preferred in industrial extraction of metals due to their suitable physical properties (Marcus & Kertes, 1969). Protonation of a lipophilic high

molecular mass tertiary amine (R_3N) and association with a monobasic anion, L^-, is described by

$$\overline{R_3N} + H^+ + L^- \rightleftarrows \overline{R_3NH^+L^-}. \tag{2.38}$$

Equation (2.38) describes the extraction of an acid, which is discussed further in Chapter 2.3.4. A distinctive feature of quaternary ammonium salts is that their ionic character is retained in both acidic and basic conditions. The anion of the amine salt can be replaced by other anionic species such as a negatively charged metal complex. Assuming the metal complex is formed by a metal cation with charge *z*+ and monobasic ligands A^-, extraction of the anionic metal specimen is described by the anion exchange reaction

$$MA_{z+p}^{p-} + p\overline{R_3NH^+L^-} \rightleftarrows \overline{(R_3NH^+)_p^{p+}MA_{z+p}^{p-}} + pL^-. \tag{2.39}$$

If the extraction system contains only one anionic ligand, L^-, the apparent extraction constant for Equation (2.39) can be written

$$K_p' = \frac{\left[\overline{(R_3NH^+)_p^{p+}ML_{z+p}^{p-}}\right][L^-]^p}{\left[ML_{z+p}^{p-}\right]\left[\overline{R_3NH^+L^-}\right]^p} \tag{2.40}$$

and the distribution ratio is given by

$$D_M = \frac{\left[\overline{(R_3NH^+)_p^{p+}ML_{z+p}^{p-}}\right]}{\sum[ML_n^{z-n}]} = K_p' \frac{\beta_p\,[L^-]^p\left[\overline{R_3NH^+L^-}\right]^p}{1 + \sum \beta_n[L^-]^n}, \tag{2.41}$$

but only when $\overline{(R_3NH^+)_p^{p+}ML_{z+p}^{p-}}$ is the only metal specimen in the organic phase (Rydberg *et al.*, 2004). It is extremely challenging to derive mass-action law expressions for the distribution of metals in systems where ion associates are extracted. The ligand concentration in the aqueous phase must be sufficiently high for the formation of anionic metal complexes. Therefore, the ionic strength of the aqueous phase is typically so high that the aqueous phase is highly non-ideal. Furthermore, speciation of the amine salts in organic diluents is affected by the nature and solvating power of the diluent, the anion species, the length of the hydrocarbon chains, temperature, and the concentration of the solute in non-polar solvents (Marcus & Kertes, 1969). The amine salts tend to aggregate and form micelles in inert diluents, which results in formation of a third phase at high extractant concentrations. Aggregation can be controlled and third-phase formation can be avoided by using sufficiently basic modifiers (*e.g.*, TBP or alcohols), using polar or aromatic diluents, or increasing the temperature (Marcus & Kertes, 1969; Rydberg *et al.*, 2004).

2.3.4 Extraction of acids

Distribution of acids is important in hydrometallurgical extraction systems not only because of the wide use of acidic extractants but also because the acids may compete with the target metal species for the available extractant molecules. Furthermore, the theory on extraction of acids is relevant in the context of Publication I, where H_3AsO_4 and H_2SO_4 were extracted by TBP and aliphatic alcohols. Extraction of weak monobasic organic acids can be described by the dissociation reaction (Equation 2.14) and partitioning between the organic and aqueous phases (Equation 2.13). The distribution ratio of the acid is

$$D_{\mathrm{HA}} = \frac{[\overline{\mathrm{HA}}]}{[\mathrm{HA}] + [\mathrm{A}^-]} = \frac{P_{\mathrm{HA}}}{1 + K_{\mathrm{a,HA}}[\mathrm{H}^+]^{-1}}. \tag{2.42}$$

The expression for D_{HA} (Equation 2.42) must be extended if the acid forms aggregates in the organic phase or if the acid protonates in the aqueous phase to form H_2A^+ (Rydberg *et al.*, 2004).

Acids can also be extracted as ion pairs and adducts but the structures of such "solvated hydrogen salts" are not well known (Rydberg *et al.*, 2004). Strong inorganic acids are mainly dissociated in aqueous solutions even at very low pH. However, a strong donor molecule can solvate the proton and then form an extractable ion associate with the anion. Oxygenated solvents (ethers, alcohols, ketones, and esters) and neutral organophosphorus compounds extract acids with a varying amount of hydrate water, whereas extraction as an anhydrous ion pair is typical with amine extractants due to their stronger basicity (Marcus & Kertes, 1969). Rydberg *et al*. (2004) have presented a simplified description of the extraction of monoprotic acids by adduct formation (omitting hydrate water)

$$\overline{\mathrm{HA}} + b\overline{\mathrm{B}} \rightleftarrows \overline{\mathrm{HAB}_b}, \tag{2.43}$$

which can be considered to take place either in the organic phase or at the interface of the liquid phases. Adduct formation (Equation 2.43) can be considered by introducing the concentrations of the adducts to Equation (2.42)

$$D_{\mathrm{HA}} = \frac{P_{\mathrm{HA}}(1 + \sum K_{\mathrm{ad},b}[\overline{\mathrm{B}}]^b)}{1 + K_{\mathrm{a,HA}}[\mathrm{H}^+]^{-1}}. \tag{2.44}$$

Distribution ratio measurements alone cannot reveal whether the reaction occurs in the bulk organic phase or at the interface. Equation (2.44) also describes extraction with adduct formation at the interface, the only difference being that the terms $P_{\mathrm{HA}}K_{\mathrm{ad},b}$ are replaced with single constants and HA in Equation (2.43) is formally written as aqueous reactant. Establishing general equations that accurately describe the distribution of acids is difficult because of the variety of acids and individual characteristics of the extraction systems. The extraction of acids is often accompanied by co-extraction of water and changes in phase volumes. Moreover, it is possible that extracted mineral acids are found

in both undissociated and dissociated forms or as multi-acid adducts in the organic phase (Kislik, 2012; Marcus & Kertes, 1969).

3 Process development methods

The selectivity of an extractant is rarely high enough to simultaneously allow high purity and recovery in a single extraction stage from complex multi-metal solutions, and chemically similar metals are often extracted together with the target metal. Plotting the percentage extracted against a characteristic variable, such as pH (Figure 3.1), total anion concentration, or free ligand concentration, is useful for evaluating favourable extraction conditions as well as the order in which the metals are extracted. Figure 3.1 illustrates hypothetical pH isotherms for four different metals that are extracted by a liquid cation exchanger. It is seen that complete separations between metals M_1–M_3 and M_3–M_4 are impossible in a single extraction stage. Additionally, M_4 cannot be extracted to the organic phase without co-extraction of the other metals, but M_1–M_3 must first be separated from M_4. However, separation efficiency and recovery can be improved by using multiple extraction stages.

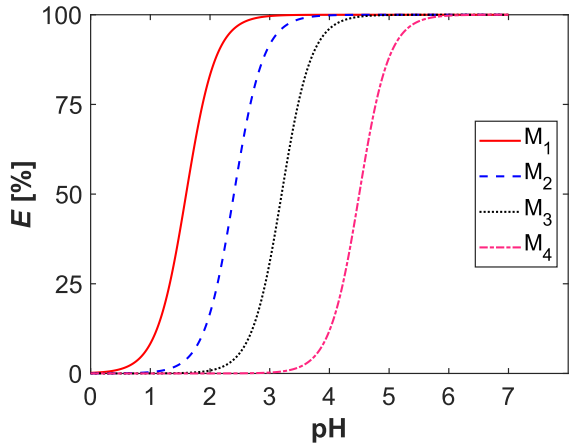

Figure 3.1 Hypothetical pH isotherms for four different metals.

3.1 Extraction with multiple stages

In crosscurrent extraction a volume of the feed is equilibrated multiple times with fresh solvent (Figure 3.2). Although the percentages extracted in each single stage are lower than 100 %, the cumulative percentage of extraction will approach 100 % as the number of successive extractions is increased, as predicted by the equation given by IUPAC

$$E_n = \left(1 - \left(\frac{V_{\mathrm{org}}}{V_{\mathrm{aq}}} D_{\mathrm{M}} + 1\right)^{-n}\right) \cdot 100\ \%, \tag{3.1}$$

where E_n is the cumulative percentage extracted in n crosscurrent extraction stages (Rice *et al.*, 1993). Equation (3.1) is valid when the distribution ratio and phase ratio are constant in addition to equilibrium being attained in each extraction stage. If the phase

ratio or distribution ratio varies from stage to stage, the cumulative percentage extracted can be calculated stagewise given that the phase ratios and distribution ratios are known. If $D_M = 1$, O/A = 0.25, and $n = 4$ in Equation (3.1), the cumulative percentage extracted will be 59 %, whereas a single equilibration at O/A = 1 extracts only 50 % of the solute (Equation 2.10). Therefore, multiple extractions with a low O/A ratio will extract more of the solute than a single extraction with an equal total amount of solvent, yielding a more concentrated extract when the extracts E_1, E_2,…,E_n are mixed.

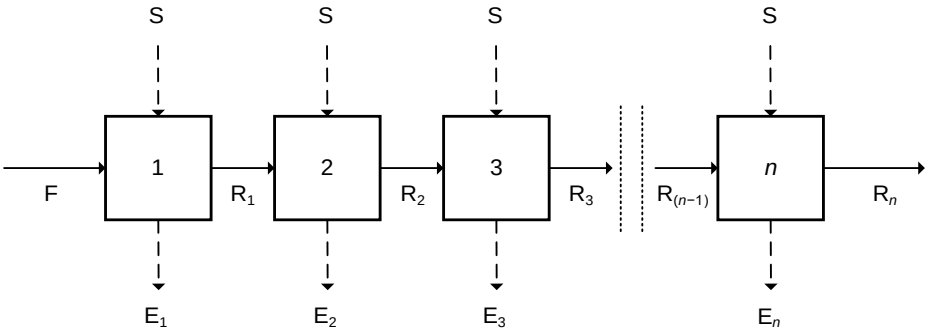

Figure 3.2 Crosscurrent solvent extraction.

Concentration of the solute in the extracts decreases after each crosscurrent contact. However, if the extract from any stage $n > 1$ in Figure 3.2 is not saturated, it can be used in stage $n-1$ to extract the solute from $R_{(n-2)}$ (or from the aqueous feed). This is the principle of countercurrent solvent extraction (Figure 3.3). The total amount of solute entering an extraction stage in a countercurrent cascade is higher than it would be if solute-free solvent were used, and the extract will be more concentrated than extract that would be obtained from crosscurrent extraction. The key idea is to operate the countercurrent cascade at sufficiently low solvent-to-feed volumetric flow ratio (S/F) so that the solute with the highest affinity towards the extractant occupies the extractant ligands. This is referred to as the *crowding effect* as the extraction of the undesired solutes is hindered by the limited availability of the free extractant ligands. The countercurrent operation enables a high metal loading in the organic phase with enhanced purity due to the crowding effect. Thus, the separation material (extractant) is efficiently utilized.

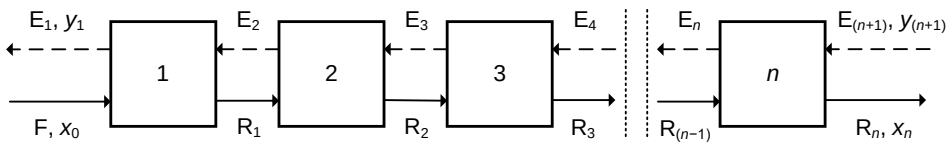

Figure 3.3 Countercurrent solvent extraction.

The material balance of a single solute on a countercurrent solvent extraction stage (Figure 3.3) can be written

$$R_{(n-1)}x_{(n-1)} + E_{(n+1)}y_{(n+1)} = R_n x_n + E_n y_n, \tag{3.2}$$

where $E_{(n+1)}$ is the solvent feed rate, E_n is the extract flowrate, $R_{(n-1)}$ is the aqueous feed rate, R_n is the raffinate flowrate, $x_{(n-1)}$ is the concentration of the solute in the aqueous feed, x_n is the concentration of the solute in the raffinate, y_n is the concentration of the solute in the extract, and $y_{(n+1)}$ is the concentration of the solute in the extract from stage n+1 (or concentration in the solvent feed). When there are no changes in phase volumes, $E_1,\ldots,E_n$ are equal to the solvent feed rate, S, and $R_1,\ldots,R_n$ are equal to F; hence, the material balance equation (Equation 3.2) can be written for the whole countercurrent cascade in the form

$$y_{(n+1)} = \frac{F}{S}(x_n - x_0) + y_1, \tag{3.3}$$

where y_1 is the concentration of the solute in the extract (Figure 3.3). The concentrations on each countercurrent stage are determined by the mass balance (Equation 3.2) and the equilibrium distribution ($y_n = D_n x_n$). A system of n+1 mass-balance equations must be solved to calculate the stream concentrations for a single solute in a countercurrent cascade. A graphical solution by the McCabe–Thiele method is described in Chapter 3.2.

3.2 McCabe–Thiele method

McCabe–Thiele diagrams (Figure 3.4) are based on the mass balance and equilibrium distribution of the target solute (here, metal M). The mass balance is solved graphically for each extraction stage and the cascade by using an *equilibrium line* and an *operating line*. The equilibrium line is a plot of analytical $c_{eq}(M)_{org}$ vs. $c_{eq}(M)_{aq}$. The curve is unique for the given chemical system and process conditions (T, p, pH). The most common method for experimental determination of the equilibrium line is to contact the aqueous feed solution with the extractant solution at various O/A ratios under constant temperature and pH (Bourget *et al*., 2011). The operating line represents the mass balance (Equation 3.3) and, thus, the terminal coordinates of the operating line are determined by the S/F ratio, the feed concentrations, and the target percentage of extraction—when constant phase ratio is assumed. The operating line is linear when the phase ratio does not vary from stage to stage (Coulson *et al*., 1983; Kislik, 2012; Ritcey, 2006).

The number of stages is determined by drawing horizontal and vertical lines between the equilibrium line and the operating line as shown in Figure 3.4. When the diagram is constructed from the aqueous feed end (a top-to-bottom construction), the first horizontal line is drawn from the intersection of the vertical aqueous feed line ($[M]_{aq}$ = 4.5 g L^{-1}) and the operating line, to the equilibrium line (Figure 3.4 a). Next, the first ideal stage is completed by drawing a vertical line from the equilibrium line to the operating line. This stepwise procedure is continued until the target percentage of extraction is met (*i.e.*, when

the $[M]_{aq}$ coordinate of the vertical line is small enough). The ideal stages can also be drawn by starting from the organic feed end, a bottom-to-top construction (Kislik, 2012; Ritcey, 2006).

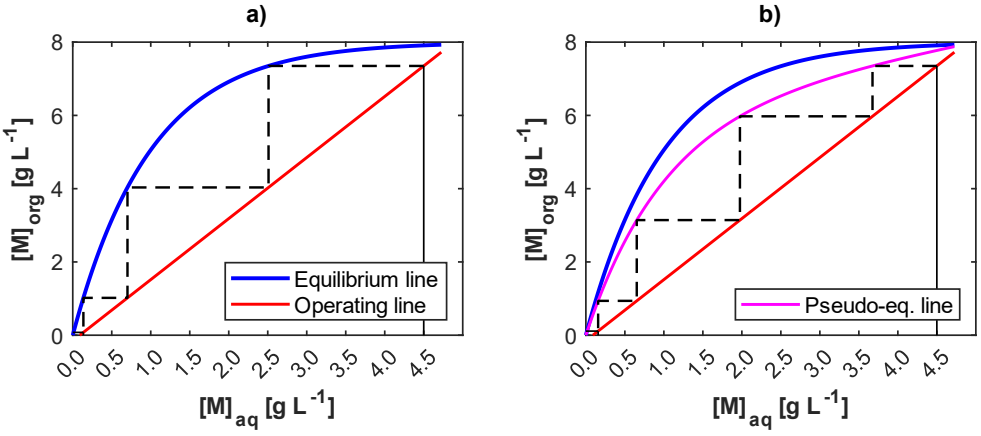

Figure 3.4 McCabe–Thiele diagrams with a hypothetical equilibrium line: a) Ideal extraction stages (M_E = 100 %); b) Extraction stages with M_E = 75 %. Operating line calculated with S/F = 0.6 and 98 % removal of M.

Chemical equilibrium is typically not attained in continuous solvent extraction equipment (Figure 1.3) because the residence time of the fluid elements within the effective mass transfer zone is shorter than the time required to reach the equilibrium. The overall rate of extraction, and hence the equilibration time, is determined by the convection and diffusion rates, the reaction kinetics, and the interfacial area between the liquid phases. The droplet size distribution, and hence the interfacial area, in a solvent extraction system is determined by the temperature-dependent physical properties of the liquids (densities, viscosities, interfacial tension), the intensity of mixing, and the hydrodynamic design of the extractor. Increasing mixing intensity increases the interfacial area and convective mass transfer while decreasing the thickness of the boundary layers at the interface. Therefore, the rate of extraction can be increased—up to certain limits—by increasing the mixing intensity. Too intensive mixing can reduce the size of the droplets so much that they behave as rigid spheres, with no internal circulation. Under these conditions, the transfer of the extractant to the interface is hindered and the rate of extraction becomes slow (Ritcey, 2006).

The number of required non-ideal extraction stages can be estimated with empirical extractor-specific parameters that relate the performance of a real extraction stage to an equilibrium stage. The extract phase Murphree efficiency is

$$M_{\mathrm{E},i} = \frac{y_{i,n} - y_{i,(n+1)}}{y^*_{i,n} - y_{i,(n+1)}}, \tag{3.4}$$

where $M_{\mathrm{E},i}$ is the extract phase Murphree efficiency for specimen i, $y_{i,n}$ is the concentration of i in the extract leaving stage n, $y^*_{i,n}$ is the concentration of i in the extract in equilibrium, and $y_{i,(n+1)}$ is the concentration of i in the extract entering stage n from stage n+1. The raffinate phase Murphree efficiency is

$$M_{\mathrm{R},i} = \frac{x_{i,(n-1)} - x_{i,n}}{x_{i,(n-1)} - x^*_{i,n}}, \tag{3.5}$$

where $M_{\mathrm{R},i}$ is the raffinate phase Murphree efficiency for specimen i, $x_{i,n}$ is the concentration of i in the raffinate leaving from stage n, $x^*_{i,n}$ is the concentration of i in the raffinate in equilibrium, and $x_{i,(n-1)}$ is the concentration of i in the extract entering stage n from stage n−1. The definitions of M_{E} and M_{R} are analogous to the definitions used in distillation calculations (Coulson *et al*., 1983). The M_{E} or M_{R} value is used to construct a pseudo-equilibrium line (Figure 3.4 b), which is used in the graphical solution of the mass-balance equations by the McCabe–Thiele method.

3.3 Simulation of countercurrent extraction by batch experiments

The performance of a countercurrent solvent extraction cascade can be experimentally estimated by batch extractions (Haghighi *et al*., 2015; Thornton, 1992). Figure 3.5 shows the experimental procedure for simulating a countercurrent cascade. On the first cycle the solvent and feed are equilibrated in as many vessels as there are extraction stages. Starting from the second cycle, the equilibrated phases from the previous cycle are transferred to a new set of vessels, as shown in Figure 3.5. The steady-state compositions are obtained after several consecutive cycles. The procedure is referred to as the *pseudo-countercurrent (pseudo-cc) method* throughout this dissertation. Pseudo-cc extractions were used to study the distribution of arsenic and H_2SO_4 in countercurrent extraction (Publication I).

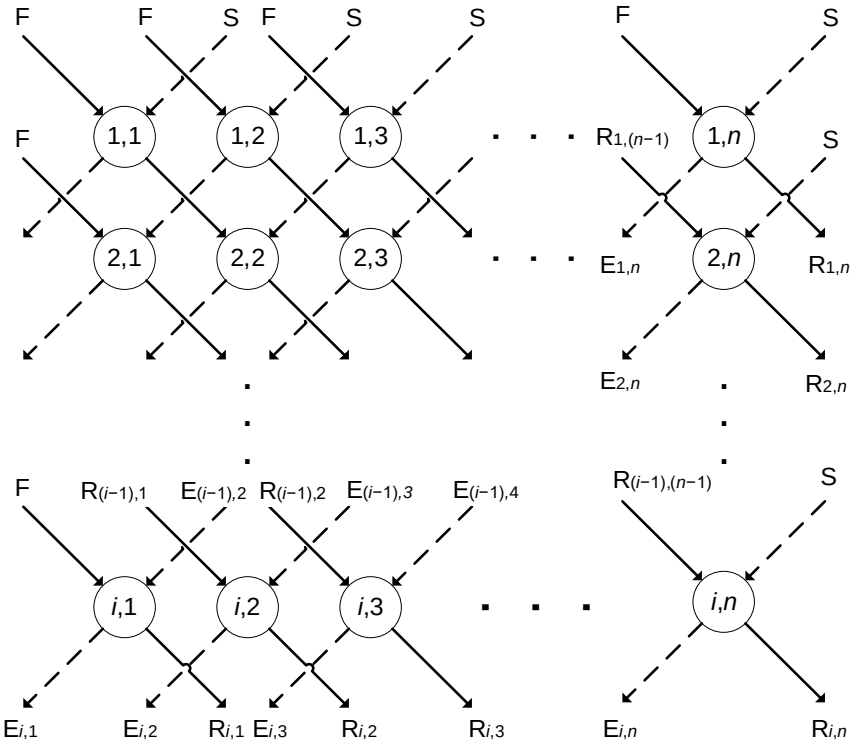

Figure 3.5 Pseudo-countercurrent method. Each circle in the figure represents one equilibration. S = solvent; F = feed; E = extract; R = raffinate; *i* is the number of cycles and *n* is the number of extraction stages. Dashed and solid lines show the transfers of the light and heavy phase, respectively.

3.4 Numerical equilibrium calculations

Numerical simulations can be used in flowsheet design to perform material balance calculations and to rigorously assess the distribution of individual chemical components within a process. Furthermore, computer simulations enable sensitivity analyses and process parameter optimization that would be more expensive and resource-intensive to perform experimentally. A numerical process simulation tool simultaneously solves the equilibrium compositions with the material balances. Therefore, the accuracy of flowsheet simulations depends on the accuracy of the equilibrium model. Modelling approaches in flowsheet simulations are briefly summarized in Chapter 1.2.

The mechanistic modelling approach presented earlier by Vasilyev *et al*. (2017, 2018, 2019) was applied in this thesis to qualitatively study the effect of the Mn:Ca ratio in the feed solution on the extraction of zinc, calcium, and manganese by D2EHPA. The extraction of zinc and calcium from concentrated $MnSO_4$ leachate was experimentally studied in Publication II. A simplified equilibrium model (Table 3.1) was used to simulate

pH isotherms for zinc, calcium, and manganese. The following assumptions and simplifications were made:

- Only liquid–liquid equilibria were considered.
- Redox reactions were not considered.
- The system was considered as ideal. All activity coefficients were set to one. No ionic strength corrections were applied for the equilibrium constants.
- Precipitation reactions of $Ca(OH)_2$, $CaSO_4$, and $CaSO_4 \cdot 2H_2O$ were omitted to exclusively study the extraction of calcium at different Mn:Ca ratios.
- The phase volumes do not change except due to pH adjustment by aqueous NaOH.
- Stoichiometries of the extraction reactions were simplified to follow chelation stoichiometry (Equation 2.21). Adduct formation, hydration, micelle formation, or polymerization of the organometallic complexes were not considered.
- Water molecules in the speciation equations were not considered, except in the ionic product of water.
- All reactions were considered as elementary reactions because the equilibrium composition was solved by integrating the system of rate equations (a system of ordinary differential equations) written for the reactions in Table 3.1. The equilibrium composition is determined by the equilibrium constants regardless of the reaction rates. The numerical solution of the model is explained in Vasilyev *et al*. (2019).

The $\log(K')$ values (Table 3.1) for the extraction reactions of manganese, zinc, and calcium were obtained by visual fitting of the simulated pH_{50} values against experimentally determined values. The experimental data for the parameter fitting were taken from Publication II, Publication III, and Pakarinen & Paatero (2011) for zinc, manganese, and calcium, respectively. The $\log(K'_{Na})$ was set to −6 to describe weak extraction. The apparent extraction constants in Table 3.1 are usable only for theoretical qualitative estimations with the given equilibrium model. A more sophisticated equilibrium model and parameter-fitting method must be developed for rigorous flowsheet calculations.

Table 3.1 Reactions included in the simplified equilibrium model. HA = D2EHPA.

Reaction equation	log(*K*) or log(*K*´)	Reference
$H^+ + HSO_4^- \rightleftarrows H_2SO_4$	−3.0	Vasilyev *et al*. (2019)
$H^+ + SO_4^{2-} \rightleftarrows HSO_4^-$	1.98	Grenthe *et al*. (1992)
$Ca^{2+} + H^+ + SO_4^{2-} \rightleftarrows CaHSO_4^+$	1.08	Ball & Nordstrom (1991)
$Ca^{2+} + SO_4^{2-} \rightleftarrows CaSO_4$	2.3	Nordstrom *et al*. (1990)
$Ca^{2+} + H_2O \rightleftarrows CaOH^+ + H^+$	−12.78	Nordstrom *et al*. (1990)
$Mn^{2+} + SO_4^{2-} \rightleftarrows MnSO_4$	2.25	Nair & Nancollas (1959)
$Mn^{2+} + H_2O \rightleftarrows MnOH^+ + H^+$	−10.59	Baes & Mesmer (1976)
$Mn^{2+} + 2\,H_2O \rightleftarrows Mn(OH)_2 + 2\,H^+$	−18.54	Wolfram & Krupp (1996)
$Mn^{2+} + 2\,H_2O \rightleftarrows Mn(OH)_2(s) + 2\,H^+$	−15.2	Ball & Nordstrom (1991)
$2\,Mn^{2+} + H_2O \rightleftarrows Mn_2OH^{3+} + H^+$	−10.56	Baes & Mesmer (1976)
$Zn^{2+} + SO_4^{2-} \rightleftarrows ZnSO_4$	2.37	Ball & Nordstrom (1991)
$Zn^{2+} + SO_4^{2-} \rightleftarrows ZnSO_4(s)$	−3.01	Ball & Nordstrom (1991)
$Zn^{2+} + 2\,SO_4^{2-} \rightleftarrows Zn(SO_4)_2^{2-}$	3.28	Ball & Nordstrom (1991)
$Zn^{2+} + 3\,SO_4^{2-} \rightleftarrows Zn(SO_4)_3^{4-}$	1.7	Puigdomenech (2009)
$Zn^{2+} + 4\,SO_4^{2-} \rightleftarrows Zn(SO_4)_4^{6-}$	1.7	Puigdomenech (2009)
$Zn^{2+} + H_2O \rightleftarrows Zn(OH)^+ + H^+$	−7.5	Y. Zhang & Muhammed (2001)
$2\,Zn^{2+} + H_2O \rightleftarrows Zn_2(OH)^{3+} + H^+$	−9	Y. Zhang & Muhammed (2001)
$Zn^{2+} + 2\,H_2O \rightleftarrows Zn(OH)_2 + 2\,H^+$	−16.4	Y. Zhang & Muhammed (2001)
$Zn^{2+} + 2\,H_2O \rightleftarrows Zn(OH)_2(s) + 2\,H^+$	−12.45	Ball & Nordstrom (1991)
$Na^+ + SO_4^{2-} \rightleftarrows NaSO_4^-$	0.7	Nordstrom *et al*. (1990)
$Na^+ + H_2O \rightleftarrows NaOH + H^+$	−14.18	Baes & Mesmer (1976)
$H^+ + OH^- \rightleftarrows H_2O$	14.00	Nordstrom *et al*. (1990)
$2\,\overline{HA} \rightleftarrows (\overline{HA})_2$	4.42	Huang & Juang (1986)
$Na^+ + \overline{HA} \rightleftarrows \overline{NaA} + H^+$	$\log(K'_{Na}) = -6$	–
$Zn^{2+} + 2\,\overline{HA} \rightleftarrows \overline{ZnA_2} + 2\,H^+$	$\log(K'_{Zn}) = 4.2$	–
$Mn^{2+} + 2\,\overline{HA} \rightleftarrows \overline{MnA_2} + 2\,H^+$	$\log(K'_{Mn}) = 1.9$	–
$Ca^{2+} + 2\,\overline{HA} \rightleftarrows \overline{CaA_2} + 2\,H^+$	$\log(K'_{Ca}) = 2.5$	–

4 Results and discussion

4.1 Extraction of arsenic from concentrated sulfuric acid

Arsenic-contaminated H_2SO_4 solutions are produced in large quantities as by-products during the pyrometallurgical processing of sulfide minerals that contain various impurities, including arsenic. In copper refineries, arsenic is volatilized during ore smelting. Then, it ends up in electrostatic precipitator dust and into the H_2SO_4 solutions that circulate in wet gas scrubbers (Dalewski, 1999; Piret, 1999; Szymanowski, 1998). However, pyrometallurgical treatments do not completely remove the arsenic and other impurities. Eventually, the impurities end up in cast copper anodes. During electrolytic purification of copper, arsenic dissolves in the H_2SO_4 electrolyte from the anodes with other impurities. The impurities decrease the quality of the product cathodes and lower the efficiency of the electrorefining cell. Furthermore, poisonous arsine gas, AsH_3, may form if the levels of arsenic get sufficiently high in the electrolyte (Szymanowski, 1998). Removal of the arsenic enables safer usage of the technical H_2SO_4 solutions in, for instance, leaching or pH adjustment. Furthermore, high purity arsenic trioxide, As_2O_3, is an essential compound for the semiconductor industry, and it can be used as a cementation reagent in zinc refining for removing cobalt. Despite having target applications, As_2O_3 is needed only in small quantities. Therefore, it is mostly considered an impurity without significant value.

Arsenic(V) can be extracted from H_2SO_4 solutions by solvating neutral organophosphorus compounds (NOPCs), such as TBP. NOPCs extract only arsenic(V) in significant amounts (Giganov *et al.*, 1978; Totsuka *et al.*, 1986), whereas alcohols and glycols also extract arsenic(III) (Baradel *et al.*, 1986a, 1986b, 1988; Baradel & Guerriero, 1988; Szymanowski, 1998). The extractants available for the solvent extraction of arsenic are discussed in Publication I.

Travkin *et al.* (1993) have described the extraction of arsenic acid by solvating organophosphorus extractants by

$$n\mathrm{H_3AsO_4} + w\mathrm{H_2O} + q\bar{\mathrm{S}} \rightleftarrows n\overline{\mathrm{H_3AsO_4 \cdot wH_2O \cdot qS}}, \qquad (4.1)$$

where S denotes an extractant molecule, and n, w, and q are stoichiometric coefficients that vary depending on the reaction conditions and the extractant. H_2SO_4 is co-extracted to the organic phase together with arsenic; an equation similar to Equation (4.1) can also be written for the extraction of H_2SO_4. Alternatively, the extracted species can be considered multiacid adducts, such as $S_q(H_3AsO_4)_n(H_2SO_4)_p(H_2O)_w$ (Demirkiran *et al.*, 2002). Increasing H_2SO_4 concentration in the feed enhances the extraction of arsenic (de Lourdes Ballinas *et al.*, 2003; Demirkiran *et al.*, 2002; Demirkiran & Rice, 2002; Iberhan & Wiśniewski, 2002; Iberhan & Wiśniewski, 2003; Navarro & Alguacil, 1996; Szymanowski, 1998; Totsuka *et al.*, 1986; Travkin *et al.*, 1993, 2001; Wiśniewski, 1997; Wiśniewski, 1998) but the co-extraction of H_2SO_4 is also increased. Co-extraction of

H_2SO_4 and water causes expansion of the organic phase and simultaneous shrinkage of the aqueous phase (*i.e.*, the volumetric phase ratio changes during extraction). The change in phase ratio is negligible in extractions with 2–3 M H_2SO_4 solutions because the absolute amounts of co-extracted H_2SO_4 and water are relatively low. Another challenge arising from a very high concentration of H_2SO_4 is third-phase formation, which will occur if TBP is used with an aliphatic diluent. Splitting of the organic phase in two layers makes phase separation in typical SX contactors (Figure 1.3) difficult, and the use of aromatic solvents is discouraged due to their hazardousness.

4.1.1 Compositions of studied sulfuric acid solutions

Two batches of arsenic-bearing concentrated H_2SO_4 solutions (Table 4.1) were received from an industrial plant for the solvent extraction experiments. Theoretical speciation analysis (Publication I, Figure 2) suggests that the arsenic is in the form of undissociated arsenic acid, H_3AsO_4 in such solutions (*i.e.*, at E_h = +0.71 V and $\log([H^+]_{tot}) = 1.3$). The experimental and analytical procedures are given in Publication I.

Table 4.1 Compositions of H_2SO_4 solutions used in solvent extraction experiments in Publication I.

	Shipment #1	Shipment #2
H_2SO_4 [g L^{-1}]	1020	963
As [g L^{-1}]	23.9	32.5
As^{3+} [%]	9.2	7.1
Ni [g L^{-1}]	2.1	2.6
Cu [mg L^{-1}]	2.5	18.9
Zn [mg L^{-1}]	0.8	< DL
Cd [mg L^{-1}]	< DL	0.1
Sb [mg L^{-1}]	117	187
Hg [mg L^{-1}]	0.7	2.0
Pb [mg L^{-1}]	1.1	2.0
Bi [mg L^{-1}]	4.9	43.3

DL= Detection limit

4.1.2 Extraction of arsenic and sulfuric acid by tributyl phosphate and a mixture of 1,2-octanediol and 2-ethylhexanol

The equilibrium distributions of arsenic and H_2SO_4 were similar in extraction by TBP and a mixture of 6 mass % 1,2-octanediol in 2-ethylhexanol (referred to as the alcohol mixture) (Figure 4.1). The changes in phase densities and volumetric phase ratios are highly significant (Publication I, Figure 8) due to the co-extraction of H_2SO_4 and water. The changes in O/A ratios were considered when the percentages of arsenic and H_2SO_4

extracted (Publication I, Figure 7) were calculated. TBP is slightly more selective for arsenic during loading than the alcohol mixture at initial O/A ≤ 1 (Table 4.2). Additionally, the separation of arsenic and H_2SO_4 by scrubbing is significantly more efficient with loaded TBP than with the alcohol mixture (Publication I, Figure 11).

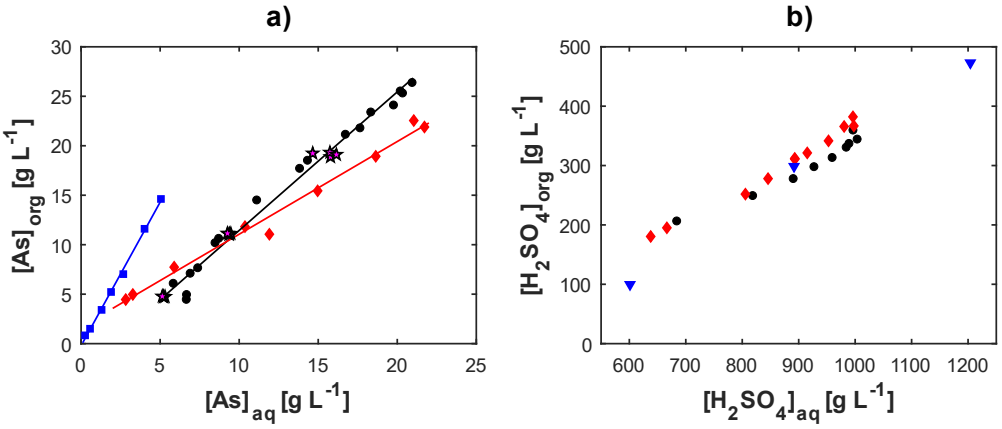

Figure 4.1 Loading isotherms for a) the extraction of arsenic and b) the extraction of H_2SO_4 from a feed solution containing 23.9 g L^{-1} arsenic and 1020 g L^{-1} H_2SO_4. Undiluted TBP (circles), pseudo-countercurrent extraction by undiluted TBP (pentagrams), 6 mass % 1,2-octanediol in 2-ethylhexanol (diamonds), undiluted TBP and 600 g L^{-1} H_2SO_4 in the feed (Navarro & Alguacil, 1996) (squares), and 2-ethylhexanol (Gromov *et al.*, 2018) (triangles).

Table 4.2 Comparison of TBP and the alcohol mixture in extraction of arsenic and H_2SO_4 from feed solution containing 23.9 g L^{-1} arsenic and 1020 g L^{-1} H_2SO_4. T = 21 ± 1 °C, t_{eq} = 20 min.

O/A	Undiluted TBP			6 mass % 1,2-octanediol in 2-ethylhexanol		
	D(As)	D(H_2SO_4)	α(As/H_2SO_4)	D(As)	D(H_2SO_4)	α(As/H_2SO_4)
0.1	1.22	0.34	3.54	1.01	0.37	2.74
0.125	1.27	0.36	3.50	1.07	0.38	2.79
0.25	1.24	0.34	3.68	1.02	0.37	2.72
0.5	1.28	0.33	3.92	1.03	0.36	2.88
0.8	1.31	0.32	4.07	0.93	0.35	2.64
1	1.22	0.31	3.92	1.14	0.35	3.26
2	1.04	0.30	3.41	1.31	0.31	4.20
3.5	0.74	0.30	2.46	1.52	0.29	5.19

4.1.3 Estimation of the required number of countercurrent extraction stages by the McCabe–Thiele method

McCabe–Thiele analysis with linear operating lines has been previously used to evaluate the required number of extraction stages for separating arsenic and H_2SO_4 from dilute to moderately concentrated H_2SO_4 solutions (Demirkiran & Rice, 2002; Navarro & Alguacil, 1996; Wiśniewski, 1998). With concentrated H_2SO_4 the change in the volumetric phase ratio is significant (Publication I, Figure 8); this must be considered in the construction of the operating line. Terminal points, ($[As]_{aq,out}$,$[As]_{org,in}$) and ($[As]_{aq,in}$,$[As]_{org,out}$), of the adjusted operating line can be calculated from the target set for fraction extracted when the feed concentrations, initial phase ratio, and equilibrium phase ratio are known. Concentrations in the extract and raffinate are given by

$$[\mathrm{As}]_{\mathrm{eq,org}} = \frac{f_E [\mathrm{As}]_{0,\mathrm{aq}} V_{0,\mathrm{aq}}}{V_{\mathrm{eq,org}}} + [\mathrm{As}]_{0,\mathrm{org}} \tag{4.2}$$

$$[\mathrm{As}]_{\mathrm{eq,aq}} = \frac{(1 - f_E)[\mathrm{As}]_{0,\mathrm{aq}} V_{0,\mathrm{aq}}}{V_{\mathrm{eq,aq}}}, \tag{4.3}$$

where f_E is the fraction of arsenic extracted from the aqueous phase, V_0 denotes the initial volume, and V_{eq} denotes the volume at equilibrium. Equations (4.2 and 4.3) assume mass transfer from the aqueous phase to the organic phase. $V_{eq,org}$ and $V_{eq,aq}$ are calculated from the phase ratio in equilibrium, which can be estimated from the initial phase ratio by using the polynomial fit given in Publication I, Figure 8.

4.1.4 Comparison of McCabe–Thiele predictions against experimental results

The McCabe–Thiele analysis with constant phase ratio (E/R = S/F = 0.79) indicates that seven extraction stages are required to extract 83.7 % arsenic (Figure 4.2 a). However, according to the pseudo-countercurrent experiments (see Chapter 3.3), 83.7 % arsenic was already extracted in three countercurrent extraction stages (Figure 4.2 b). The concentration of arsenic is not lowered by 83.7 % due to the change in phase ratio. Although the approach explained in Chapter 4.1.3 fails to describe the curvature in the operating line, the McCabe–Thiele prediction was improved by constructing the operating line using Equations (4.2 & 4.3) (Figure 4.2). Note that the slope of the operating line in Figure 4.2 b is not equal to F/S or R/E.

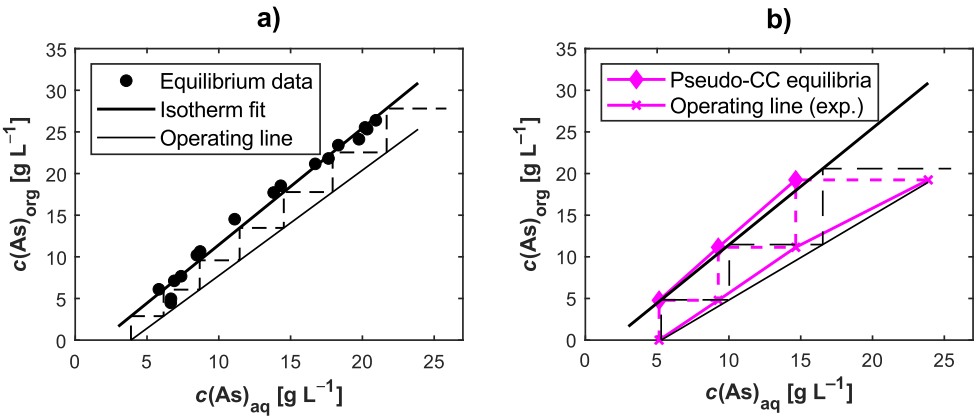

Figure 4.2 Prediction of countercurrent extraction of arsenic by the McCabe–Thiele method. a) Volumetric phase ratio is assumed to be constant (S/F = E/R = 0.79); b) Comparison of experimental distributions with the McCabe–Thiele analysis where the change in volumetric O/A ratio from S/F = 0.79 to E/R = 1.43 is considered. Operating line equations: a) $c(\mathrm{As})_{org} = 1.266 \cdot c(\mathrm{As})_{aq} - 4.915$, b) $1.019 \cdot c(\mathrm{As})_{aq} - 5.383$.

Aside from changes in phase ratios, the speciation of arsenic and H_2SO_4 change during the back-extraction (Publication I, Figure 10). H_3AsO_4 ($pK_{a,1} = 2.26$) (Rumble, 2021) starts to dissociate into H^+ and $H_2AsO_4^-$ when the total concentration of protons is low enough. $H_2AsO_4^-$ has much higher affinity for the aqueous phase and this explains why D(As) is so dependent on the concentration of H_2SO_4 in the system. Additionally, it is well known that the McCabe–Thiele method cannot be applied when speciation changes affect the distribution ratios. This is also seen in Figure 4.3, as the stripping of arsenic cannot be described by a single isotherm. The stripping raffinate from the pseudo-countercurrent experiments contained 40.1 g L^{-1} arsenic, whereas the maximum $[As]_{aq}$ was 27.9 g L^{-1} in the conventional batch stripping experiments.

In this case, process design can only be accurately done through experimental methods or numerical simulations. Mechanistic description of the H_3AsO_4–H_2SO_4–H_2O–TBP system is challenging because the extraction reactions and their equilibrium constants are not precisely known. The amount of co-extracted water in TBP varies with the concentration of H_2SO_4 in the organic phase (Hesford & McKay, 1960). Here, the mass-balance calculations indicated a 1:2:1 ratio of H_2SO_4:H_2O:TBP in the loaded organic phase, when $c(H_2SO_4)_{org}$ was 200–300 g L^{-1}. When $c(H_2SO_4)_{org}$ decreased below 15 g L^{-1} in stripping, the stoichiometric ratio H_2O:TBP was 7:1. More equilibrium data with analytically determined $c(H_2O)_{org}$ are required to develop accurate stoichiometric descriptions for a mechanistic model. Any *ad hoc* parametric descriptions would also require a large amount of experimental data to cover the full concentration domains. Therefore, the experimental pseudo-countercurrent method is valuable in the development of SX processes for concentrated acid solutions. Equilibrium data are

accurately and conveniently simultaneously obtained when the number of extraction stages is evaluated by the pseudo-cc method. Besides being useful in evaluation of the countercurrent cascades, the pseudo-cc results are also useful in the development of simulation tools. If the flowsheet simulations assume ideal extraction stages, the equilibria from pseudo-cc experiments are likely the best reference data for validating the simulations.

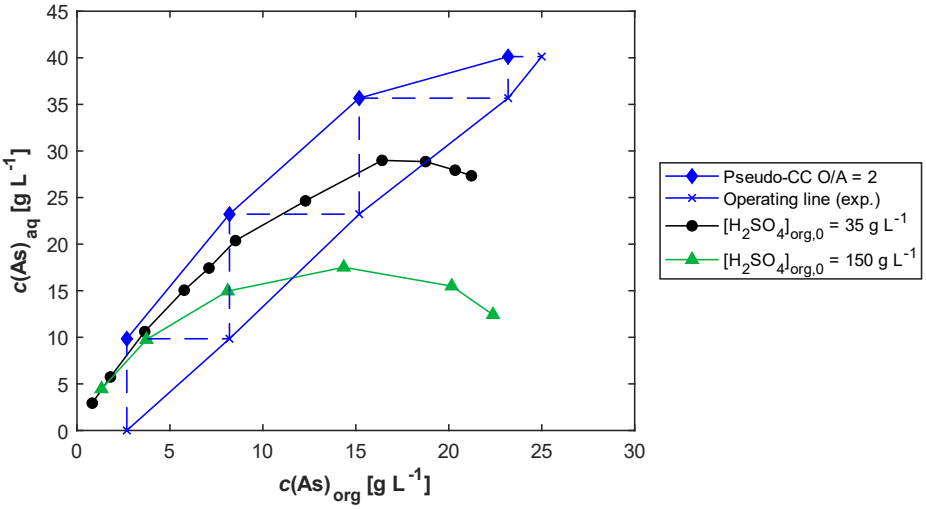

Figure 4.3 McCabe–Thiele plot from four-stage pseudo-countercurrent stripping experiments and influence of the initial H_2SO_4 concentration in loaded TBP on distribution of arsenic in stripping of loaded TBP.

4.2 Purification of concentrated manganese sulfate solution

Manganese and zinc are widely used elements in the metallurgical industry. Most manganese is used in steelmaking (Matricardi & Downing, 1995), but it is also a key element in the production of Ni–Co–Mn (NCM) cathode-active materials for LIBs. Zinc is also used in battery manufacturing, although its primary uses are in corrosion protection, manufacturing of die castings, and the production of brass (Brodd, 1992; Goodwin, 1998). Anode sludges from zinc electrowinning (ZnEW) usually contain around 40 mass % manganese and 6–10 mass % lead on a dry basis (Ayala & Fernández, 2013; Kauppinen *et al.*, 2020; Zhang *et al.*, 2018). The presence of zinc, calcium, magnesium, sodium, potassium, and strontium in the sludges at lower than 10 mass % total concentration has been reported; there may also be other base metals in small amounts (0.1 % or less each) (Ayala & Fernández, 2013; Kauppinen *et al.*, 2020; Zhang *et al.*, 2018). Aside from formation during ZnEW, manganese-bearing anode sludges are also formed during electrolytic refining of copper and manganese (Wang *et al.*, 2019; Zhang & Cheng, 2007). Because of their significant manganese content, the anode sludges serve as secondary sources of manganese.

Concentrated $MnSO_4$ solutions (Table 4.3) were obtained by leaching ZnEW anode sludge with H_2SO_4 and H_2O_2 as described by Kauppinen *et al*. (2020). These solutions were then used in the solvent extraction studies (Figure 4.4). Concentration of manganese in PLS 1 was near the solubility limit of $MnSO_4$ (4.2 mol $(kg\,H_2O)^{-1}$ (231.6 g L^{-1} manganese) at 25 °C (Söhnel & Novotný, 1985)). The composition of the feed solution in the continuous experiments (PLS 2) was slightly different from PLS 1 due to the scale-up of the reductive leaching and subsequent solid–liquid separation. The leachate used in the continuous experiments (PLS 2) was initially more acidic (pH < 0) than PLS 1. Thus, the PLS 2 was partially neutralized to pH = 1.2. Adjusting the pH of concentrated $MnSO_4$ solutions is restricted, as the addition of alkali metal hydroxides or NH_3 in large quantities may result in the precipitation of manganese hydroxides or Tutton's salt $(C_2Mn(SO_4)_2{\cdot}n(H_2O)$, where C denotes an univalent cation, for example, Na^+, K^+, or NH_4^+ (Montgomery *et al*., 1966).

Table 4.3 Metal concentrations in the first and the second anode sludge leachates, abbreviated as PLS 1 and PLS 2, respectively.

Analysis	**Unit**	**PLS 1**	**PLS 2**
[Mn]	g L^{-1}	**180** ± 11	**161** ± 9
[Na]	g L^{-1}	**–**	**17.7** ± 2
[Mg]	mg L^{-1}	**–**	**215** ± 10
[Al]	mg L^{-1}	**83** ± 29	**63** ± 46
[K]	mg L^{-1}	**4120** ± 168	**3000** ± 281
[Ca]	mg L^{-1}	**291** ± 127	**204** ± 42.9
[Fe]	mg L^{-1}	**37.5** ± 5	**135** ± 12.4
[Zn]	mg L^{-1}	**449** ± 14	**999** ± 41.5
E_h (22 ± 1 °C)	mV	**+800**	**+760**
pH (22 ± 1 °C)	–	**0.6**	**1.2**

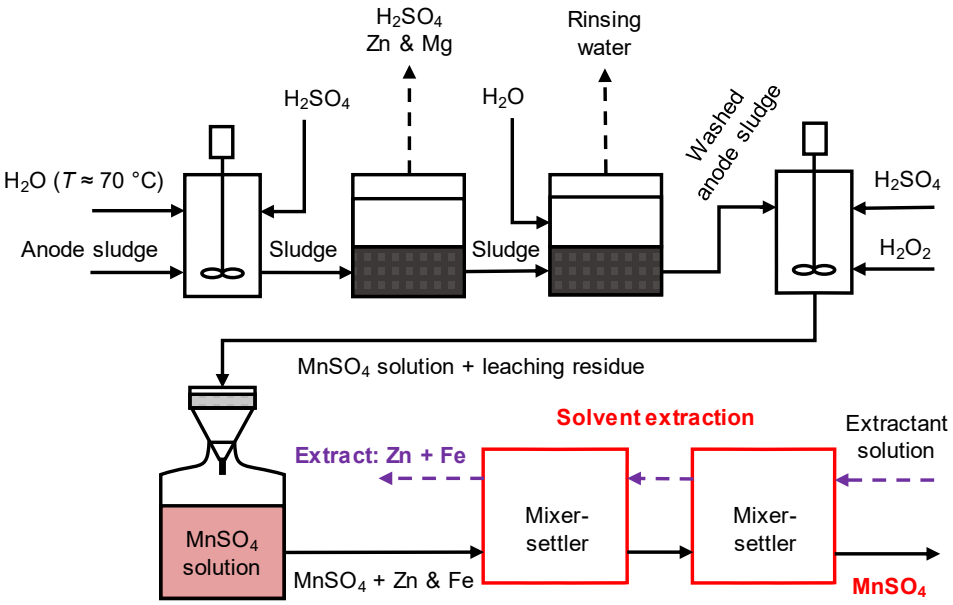

Figure 4.4 Summary of the anode sludge processing steps.

Bis-(2-ethylhexyl) hydrogen phosphate (D2EHPA) and bis-(2,4,4-trimethylpentyl)-phosphinic acid (BTMPPA, CYANEX 272) (diluted in Exxsol D80 aliphatic diluent) were used to study the extraction of impurity metals (in this chapter, metals other than manganese) from the leachate. A detailed discussion on different extractants and their characteristics is given in Publication II. D2EHPA and BTMPPA mainly extract the metal ions as chelates or organometallic self-adducts. Considering that these extractants exist mostly as dimers in aliphatic diluents (Marcus & Kertes, 1969), the extraction reactions are formally described by

$$\mathrm{M}^{z+} + \frac{z+b}{2}\overline{(\mathrm{HA})_2} \rightleftarrows \overline{\mathrm{MA}_z(\mathrm{HA})_b} + z\mathrm{H}^+. \qquad (4.4)$$

Usually, aluminium, calcium, iron and zinc are extracted by D2EHPA at a lower pH than manganese (Cheng, 2000; Lee *et al.*, 2010; Mohapatra *et al.*, 2007; Pakarinen & Paatero, 2011; Pereira *et al.*, 2007; Principe & Demopoulos, 2004). BTMPPA also extracts aluminium, iron, and zinc ahead of manganese (Flett, 2005; Mohapatra *et al.*, 2007; Pakarinen & Paatero, 2011), but the extraction of calcium is negligible at pH values below 5; BTMPPA extracts manganese ahead of calcium (Pakarinen & Paatero, 2011).

4.2.1 Effect of pH and extractant concentration on extraction of iron, zinc, and manganese

Iron and zinc were efficiently removed from the concentrated $MnSO_4$ leachate (Figure 4.5) at pH 3.0 and above. As a more acidic reagent, D2EHPA can extract the metals at lower pH values than BTMPPA (Pakarinen & Paatero, 2011). Over 80 % of the iron was extracted by 0.2 M D2EHPA at pH 0.8, whereas, with 0.2 M BTMPPA pH > 1.5 was required. The interpolated pH_{50} values of zinc extraction were 1.48 and 2.12 for 0.2 M D2EHPA and 0.2 M BTMPPA, respectively. The effect of pH on the extraction of zinc (Figure 4.5) was qualitatively similar to earlier results published in the literature (Biswas *et al*., 2016; Chen *et al*., 2018b; Cheng, 2000; Innocenzi & Veglio, 2012; Pereira *et al*., 2007; Salgado *et al*., 2003). An increase in extractant concentration decreased the pH required to achieve a specific percentage of extraction (Figure 4.5), which is in qualitative agreement with Equation (2.25) as well as the results from Pereira *et al*. (2007). Extraction of manganese by 0.8 M BTMPPA was 1.9–5.8 % and, by 0.8 M D2EHPA, 3.3–11.4 % as determined from the raffinate phase concentrations (Figure 4.5). The concentration of aluminium in the organic samples throughout this study was below 20 mg L^{-1}, meaning that aluminium was only weakly extracted (E(Al) < 30 %) by both extractants.

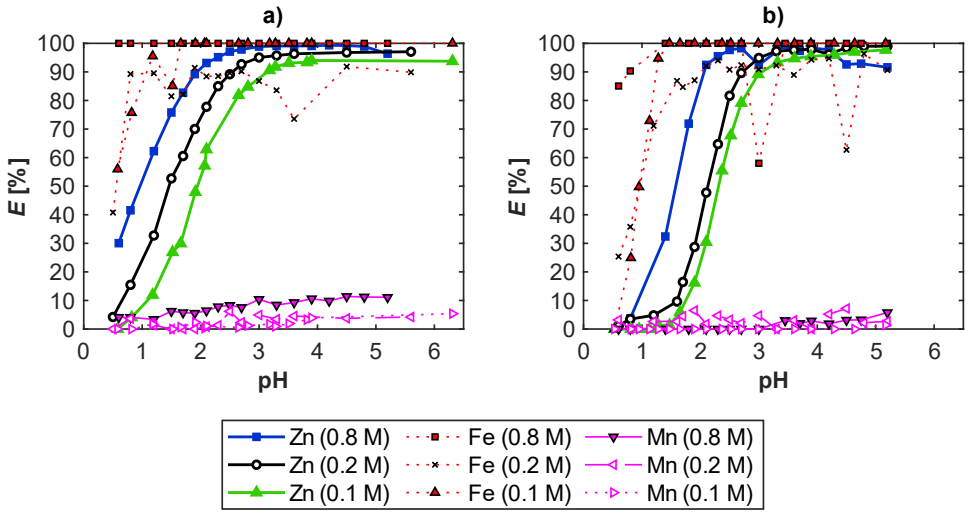

Figure 4.5 Effect of pH on extraction of zinc, iron, and manganese from the anode sludge leachate. a) D2EHPA; and b) BTMPPA. Concentration of the extractant is given in brackets. T = 25 ± 1 °C, t_{eq} = 15 min, O/A = 1. $[Zn]_0$ = 450 mg L^{-1}, $[Fe]_0$ = 40 mg L^{-1}, $[Ca]_0$ = 320–350 mg L^{-1}, and $[Mn]_0$ = 180 g L^{-1}.

4.2.2 Extraction of calcium

The extraction of calcium by both BTMPPA and D2EHPA was negligible between pH = 0.5 and pH = 6 (Publication II, Figure 4). The calcium levels were below the detection limit (approximately 25 mg L^{-1}) in almost all the organic samples from the determination of the loading isotherms (Publication II, Figure 5). Extractions with 0.2 M extractant solutions were repeated at 15 °C because Pakarinen & Paatero (2011) reported an increase in the extraction of calcium with decreasing temperature. Here, the decrease in temperature from 25 °C to 15 °C did not have a significant effect on the extraction of the metals, including calcium (Publication II, Figure 4). Calcium rejection by D2EHPA is an anomalous observation when compared against earlier extraction studies where significant amounts of calcium were extracted (Cheng, 2000; Haghighi *et al.*, 2015; Pakarinen & Paatero, 2011). Theoretical equilibrium calculations show decreasing calcium extraction with an increasing Mn:Ca ratio in the aqueous feed solution (Figure 4.6). The equilibrium model and fitting of the apparent extraction constants are explained in Chapter 3.4. The included reactions and their equilibrium constants are listed in Table 3.1. Sensitivity analysis of the log(K'_{Ca}) value (Figure 4.7) showed that the extraction of calcium was incomplete, even if the log(K'_{Ca}) value was higher than the value obtained by fitting (Table 3.1).

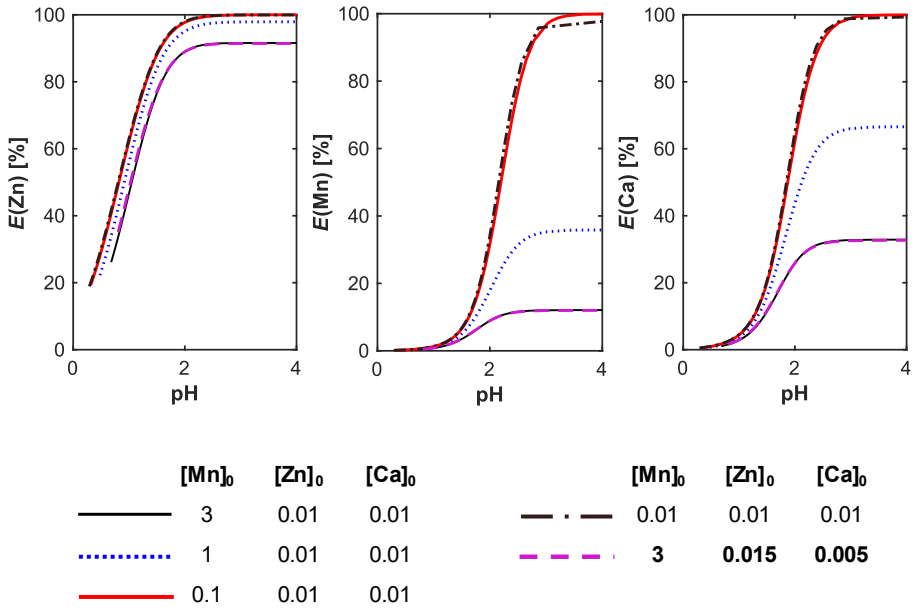

Figure 4.6 Effect of feed solution composition on the extraction of zinc, manganese, and calcium from sulfate media by 0.75 M D2EHPA as predicted by theoretical equilibrium calculations. The simulated extraction curves for the anode sludge leachate are marked with a dashed line. Concentrations given in [mol L^{-1}]. $[H_2SO_4]_0$ = 0.5 mol L^{-1}.

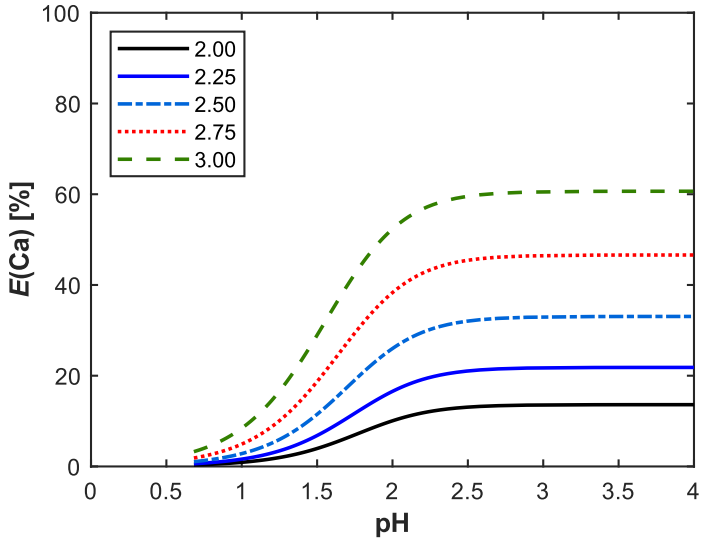

Figure 4.7 Effect of log(K'_{Ca}) value on simulated pH isotherms describing the extraction of calcium by 0.75 M D2EHPA. $[Mn]_0$ = 3 mol L^{-1}; $[Zn]_0$ = 5 mmol L^{-1}; $[Ca]_0$ = 5 mmol L^{-1}; $[H_2SO_4]_0$ = 0.5 mol L^{-1}.

4.2.3 Zn/Mn and Fe/Mn selectivity of the extractants

Selectivities of zinc and iron over manganese were evaluated by comparing the formal mole fraction of manganese in the organic phase as defined by

$$f^*_{\mathrm{Mn,org}} = \frac{[\mathrm{Mn}]_{\mathrm{org}}}{[\mathrm{M}]_{\mathrm{org,tot}}} \cong \frac{[\mathrm{Mn}]_{\mathrm{org}}}{[\mathrm{Fe}]_{\mathrm{org}} + [\mathrm{Zn}]_{\mathrm{org}} + [\mathrm{Mn}]_{\mathrm{org}}}, \quad (4.5)$$

where $f^*_{\mathrm{Mn,org}}$ is the mole fraction of manganese in the organic phase with respect to the total concentration of metals in the organic phase and $[M]_{org,tot}$ is the total concentration of metals in the organic phase [mol L^{-1}]. The total concentration of metals in the organic phase was approximated as the sum of $[Fe]_{org}$, $[Zn]_{org}$, and $[Mn]_{org}$ because the concentrations of other metals in the organic samples were negligible with respect to $[Fe]_{org}$, $[Zn]_{org}$, and $[Mn]_{org}$. Equation (4.5) was used for the selectivity comparisons because, in this case, [Fe] in the aqueous phase was lowered below the detection limit and distribution coefficients or separation factors could not be calculated for iron.

BTMPPA had higher selectivity towards zinc and iron than D2EHPA (Figure 4.8). The fraction of manganese in the organic phase decreased with both extractants when the number of available extractant ligands decreased (Figure 4.8 a, c) regardless of the pH or temperature used in the experiment. The lowest $f^*_{\mathrm{Mn,org}}$ was 28.9 mol % for crowded D2EHPA at a 0.2 M extractant concentration and pH 2.7, whereas, with crowded 0.2 M BTMPPA the $f^*_{\mathrm{Mn,org}}$ was 10.0 mol %. The effect of pH on selectivity was more

pronounced with D2EHPA than with BTMPPA (Figure 4.8). Crowding of 0.8 M D2EHPA at pH 3.0 lowered the $f^*_{Mn,org}$ to 35 mol %, but, at pH 1.7, the $f^*_{Mn,org}$ in the loaded D2EHPA did not decrease below 65 mol %. On the other hand, $f^*_{Mn,org}$ in the crowded 0.8 M BTMPPA lowered below 10 mol % at pH 1.7. Co-extraction of manganese can thus be limited by crowding the extractants (Figure 4.8 b, d).

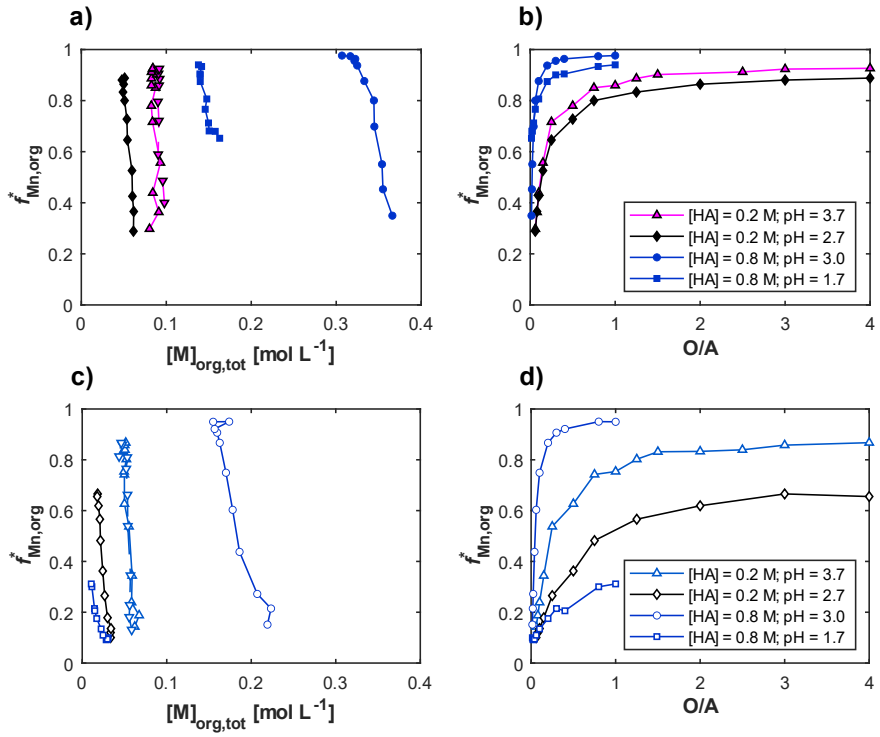

Figure 4.8 Selectivity of the extractants under different conditions. a) Effect of metal loading on the fraction of manganese in D2EHPA; b) Effect of volumetric phase ratio on the fraction of manganese in D2EHPA; c) Effect of metal loading on the fraction of manganese in BTMPPA; d) Effect of volumetric phase ratio on the fraction of manganese in BTMPPA. T = 25 ± 1 °C. $[Zn]_0$ = 450 mg L^{-1}, $[Fe]_0$ = 40 mg L^{-1}, $[Ca]_0$ = 320–350 mg L^{-1} and $[Mn]_0$ = 180 g L^{-1}. HA denotes the extractant and $f^*_{Mn,org}$ is defined in Equation (4.5).

4.2.4 Separation of co-extracted manganese from zinc and iron during backextraction

The co-extracted manganese was recovered at 99.5–99.8 mass % relative purity by stripping the loaded 0.8 M extractants with 0.5 M H_2SO_4 at high O/A ratios (Figure 4.9). Stripping recoveries of manganese at P_R(Mn) > 99.5 mass % were 55.7 % and 71.5 % from D2EHPA and BTMPPA, respectively. The manganese-rich fractions of the stripping

raffinates contained 29.4–33.9 g L^{-1} manganese, 13–16 mg L^{-1} aluminium, 1.5–5.2 mg L^{-1} zinc, and < 1 mg L^{-1} iron. Increasing the amount of stripping acid (*i.e.*, lowering O/A and/or increasing the concentration of H_2SO_4) lowers the pH so that zinc and iron are also stripped according to the pH isotherms (Figure 4.5). Thus, in stripping, the relative purity of manganese was lowered with decreasing O/A.

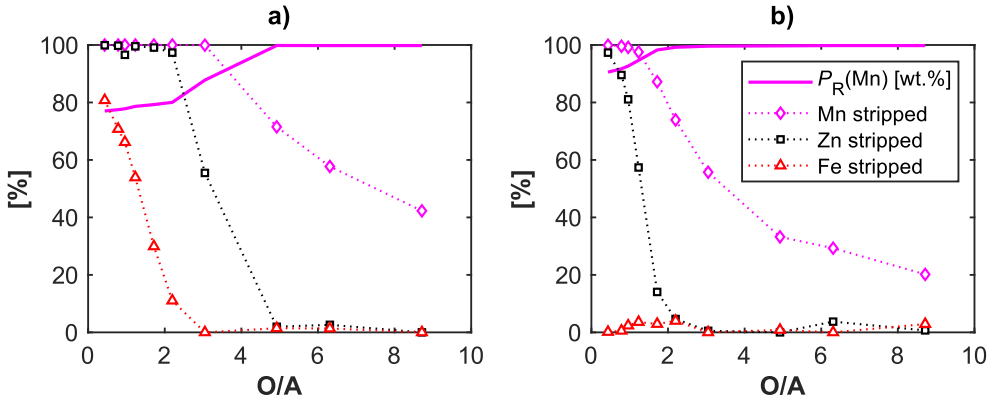

Figure 4.9 Effect of phase ratio on stripping of manganese, zinc, and iron from a) loaded 0.8 M BTMPPA and b) loaded 0.8 M D2EHPA at 25 ± 1 °C with 0.5 M H_2SO_4. Initial metal loadings: $[Mn]_{BTMPPA}$ = 8.2 g L^{-1}, $[Zn]_{BTMPPA}$ = 1.09 g L^{-1}, $[Fe]_{BTMPPA}$ = 79.9 mg L^{-1}; $[Mn]_{D2EHPA}$ = 16.8 g L^{-1}, $[Zn]_{D2EHPA}$ = 1.09 g L^{-1}, and $[Fe]_{D2EHPA}$ = 76.4 mg L^{-1}.

4.2.5 Characteristics of the continuous countercurrent process

Only zinc, iron, and manganese were extracted in significant amounts from the anode sludge leachate. Because iron is extracted at the lowest pH and the leachate (Table 4.3) contains significantly less iron than zinc, adjustment of the process parameters for efficient zinc removal will provide simultaneous removal of both zinc and iron. Two continuous countercurrent extraction stages operating at ambient temperature, pH = 3, S/F = 0.43, and 0.8 M extractant concentration yielded a raffinate with less than 10 mg L^{-1} zinc (Figure 4.10), as predicted by the top-to-bottom-type McCabe–Thiele analysis (Figure 4.11). However, the measured stagewise concentrations differed from those predicted. Interpolation or extrapolation of steep equilibrium curves can easily result in relatively large errors. Although the performance of 0.8 M D2EHPA is summarized in Figure 4.10, BTMPPA also removed similar amounts of zinc and iron from the leachate (Publication II, Chapter 3.3).

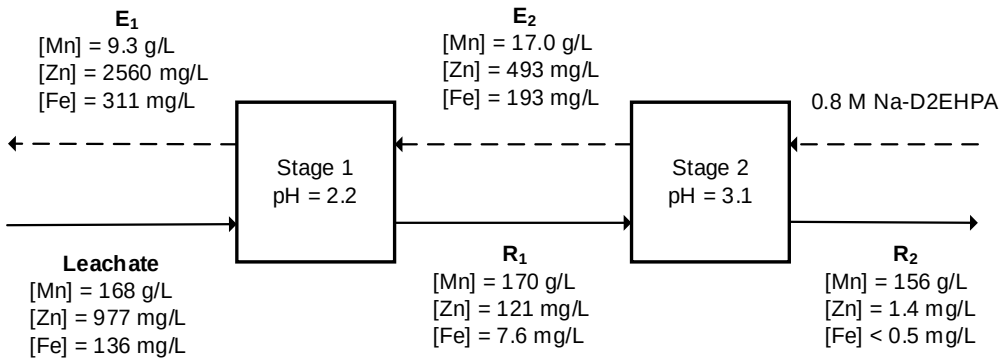

Figure 4.10 The solution compositions in two-stage countercurrent extraction of zinc and iron from concentrated $MnSO_4$ solution by 0.8 M Na-D2EHPA. S/F = 0.43; τ_{mix} = 6 min; T = 22 ± 1 °C. Pre-neutralization: 100 mL 5 M NaOH in one liter of 0.8 M D2EHPA (64.2 % saponification).

Increasing the mean residence time in the mixer (τ_{mix}) from 3.6 min to 6 min improved the separation with BTMPPA but the change in τ_{mix} had marginal—if any—effect on the extraction by D2EHPA (Publication II, Table 3). High extraction of zinc and iron is typical for both BTMPPA and D2EHPA; the fraction of zinc extracted here is similar to that obtained by Pereira *et al*. (2007) with 20 % D2EHPA in three extraction stages at S/F = 1, pH = 2.5, and T = 28 ± 1 °C. However, Pereira *et al*. (2007) reported a decrease of [Fe] from 241 mg L^{-1} to 116 mg L^{-1}, whereas, here, [Fe] lowered from 135 mg L^{-1} to below 2 mg L^{-1}. The average concentrations given in Figure 4.10 do not completely align with the mass balance; the errors can be explained by deviations in the ICP-MS analyses (Table 4.3), precipitation of the metals, and fluctuation in the feed flowrates. The zinc- and iron-barren raffinate is suggested for the co-precipitation synthesis of NCM cathode precursors (Publication II).

Although no solids were observed in the extracts or raffinates, precipitation and gelation were observed in the settlers. The precipitates were likely manganese and iron hydroxides, but the precipitation of Tutton's salts is also possible. A stoichiometric excess of extractant with respect to the amount of zinc and iron is recommended to enable the extraction at the lowest possible pH, possibly avoiding precipitation. Increasing the amount of active extractant will increase the co-extraction of manganese. However, avoiding precipitation is more important because the co-extracted manganese can be recovered selectively by stripping (Figure 4.9). The estimated loss of manganese to the impure stripping fractions due to co-extraction was 0.1–0.3 % for BTMPPA and 1.2–2.1 % for D2EHPA (28.5 % and 44.3 % of the loaded manganese, respectively) (Publication II, Table 3). Zinc and manganese are completely stripped from the loaded extractants by an adequate amount of acid (*e.g.*, H_2SO_4 or HCl). Complete stripping of iron from D2EHPA requires 5 N HCl, whereas iron is more effectively stripped by H_2SO_4 (8–10 N) from BTMPPA (Sandhibigraha *et al*., 2000).

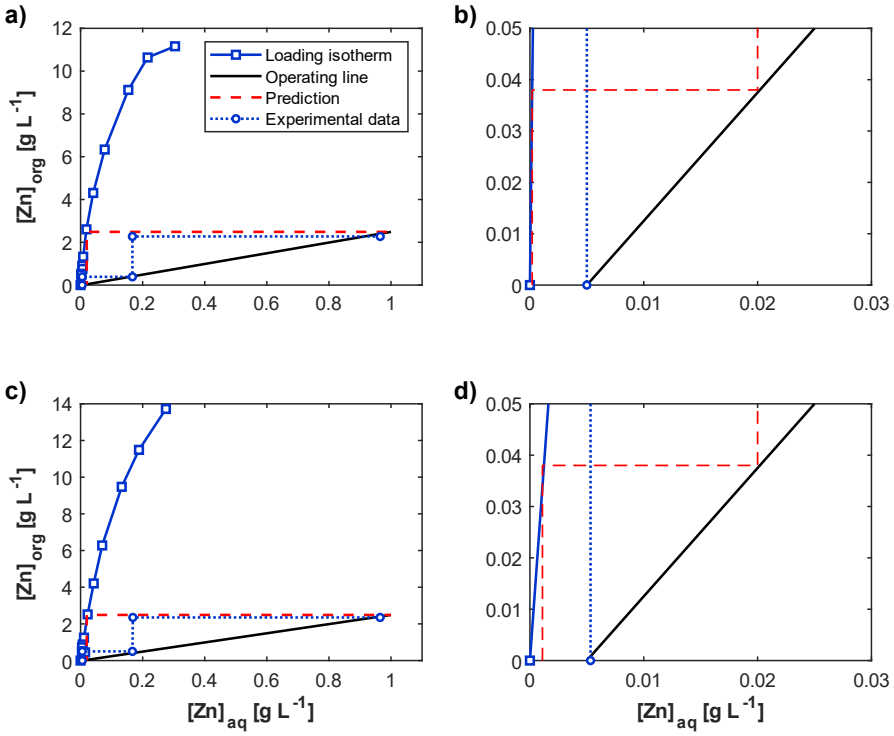

Figure 4.11 McCabe–Thiele analysis of the countercurrent extraction of zinc at pH = 3.0 by a) & b) 0.8 M BTMPPA and c) & d) 0.8 M D2EHPA from the anode sludge leachate in comparison with the experimental results. The loading isotherms for zinc were determined using anode sludge leachate with $[Zn]_0$ = 450 mg L^{-1}, $[Fe]_0$ = 40 mg L^{-1}, $[Ca]_0$ = 320–350 mg L^{-1}, and $[Mn]_0$ = 180 g L^{-1}. The experimental data was extrapolated to (0,0) (subfigures b & d).

4.3 A solvent extraction flowsheet for producing multi-metal solutions for the synthesis of cathode precursors

Hydrometallurgical recycling of lithium-ion batteries involves the liberation of metals from the spent cathode powders by reductive acid leaching. Many different mineral and carboxylic acids can be used for leaching (Chagnes & Pospiech, 2013; Li *et al.*, 2018; Meshram *et al.*, 2014) but H_2SO_4 with H_2O_2 as a reductant can be recommended due to high leaching recoveries and economical advantage (Chen & Ho, 2018). The LIB leachates contain the key cathode metals (lithium, cobalt, nickel, and manganese) and the presence of aluminium, iron, and copper in small quantities is common (Li *et al.*, 2018; Meshram *et al.*, 2014).

The processing of LIB leachates begins with the removal of impurities (here aluminium, iron, and copper), which can be done by NaOH precipitation (Joo *et al*., 2016), ion exchange (Virolainen *et al*., 2021), or solvent extraction (Nayl *et al*., 2015). The extractive method is recommended because of the potential loss of cobalt during hydroxide precipitation (Peng *et al*., 2020; Suzuki *et al*., 2012). Additionally, part of the manganese may be lost together with the impurity metals during ion exchange (Virolainen *et al*., 2021).

Nickel, cobalt, and manganese are extracted to the organic phase by suitable extractants from the impurity-free leachate, while most of the lithium remains in the raffinate. Acidic organophosphorus extractants such as D2EHPA, CYANEX 272 (BTMPPA), and PC88-A (2-ethylhexoxy(2-ethylhexyl)phosphinic acid, also known as 2-ethylhexyl hydrogen 2-ethylhexylphosphonate) are well-known extractants for this kind of metal separation. Manganese can be separated from lithium, cobalt, and nickel by D2EHPA, but the separation of cobalt and nickel by D2EHPA is difficult (Cheng, 2000; Sole, 2018). On the other hand, CYANEX 272 has excellent Co/Ni selectivity, but weak Mn/Co selectivity (Sole, 2018). Chen & Ho (2018) suggested the separation of lithium, nickel, cobalt, and manganese by separate CYANEX 272 and D2EHPA circuits. CYANEX 272 and D2EHPA were selected as the extractants also for the work in Publication III because the overall material efficiency could be improved with the industry-proven extractants by an improved flowsheet.

4.3.1 **Flowsheet**

Solvent extraction processes are often designed to separate metals into their own fractions, from where they can be precipitated or crystallized as pure metal salts, or electrowon (Chen & Ho, 2018; Chen *et al*., 2015a; X. Chen *et al*., 2015b; Liu *et al*., 2020; Suzuki *et al*., 2012; Tanong *et al*., 2017; Virolainen *et al*., 2017; Wang *et al*., 2012). However, a multi-metal solution with specific amounts of nickel, cobalt, and manganese (NCM solution) can also be one product of the solvent extraction process (Liu *et al*., 2021; Shuya *et al*., 2020; Yang *et al*., 2017).

A solvent extraction flowsheet (Figure 4.12) for producing Li_2SO_4, $CoSO_4$, $MnSO_4$, and NCM synthesis mixtures from cobalt-rich LIB leachates was conceptualized based on the separation characteristics of CYANEX 272 and D2EHPA as well as the requirements set by hydroxide co-precipitation synthesis of NCM cathode precursors. The NCM mixture is obtained from the process (Figure 4.12) by stripping a mixed D2EHPA solution that contains nickel, cobalt, and manganese. To produce a multi-metal sulfate mixture for the co-precipitation synthesis of, for example, NCM811, the Ni:Co and Ni:Mn molar ratios in the organic phase must be 8. If one or both of the ratios is higher than 8, the composition in the final NCM mixture can be adjusted to the desired stoichiometric ratio using the concentrated $CoSO_4$ and $MnSO_4$ products from the same process.

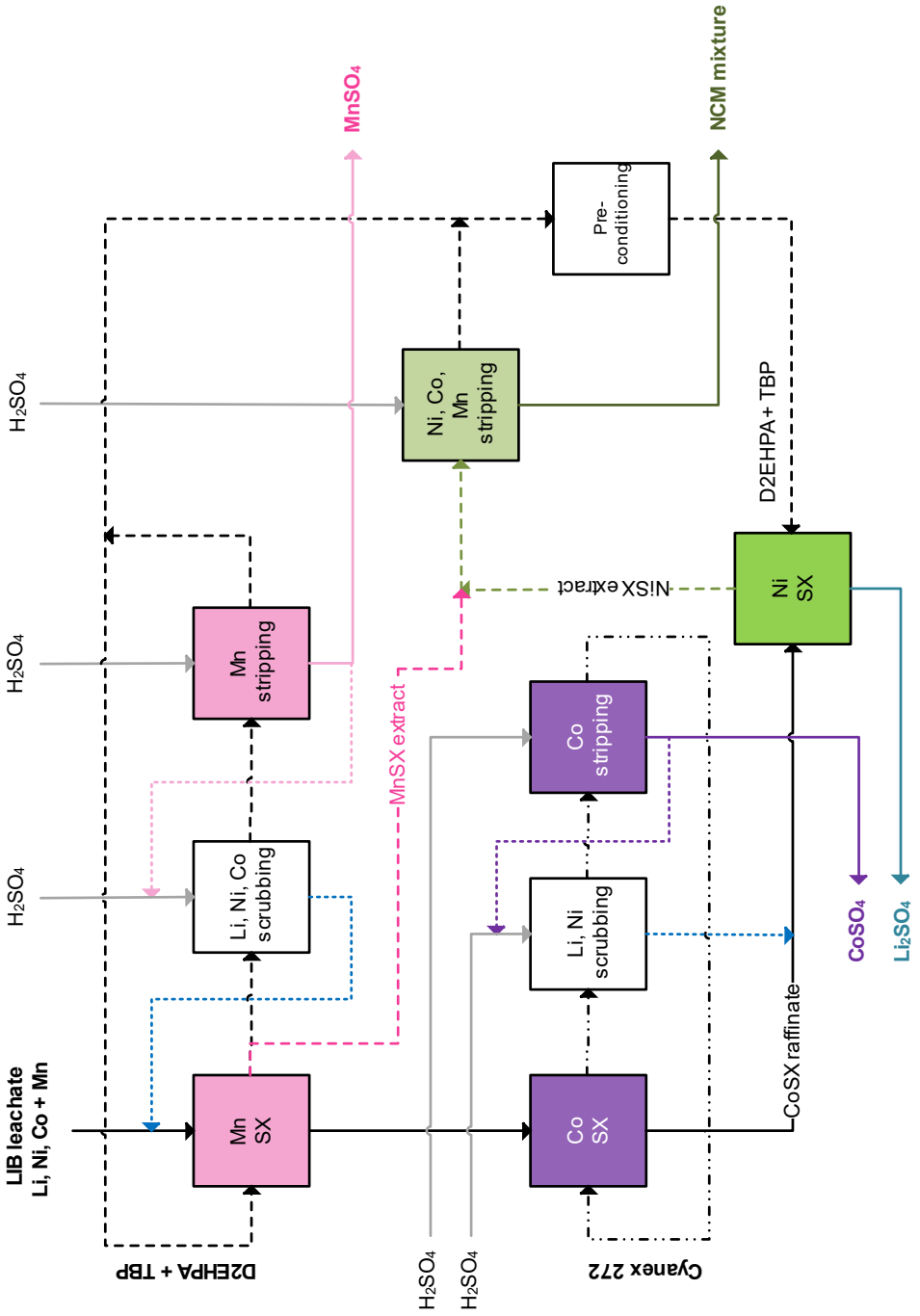

Figure 4.12 A simplified diagram of a solvent extraction process for the processing of lithium-ion battery leachates. The blocks studied in Publication III are coloured.

A loaded D2EHPA solution with suitable amounts of nickel, cobalt, and manganese (NCM-D2EHPA) is obtained by mixing the NiSX extract with an extract bleed from MnSX. Alternatively, the partially loaded D2EHPA from the MnSX circuit could be used to extract nickel. Cobalt can be delivered to the NCM-D2EHPA within the NiSX extract and/or within the MnSX extract bleed because of the co-extraction of cobalt in both MnSX and NiSX. Therefore, the CoSX raffinate does not need to be completely free from cobalt. A simulated leachate with 2.5 g L^{-1} lithium, 2.0 g L^{-1} nickel, 16.8 g L^{-1} cobalt, 2.1 g L^{-1} manganese, and 15 g L^{-1} H_2SO_4 was used in the solvent extraction experiments. The leachate composition was taken from Porvali *et al*. (2019) and the experimental methods are explained in Publication III.

4.3.2 Effect of pH on extraction of manganese, cobalt, nickel, and lithium

The pH_{50} values in extraction by 0.8 M D2EHPA (5 vol% TBP) were approximately 2.0 for manganese, 4.0 for cobalt, and 4.7 for nickel as determined by graphical interpolation (Figure 4.13 a). The pH_{50} values are similar to those given by Sole (2018). Figure 4.13 shows that complete extraction of manganese cannot be achieved by a single extraction stage without significant co-extraction of the other metals. The extraction of sodium is shown in Figure 4.13 because Na^+ ions were introduced to the extraction system due to pH adjustment by NaOH. The extraction of nickel, lithium, and sodium occurred at a significantly lower pH when the leachate did not contain manganese and cobalt (Figure 4.13 b). Extraction of nickel was 91.2 % from the manganese- and cobalt-free leachate at pH = 4.85 but further increases in pH had a limited effect in increasing the extraction of nickel and lithium (Figure 4.13 b).

The pH_{50} values in extraction by 0.8 M CYANEX 272 were 3.8 for manganese and 4.4 for cobalt (Figure 4.14). The pH isotherm for cobalt is quite similar to the pH isotherm reported by Virolainen *et al*. (2017) for 1 M CYANEX 272; the minor differences are explained by different extractant concentrations. The extraction of nickel, lithium, and sodium by 0.8 M CYANEX 272 was weak over the studied pH range (0.8–6.4) at O/A = 1. Also, the extraction of cobalt was incomplete (Figure 4.14 a). Cobalt loading in the loaded 0.8 M CYANEX 272 was 71.6 % of the theoretical extractant capacity at pH = 6.4 and a further increase in pH resulted in gelation of the cobalt-loaded organic phase. Polymerization of the cobalt-loaded BTMPPA results in a rapid increase in viscosity when the loading of cobalt in the organic phase reaches 70–75 % of the theoretical extractant capacity (Xun & Golding, 1987). Therefore, the pH isotherms were also determined at O/A = 2.5 to enable more efficient extraction while maintaining the metal loading below the range in which the rapid viscosity increase takes place. More than 99 % of the nickel was extracted at pH ≥ 7 and O/A = 2.5. Furthermore, significant fractions of lithium and sodium were extracted (Figure 4.14 b). The extraction of manganese and cobalt by 0.8 M CYANEX 272 was practically complete (> 99.99 %) at pH ≥ 7 and O/A = 2.5 (Figure 4.14 b).

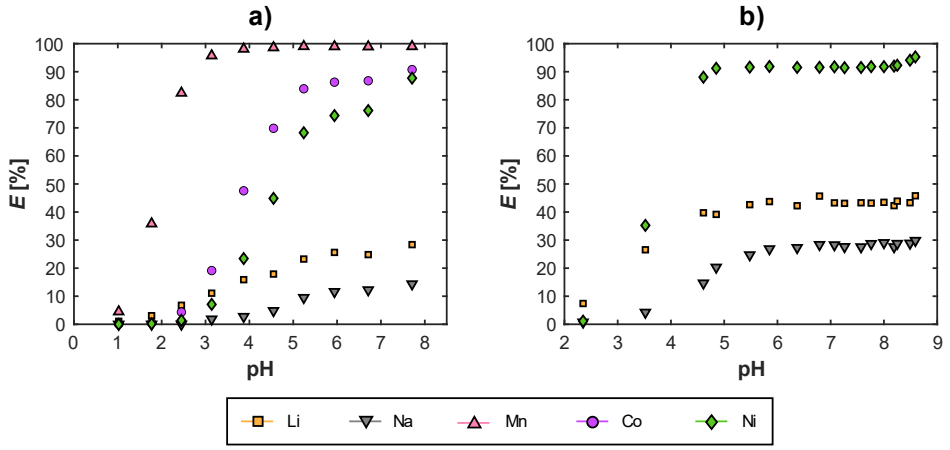

Figure 4.13 Effect of pH on the extraction of lithium, nickel, cobalt, manganese, and sodium by 0.8 M D2EHPA (modifier: 5 vol% TBP; diluent: Exxsol D80). T = 25 ± 1 °C; t_{eq} = 15 min; O/A = 1. Initial aqueous concentrations [g L^{-1}]: a) Li: 2.52, Ni: 2.05, Co: 16.5, Mn: 2.09; b) Li: 2.29, Na: 26.2, Ni: 1.94.

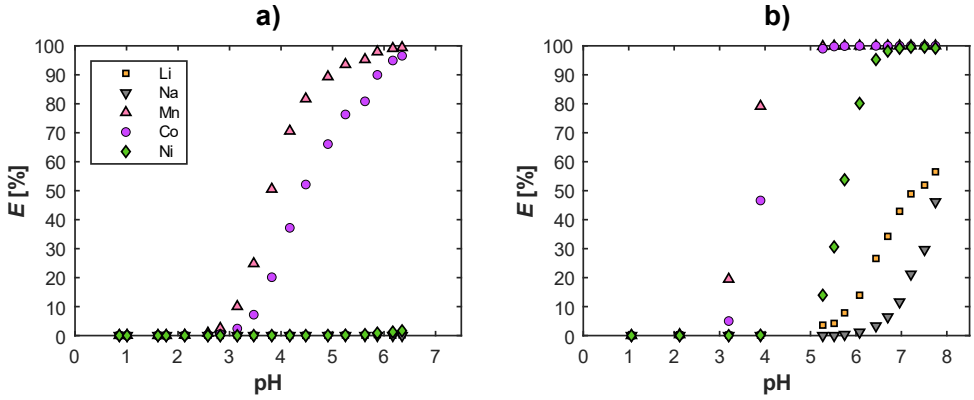

Figure 4.14 Effect of pH on the extraction of lithium, nickel, cobalt, manganese, and sodium by 0.8 M CYANEX 272 (diluted in Exxsol D80) at a) O/A = 1 and b) O/A =2.5. T = 25 ± 1 °C; t_{eq} = 15 min. Initial aqueous concentrations [g L^{-1}]: Li: 2.52, Ni: 2.05, Co: 16.5, Mn: 2.09.

4.3.3 Countercurrent separation of manganese from lithium, cobalt, and nickel by 0.8 M D2EHPA

The pH for extraction of manganese was chosen to be 2.5 as more than 80 % manganese was extracted at O/A = 1 while the extraction percentages of nickel, cobalt, and lithium were maintained below 10 % (Figure 4.13 a). McCabe–Thiele analysis suggested that

99.5 % of the Mn could be removed by 0.8 M D2EHPA in three ideal countercurrent extraction stages operating with S/F = 0.8 at pH = 2.50 (Figure 4.15). Extraction of manganese was 94.2 % in three countercurrent stages (Table 4.4) and the raffinate contained 115 mg L^{-1} manganese. The amount of manganese extracted in the countercurrent experiments was lower than predicted because the raffinate exit stage operated at pH = 2.1, whereas the McCabe–Thiele analysis assumes pH = 2.5 for all stages. Furthermore, chemical equilibrium is not attained in continuous extraction equipment. The prediction for raffinate exit stage composition was determined from Figure 4.15 by graphical extrapolation of the experimental data.

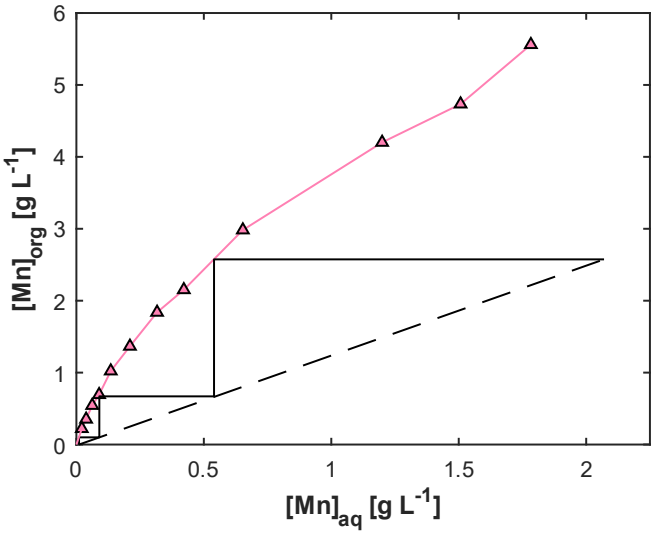

Figure 4.15 A McCabe–Thiele analysis applied to the equilibrium distribution of manganese between 0.8 M D2EHPA (5 vol% TBP, diluted in Exxsol D80) and simulated LIB leachate. T = 25 ± 1 °C; pH = 2.5; t_{eq} = 15 min. Initial aqueous concentrations [g L^{-1}]: Li: 2.63, Ni: 1.98, Co: 16.2, Mn: 2.07. The operating line was calculated with S/F = 0.8 and 99.5 % manganese removal.

Table 4.4 Compositions of the extract and raffinate from three-stage countercurrent extraction by 0.8 M D2EHPA. S/F = 0.8; T = 21 ± 1 °C; τ_{mix} = 4 min.

	[Li]	[Na]	[Mn]	[Co]	[Ni]	pH_{avg}
			[mg L^{-1}]			
Simulated leachate	*2340*	*6930*	*2070*	*16200*	*1820*	Stage 1: 2.49 ± 0.02
Raffinate	2180	8300	115	15700	1790	Stage 2: 2.52 ± 0.06
Extract	151	21.2	2970	541	17.7	Stage 3: 2.08 ± 0.03

Because any manganese left in the MnSX raffinate will be extracted by CYANEX 272 in the next CoSX step of the process (Figure 4.12), eventually decreasing the purity of the $CoSO_4$ product, maximizing the extraction of manganese is a higher priority than minimizing the co-extraction of lithium, cobalt, nickel, and sodium. Small co-extraction of lithium, cobalt, nickel, and sodium is not a concern considering the production of NCM mixtures. However, scrubbing of the manganese-rich D2EHPA is required to produce a purified $MnSO_4$ fraction (Publication III). The separation of manganese from the other metals during extraction can be improved by lowering S/F and increasing the number of extraction stages.

4.3.4 Separation of cobalt from lithium and nickel

Figure 4.13 shows that manganese can be completely extracted from the simulated leachate. Therefore, a manganese-free leachate was used to study the effect of O/A on the separation of cobalt from lithium and nickel by 0.8 M CYANEX 272 at pH = 5.3. Cobalt was very selectively extracted over nickel and lithium at O/A ratios between 0.04–1.5 (Figure 4.16 b), meaning that a sufficiently high amount of cobalt may be extracted in a single extraction stage without the extract phase becoming too viscous (see Chapter 4.3.2). A small amount of cobalt can be allowed in the CoSX raffinate because the residual cobalt will be extracted by D2EHPA in the nickel extraction step of the process (Figure 4.12). Although the concentrations of lithium and nickel were low (< 0.3 g L^{-1}) in the CYANEX 272 extracts (Figure 4.16 a), their extraction became significant after the aqueous phase was practically free from cobalt (Figure 4.16 b).

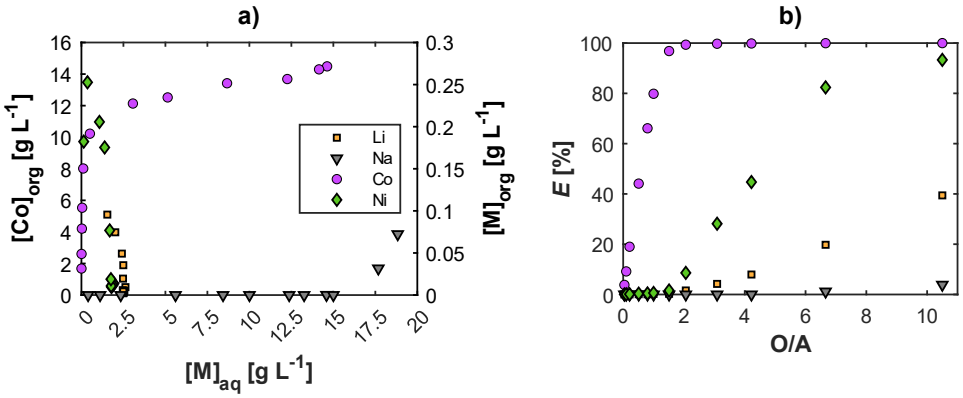

Figure 4.16 Distributions of lithium, nickel, cobalt, and sodium between 0.8 M CYANEX 272 (diluted in Exxsol D80) and manganese-free simulated LIB leachate: a) loading isotherms; b) effect of volumetric phase ratio on percentages of metals extracted. T = 25 ± 1 °C; pH = 5.3; t_{eq} = 15 min. Initial aqueous concentrations [g L^{-1}]: Li: 2.70, Ni: 1.91, Co: 15.2.

The loaded 0.8 M CYANEX 272 was prepared for the stripping experiments (Publication III, Figure 8) by single extraction at pH = 4.95 and O/A = 1.5. Batch stripping of the loaded CYANEX 272 with 2 M H_2SO_4 at O/A = 10 back-extracted all the lithium and nickel as well as 99.9 % of the cobalt, resulting in a 99.8 mass % relative purity for cobalt. The concentration of cobalt in the stripping raffinates reached over 100 g L^{-1} at O/A = 10–50 (Publication III, Figure 8). Lithium and nickel can be scrubbed before the stripping of cobalt to obtain the $CoSO_4$ fraction at even higher purity (Vasilyev *et al*., 2019; Virolainen *et al*., 2017).

4.3.5 Separation of nickel and lithium

Two countercurrent stages operating at S/F = 0.5 and pH = 7.0–7.7 extracted 98.1 % of nickel (Table 4.5) but $[Ni]_{org}/[Li]_{org}$ remained relatively low. The concentration of lithium in the organic phase did not decrease when the O/A ratio was lowered (Publication III, Figure 9 b), which suggests that the Ni^{2+} ions cannot displace the extracted Li^+ ions from D2EHPA. Further studies are recommended to determine if displacement of Li^+ by Ni^{2+} occurs in the absence of sodium. The co-extracted lithium can likely be recovered, so extraction of lithium does not need to be eliminated, but it is recommended to maximize the $[Ni]_{org}/[Li]_{org}$ ratio during the extraction of nickel. Any residual nickel, cobalt, or manganese in the lithium-rich raffinate can be precipitated as, for example, mixed hydroxides that can be recycled to the process feed. Lithium can be precipitated from the nickel-, cobalt-, and manganese-free raffinate as Li_2CO_3 (Chen & Ho, 2018).

Table 4.5 Compositions of extract and raffinate in two-stage countercurrent extraction of nickel and lithium from the CoSX raffinate by pre-neutralized 0.8 M D2EHPA. S/F = 0.5; T = 21 ± 1 °C; τ_{mix} = 4 min. Pre-neutralization: 81.5 mL 10 M NaOH in one liter of 0.8 M D2EHPA (5 vol% TBP) (100 % saponification).

	[Li]	**[Na]**	**[Mn]**	**[Co]**	**[Ni]**	**pH_{avg}**
			[mg L^{-1}]			
CoSX raffinate (aq. feed)	*2580*	*20900*	*0*	*98.5*	*2000*	Stage 1: 7.7 ± 0.1 Stage 2: 7.2 ± 0.1
Raffinate	1680	26700	0	1.03	38.7	
Extract	1770	9150	0	191	3830	

4.3.6 Production of NCM synthesis mixture

Mixing the MnSX extract (Table 4.4) with the NiSX extract (Table 4.5) at a 0.15:1 volumetric ratio yields NCM-D2EHPA where n(Ni):n(Mn) = 8.06 and n(Ni):n(Co) = 14.16. The Ni:Co:Mn stoichiometric ratio can be accurately adjusted to, for example, 8:1:1 by changing the mixing ratio of the D2EHPA extracts as well as by the addition of the concentrated $CoSO_4$ raffinate (Figure 4.12) after complete stripping of the NCM-D2EHPA.

Table 4.6 shows the composition of the raffinate from continuous stripping of NCM811-D2EHPA. The total concentration of nickel, cobalt, and manganese ([NCM]) increased from 112 mmol L^{-1} to 478 mmol L^{-1}. In addition to the possibility of concentrating the NCM mixture, controlling the amount of lithium and sodium in NCM-D2EHPA is important because their backextraction consumes stripping acid and they have the lowest solubilities—grams of metal per kg of H_2O—among the metal sulfates studied here (Publication III, Figure 12). It is likely that lithium can be recovered from the NCM synthesis mixture by carbonate precipitation after precipitating the NCM precursor because the solubility limit of LiOH in water enables 36 grams of lithium per kilogram of water at 25 °C (Söhnel & Novotný, 1985).

Table 4.6 Compositions of extract and raffinate in continuous stripping of nickel, cobalt, manganese, lithium, and sodium from 0.8 M NCM-D2EHPA with 3 M H_2SO_4. S/F = 10; T = 21 ± 1 °C; τ_{mix} = 7.3 min.

	[Li]	[Na]	[Mn]	[Co]	[Ni]	pH_{avg}
			[mmol L^{-1}]			
NCM-D2EHPA (org. feed)	55.2	391	11.2	11.1	89.9	
Raffinate	228	1770	30.1	49.2	399	1.6 ± 0.1
Extract	9.38	40.4	6.68	1.55	11.8	

The volumetric phase ratio changes during the stripping of the NCM-D2EHPA. The extract-to-raffinate ratio was differed from S/F = 10. Therefore, the mass balances are not closed with the concentrations in Table 4.6. The change in phase ratio can easily be observed visually, especially in batch extraction. The changes in phase volumes are likely explained by the break-up of microemulsion or reversed micelle structures, and by the release of hydrated water; this must be considered in process optimization.

Preparing a nickel-rich sulfate solution from a cobalt-rich LIB leachate without additional input of transition metal salts is a task with increased complexity (Figure 4.12). When the molar ratios of nickel, cobalt, and manganese in the LIB leachate match with a commercial NCM cathode composition or when additional $NiSO_4$, $CoSO_4$, and $MnSO_4$ are used to tune the solution composition (Liu *et al.*, 2021; Shuya *et al.*, 2020; Yang *et al.*, 2017), a more straightforward solvent extraction process than the concept in Figure 4.12 can be used. Adjusting the Ni:Co:Mn molar ratio in the cobalt-rich leachate (Chapter 4.3.1) to 8:1:1 using transition metal salts requires approximately 590 kg $NiSO_4 \cdot 6H_2O$ and 42 kg $MnSO_4 \cdot H_2O$ per 1.0 m^3 of leachate. The requirement for compensating the deficit is high because considerably more metals should be introduced to the process than are delivered into it from the 1.0 m^3 of leachate. Then, the solution should be diluted if 2 mol L^{-1} is the target total concentration. Thus, 1.4–1.5 m^3 of NCM811 synthesis mixture would be obtained. The process concept in Figure 4.12 produces approximately 21 L of NCM811 synthesis mixture at [NCM] = 2 mol L^{-1} from 1 m^3 of leachate (Chapter 4.3.1), assuming 100 % material recovery. The material loops

of the transition metals are closed in the concept of Figure 4.12. Purified Li_2SO_4, $CoSO_4$, and $MnSO_4$ fractions are obtained.

5 Conclusions

Metals and metallic materials are crucial for the most important infrastructure and technological developments within modern society. Hydrometallurgical solvent extraction is an industrially significant and efficient method for the separation and purification of metal salts from aqueous solutions. This thesis focused on the conceptual development of solvent extraction processes for concentrated sulfate solutions. Simplified theoretical calculations and batch equilibrium data were used in the conceptual process design. The technical feasibility of the studied processes was validated in continuous countercurrent mixer-settler equipment that have the characteristics of industrial-scale mixer-settlers. This research contributed to three different separation processes: I) separation of arsenic from concentrated H_2SO_4, II) purification of concentrated $MnSO_4$ leachate, and III) production of a mixed sulfate solution with tailored composition from a lithium-ion battery leachate.

The extraction of arsenic from 10.4 M H_2SO_4 by undiluted TBP and aliphatic alcohols is accompanied by significant changes in the volumetric phase ratio due to co-extraction of H_2SO_4 and water. Aside from the measured equilibrium distributions, changes in the volumetric phase ratios were quantified. Experimental pseudo-countercurrent method was used to study the countercurrent distribution of arsenic in three extraction stages (S/F = 0.79), two scrubbing stages (S/F = 4.03), and four stripping stages (S/F = 2.01). Undiluted TBP extracted 83.7 % of the arsenic from 10.4 M H_2SO_4 in three pseudo-countercurrent stages. The McCabe–Thiele method was unreliable in predicting the performance of the countercurrent stripping of arsenic- and H_2SO_4-loaded TBP. Changes in the aqueous speciation affect the distribution of arsenic. Therefore, the distribution cannot be predicted by a single isotherm. Future research on the structure and stoichiometry of the extracted species is recommended. Experimental comparison of the pseudo-countercurrent extractions against continuous countercurrent extractions with the same chemical system are invited.

A purification process was developed for a concentrated $MnSO_4$ leachate that contained zinc, iron, magnesium, aluminium, and calcium as impurity metals. Over 99 % of the zinc and > 98 % of the iron were removed from the leachate by 0.8 M Na-BTMPPA in two countercurrent extraction stages, whereas the removal of manganese during extraction was 5.2 %. Selective stripping recovered 71.5 % of the co-extracted manganese from the loaded BTMPPA at > 99.5 % relative purity. D2EHPA was also efficient in removing zinc and iron (> 99 %), but more manganese was co-extracted. According to simplified theoretical calculations, the extraction of calcium by D2EHPA is decreased by increasing the Mn:Ca ratio in the sulfate solution. Theoretical calculations predicted approximately 30 % extraction of calcium from the concentrated $MnSO_4$ leachate but predicted complete removal of calcium for dilute metal solutions. Because increasing the amount of extractant in the system decreases the required pH for extraction, further studies of the system are recommended with higher S/F ratio and extractant concentration. Maintaining a low pH is encouraged to avoid aqueous precipitation reactions.

Hydrometallurgical solvent extraction processes are typically designed to fractionate different metals into their own purified fractions. Here, a solvent extraction flowsheet was developed for producing a nickel-rich sulfate mixture with specific Ni:Co:Mn stoichiometric ratio from a cobalt-rich lithium-ion battery leachate. Such solutions are used in the co-precipitation synthesis of ternary cathode precursors for lithium-ion batteries. An NCM mixture is obtained from the process without additional inputs of lithium, nickel, cobalt, or manganese. Simultaneously, excess lithium, cobalt, and manganese are obtained in their own purified fractions. The key separations within the process concept were studied by batch equilibrium experiments and continuous laboratory-scale countercurrent experiments in industrial-type mixer-settlers. A sulfate mixture with 478 mmol L^{-1} total concentration of nickel, cobalt, and manganese was obtained. The stoichiometric ratios were n(Ni):n(Mn) = 8.06 and n(Ni):n(Co) = 14.16. The cobalt deficiency can be compensated by addition of the pure $CoSO_4$ fraction that is obtained from the same process.

Solvent extraction systems with concentrated solutions are more likely to exhibit phenomena and limitations that either do not occur or are less prominent in dilute extraction systems; for instance, third-phase formation, emulsification, and gelation are usually so problematic that they prevent industrial operation. Moreover, the extractability of metals may be different in dilute solutions and concentrated solutions. The McCabe–Thiele method and theoretical calculations based on simplified equilibrium models are applicable in the conceptual design of the solvent extraction flowsheets. The presented flowsheets could be improved and optimized by numerical simulations that are based on sophisticated and validated equilibrium models in which non-ideality and speciation in the organic phase are also considered.

References

Acharya, S., & Mishra, S. (2017). Studies on solvent extraction of La(III) using [A336][NO_3^-] and modeling by statistical analysis and neural network. *Separation Science and Technology*, *52*(10), 1660–1669. https://doi.org/10.1080/01496395.2017.1296870.

Anitha, M., & Singh, H. (2008). Artificial neural network simulation of rare earths solvent extraction equilibrium data. *Desalination*, *232*(1–3), 59–70. https://doi.org/10.1016/j.desal.2007.10.037.

Ayala, J., & Fernández, B. (2013). Reuse of anode slime generated by the zinc industry to obtain a liquor for manufacturing electrolytic manganese. *JOM*, *65*(8), 1007–1014. https://doi.org/10.1007/s11837-013-0667-3.

Baes, C. F., & Mesmer, R. E. (1976). *The Hydrolysis of Cations*. John Wiley & Sons.

Ball, J. W., & Nordstrom, D. K. (1991). *User's manual for WATEQ4F, with revised thermodynamic data base and text cases for calculating speciation of major, trace, and redox elements in natural waters*. U.S. Geological Survey. https://doi.org/https://doi.org/10.3133/ofr91183.

Baradel, A., & Guerriero, R. (1988). *Process for separating arsenic from acid solutions which contain it*, US Patent No. 4737350.

Baradel, A., Guerriero, R., Meregalli, L., & Vittadini, I. (1986a). Extraction of As from copper refining electrolyte, *JOM 38*(2), 32–37). https://doi.org/10.1007/BF03257918.

Baradel, A., Guerriero, R., Meregalli, L., & Vittadini, I. (1986b). New extractant for arsenic separation from industrial solutions. In *ISEC '86 International Solvent Extraction Conference: Preprints, Volume II* (pp. 401–408). DECHEMA, Frankfurt am Main, Germany.

Baradel, A., Guerriero, R., & Veronese, G. (1988). *Process for separating arsenic from acid solutions which contain it* (US Patent No. 4701311).

Biswas, R. K., Habib, M. A., Karmakar, A. K., & Tanzin, S. (2016). Recovery of manganese and zinc from waste Zn-C cell powder: Mutual separation of Mn(II) and Zn(II) from leach liquor by solvent extraction technique. *Waste Management*, *51*, 149–156. https://doi.org/10.1016/j.wasman.2015.09.041.

Bourget, C., Soderstrom, M., Jakovljevic, B., & Morrison, J. (2011). Optimization of the design parameters of a CYANEX 272 circuit for recovery of nickel and cobalt. *Solvent Extraction and Ion Exchange*, *29*(5–6), 823–836. https://doi.org/10.1080/07366299.2011.595640.

Brodd, R. (1992). Batteries (Introduction). In J. I. Kroschwitz & M. Howe-Grant (Eds.), *Kirk-Othmer Encyclopedia of Chemical Technology Vol. 3* (4th ed., pp. 963–991). John Wiley & Sons, Inc.

Casas, J. M., Etchart, J. P., & Cifuentes, L. (2003). Aqueous speciation of arsenic in sulfuric acid and cupric sulfate solutions. *AIChE Journal*, *49*(8), 2199–2210. https://doi.org/10.1002/aic.690490827.

Chagnes, A. (2020). Simulation of solvent extraction flowsheets by a global model combining physicochemical and engineering approaches—Application to cobalt(II) extraction by D2EHPA. *Solvent Extraction and Ion Exchange*, *38*(1), 3–13. https://doi.org/10.1080/07366299.2019.1691135.

Chagnes, A., & Pospiech, B. (2013). A brief review on hydrometallurgical technologies for recycling spent lithium-ion batteries. *Journal of Chemical Technology and Biotechnology*, *88*(7), 1191–1199. https://doi.org/10.1002/jctb.4053.

Chen, H., Jobson, M., Masters, A. J., Gonzalez-Miquel, M., & Halstead, S. (2018a). Flowsheet simulation of cobalt-nickel separation by solvent extraction with trihexyl(tetradecyl)phosphonium chloride. *Industrial and Engineering Chemistry Research*, *57*(30), 10049–10060. https://doi.org/10.1021/acs.iecr.7b05254.

Chen, W. S., & Ho, H. J. (2018). Recovery of valuable metals from lithium-ion batteries NMC cathode waste materials by hydrometallurgical methods. *Metals*, *8*(5). https://doi.org/10.3390/met8050321.

Chen, W. S., Liao, C. T., & Chang, C. H. (2018b). Recovery of zinc and manganese from spent Zn-Mn batteries using solvent extraction. *Key Engineering Materials*, *775 KEM*, 427–433. https://doi.org/10.4028/www.scientific.net/KEM.775.427.

Chen, X., Chen, Y., Zhou, T., Liu, D., Hu, H., & Fan, S. (2015a). Hydrometallurgical recovery of metal values from sulfuric acid leaching liquor of spent lithium-ion batteries. *Waste Management*, *38*(1), 349–356. https://doi.org/10.1016/j.wasman.2014.12.023.

Chen, X., Zhou, T., Kong, J., Fang, H., & Chen, Y. (2015b). Separation and recovery of metal values from leach liquor of waste lithium nickel cobalt manganese oxide based cathodes. *Separation and Purification Technology*, *141*, 76–83. https://doi.org/10.1016/j.seppur.2014.11.039.

Cheng, C. Y. (2000). Purification of synthetic laterite leach solution by solvent extraction using D2EHPA. *Hydrometallurgy*, *56*(3), 369–386. https://doi.org/10.1016/S0304-386X(00)00095-5.

Coulson, J. M., Richardson, J. F., Backhurst, J. R., & Harker, J. H. (1983). *Chemical Engineering* (3rd ed.). Pergamon Press.

Dalewski, F. (1999). Removing arsenic from copper smelter gases. *JOM*, *51*(9), 24–26. https://doi.org/10.1007/s11837-999-0153-0.

de Lourdes Ballinas, M., Rodríguez de San Miguel, E., Muñoz, M., & de Gyves, J. (2003). Arsenic(V) extraction from sulfuric acid media using DBBP-D2EHPA organic mixtures. *Industrial and Engineering Chemistry Research*, *42*(3), 574–581. https://doi.org/10.1021/ie020402a.

Demirkiran, A., & Rice, N. M. (2002). The extraction of arsenic (V) from copper refinery electrolytes with tri-n-butyl phosphate: II - flowsheet development. In *Proceedings of the International Solvent Extraction Conference* (pp. 890–895), Melville, South Africa.

Demirkiran, A., Rice, N. M., & Wright, A. R. (2002). The extraction of arsenic (V) and sulphuric acid from acidic sulphate media by tri-n-butyl phosphate (TBP) in Shellsol A or T: I - an equilibrium study. In *Proceedings of the International Solvent Extraction Conference* (pp. 884–889), Melville, South Africa.

Flett, D. S. (2005). Solvent extraction in hydrometallurgy: The role of organophosphorus extractants. *Journal of Organometallic Chemistry*, *690*(10), 2426–2438. https://doi.org/10.1016/j.jorganchem.2004.11.037.

Giganov, G. P., Travkin, V. F., & Ankina, N. P. (1978). Extraction of arsenic from acidic solutions by tributyl phosphate. *Tsvetnye Metally*, *8*, 27–29.

Goodwin, F. E. (1998). Zinc and Zinc Alloys. In J. I. Kroschwitz & M. Howe-Grant (Eds.), *Kirk-Othmer Encyclopedia of Chemical Technology Vol. 25* (4th ed., pp. 789–839). John Wiley & Sons, Inc.

Grenthe, I., Wanner, H., Forest, I., & OECD Nuclear Energy Agency. (1992). *Chemical Thermodynamics of Uranium*. North-Holland. https://inis.iaea.org/search/search.aspx?orig_q=RN:25000186.

Grinbaum, B. (2002). An integrated method for development and scaling up of extraction processes. In Y. Marcus & A. K. SenGupta (Eds.), *Ion Exchange and Solvent Extraction, Volume 15* (pp. 1–106). Marcel Dekker, Inc. https://doi.org/https://doi.org/10.1201/9781482270976.

Gromov, P. B., Kasikov, A. G., Shchelokova, E. A., & Petrova, A. M. (2018). Regeneration of sulfuric acid from electrolyte waste of the copper - smelting plant using solvent extraction. *Hydrometallurgy*, *175*, 187–192. https://doi.org/10.1016/j.hydromet.2017.11.008.

Habashi, F. (1999). *Textbook of Hydrometallurgy* (2nd ed.). Métallurgie Extractive Québec.

Haghighi, H. K., Moradkhani, D., & Salarirad, M. M. (2015). Separation of zinc from manganese, magnesium, calcium and cadmium using batch countercurrent extraction simulation followed by scrubbing and stripping. *Hydrometallurgy*, *154*, 9–16. https://doi.org/10.1016/j.hydromet.2015.03.007.

Helgeson, H. C., & Kirkham, D. H. (1974). Calculation of the thermodynamic and transport properties of aqueous species at high pressures and temperatures: *American Journal of Science*, *274*, 1199–1261.

Hesford, E., & McKay, H. A. C. (1960). The extraction of mineral acids by tri-n-butyl phosphate (TBP). *Journal of Inorganic and Nuclear Chemistry*, *13*, 156–164.

Hörbrand, T., Baumann, T., & Moog, H. C. (2018). Validation of hydrogeochemical databases for problems in deep geothermal energy. *Geothermal Energy*, *6*(1). https://doi.org/10.1186/s40517-018-0106-3.

Huang, T. C., & Juang, R. S. (1986). Extraction equilibrium of zinc from sulfate media with bis(2-ethylhexyl) phosphoric acid. *Industrial & Engineering Chemistry Fundamentals*, *25*(4), 752–757. https://doi.org/10.1021/i100024a046.

Iberhan, L., & Winiewski, M. (2002). Extraction of arsenic(III) and arsenic(V) with Cyanex 925, Cyanex 301 and their mixtures. *Hydrometallurgy*, *63*(1), 23–30. https://doi.org/10.1016/S0304-386X(01)00198-0.

Iberhan, L., & Wiśniewski, M. (2003). Removal of arsenic(III) and arsenic(V) from sulfuric acid solution by liquid-liquid extraction. *Journal of Chemical Technology and Biotechnology*, *78*(6), 659–665. https://doi.org/10.1002/jctb.843.

Innocenzi, V., & Veglio, F. (2012). Separation of manganese, zinc and nickel from leaching solution of nickel-metal hydride spent batteries by solvent extraction. *Hydrometallurgy*, *129–130*, 50–58. https://doi.org/10.1016/j.hydromet.2012.08.003.

Joo, S. H., Shin, D. J., Oh, C. H., Wang, J. P., Senanayake, G., & Shin, S. M. (2016). Selective extraction and separation of nickel from cobalt, manganese and lithium in pre-treated leach liquors of ternary cathode material of spent lithium-ion batteries using synergism caused by Versatic 10 acid and LIX 84-I. *Hydrometallurgy*, *159*, 65–74. https://doi.org/10.1016/j.hydromet.2015.10.012.

Kauppinen, T., Vielma, T., Salminen, J., & Lassi, U. (2020). Selective recovery of manganese from anode sludge residue by reductive leaching. *ChemEngineering*, *4*(2), 1–13. https://doi.org/10.3390/chemengineering4020040.

Kislik, V. S. (2012). *Solvent Extraction: Classical and Novel Approaches* (1st ed.). Elsevier. https://doi.org/10.1016/C2010-0-65805-6.

Lee, J. Y., Pranolo, Y., Cheng, C. Y., & Zhang, Z. W. (2010). The recovery of zinc and manganese from synthetic spent-battery leach solutions by solvent extraction. *Solvent Extraction and Ion Exchange*, *28*(1), 73–84. https://doi.org/10.1080/07366290903409043.

Li, L., Zhang, X., Li, M., Chen, R., Wu, F., Amine, K., & Lu, J. (2018). The recycling of spent lithium-ion batteries: a review of current processes and technologies. *Electrochemical Energy Reviews*, *1*(4), 461–482. https://doi.org/10.1007/s41918-018-0012-1.

Liu, T., Chen, J., Li, H., & Li, K. (2020). An integrated process for the separation and recovery of valuable metals from the spent $LiNi_{0.5}Co_{0.2}Mn_{0.3}O_2$ cathode materials. *Separation and Purification Technology*, *245*, 116869. https://doi.org/10.1016/j.seppur.2020.116869.

Liu, T., Chen, J., Shen, X., & Li, H. (2021). Regulating and regenerating the valuable metals from the cathode materials in lithium-ion batteries by nickel-cobalt-manganese co-extraction. *Separation and Purification Technology*, *259*, 118088. https://doi.org/10.1016/j.seppur.2020.118088.

Marcus, Y. (2004). Principles of solubility and solutions. In J. Rydberg, M. Cox, C. Musikas, & G. R. Choppin (Eds.), *Solvent Extraction Principles and Practice* (2nd ed.). Marcel Dekker, Inc.

Marcus, Y., & Kertes, A. S. (1969). *Ion Exchange and Solvent Extraction of Metal Complexes*. Wiley-Interscience.

Matricardi, L. R., & Downing, J. (1995). Manganese and manganese alloys. In J. I. Kroschwitz & M. Howe-Grant (Eds.), *Kirk-Othmer Encyclopedia of Chemical Technology Vol. 15* (4th ed., pp. 963–990). John Wiley & Sons, Inc.

Meshram, P., Pandey, B. D., & Mankhand, T. R. (2014). Extraction of lithium from primary and secondary sources by pre-treatment, leaching and separation: A comprehensive review. *Hydrometallurgy*, *150*, 192–208. https://doi.org/10.1016/j.hydromet.2014.10.012.

Mohapatra, D., Hong-In, K., Nam, C. W., & Park, K. H. (2007). Liquid-liquid extraction of aluminium(III) from mixed sulphate solutions using sodium salts of Cyanex 272 and D2EHPA. *Separation and Purification Technology*, *56*(3), 311–318. https://doi.org/10.1016/j.seppur.2007.02.017.

Montgomery, H., Chastain, R. V., & Lingafelter, E. C. (1966). The crystal structure of Tutton's salts. V. Manganese ammonium sulfate hexahydrate. *Acta Crystallographica*, *20*(6), 731–733. https://doi.org/10.1107/S0365110X66001762.

Nair, V. S. K., & Nancollas, G. H. (1959). Thermodynamics of ion association. Part VI.

Some transition-metal sulphates. *Journal of the Chemical Society (Resumed)*, 3934–3939. https://doi.org/10.1039/jr9590003934.

Navarro, P., & Alguacil, F. J. (1996). Removal of arsenic from copper electrolytes by solvent extraction with tributylphosphate. *Canadian Metallurgical Quarterly*, *35*(2), 133–141. https://doi.org/10.1016/0008-4433(95)00044-5.

Nayl, A. A., Hamed, M. M., & Rizk, S. E. (2015). Selective extraction and separation of metal values from leach liquor of mixed spent Li-ion batteries. *Journal of the Taiwan Institute of Chemical Engineers*, *55*, 119–125. https://doi.org/10.1016/j.jtice.2015.04.006.

Nordstrom, D. K., Plummer, L. N., Langmuir, D., Busenberg, E., May, H. M., Jones, B. F., & Parkhurst, D. L. (1990). Revised Chemical Equilibrium Data for Major Water—Mineral Reactions and Their Limitations. In *Chemical Modeling of Aqueous Systems II. A.C.S. Symp. Ser. 416* (pp. 398–413). American Chemical Society, Washington, DC. https://doi.org/10.1021/bk-1990-0416.ch031.

Omelchuk, K., & Chagnes, A. (2018). New cationic exchangers for the recovery of cobalt(II), nickel(II) and manganese(II) from acidic chloride solutions: Modelling of extraction curves. *Hydrometallurgy*, *180*, 96–103. https://doi.org/10.1016/j.hydromet.2018.07.003.

Pakarinen, J., & Paatero, E. (2011). Effect of temperature on Mn-Ca selectivity with organophosphorus acid extractants. *Hydrometallurgy*, *106*(3–4), 159–164. https://doi.org/10.1016/j.hydromet.2011.01.003.

Peng, C., Chang, C., Wang, Z., Wilson, B. P., Liu, F., & Lundström, M. (2020). Recovery of high-purity MnO_2 from the acid leaching aolution of apent Li-ion batteries. *JOM*, *72*(2), 790–799. https://doi.org/10.1007/s11837-019-03785-1.

Pereira, D. D., Rocha, S. D. F., & Mansur, M. B. (2007). Recovery of zinc sulphate from industrial effluents by liquid-liquid extraction using D2EHPA (di-2-ethylhexyl phosphoric acid). *Separation and Purification Technology*, *53*(1), 89–96. https://doi.org/10.1016/j.seppur.2006.06.013.

Piret, N. L. (1999). Removal and safe disposal of arsenic in copper processing. *Jom*, *51*(9), 16–17. https://doi.org/10.1007/s11837-999-0150-3.

Pitzer, K. S. (1991). *Activity Coefficients in Electrolyte Solutions* (2nd ed.). CRC Press.

Porvali, A., Aaltonen, M., Ojanen, S., Velazquez-Martinez, O., Eronen, E., Liu, F., Wilson, B. P., Serna-Guerrero, R., & Lundström, M. (2019). Mechanical and hydrometallurgical processes in HCl media for the recycling of valuable metals from Li-ion battery waste. *Resources, Conservation and Recycling*, *142*, 257–266. https://doi.org/10.1016/j.resconrec.2018.11.023.

Principe, F., & Demopoulos, G. P. (2004). Comparative study of iron(III) separation from zinc sulphate-sulphuric acid solutions using the organophosphorus extractants, OPAP and D2EHPA. Part I: Extraction. *Hydrometallurgy*, *74*(1–2), 93–102. https://doi.org/10.1016/j.hydromet.2004.01.004.

Puigdomenech, I. (2009). *HYDRA: Hydrochemical Equilibrium Constant Database* (2.6.2015). https://www.kth.se/che/medusa/chemeq-1.369367.

Rice, N. M., Irving, H. M. N. H., & Leonard, M. A. (1993). Nomenclature for liquid-liquid distribution (solvent extraction). *Pure and Applied Chemistry*, *65*(11), 2373–2396. https://doi.org/10.1351/pac199365112373.

Ritcey, G. M. (2006). *Solvent Extraction: Principles and Applications to Process Metallurgy, Vol. 1* (2nd ed.). G.M. Ritcey & Associates Incorporated, Ottawa.

Rumble, J. R. (2021). *CRC Handbook of Chemistry and Physics* (J. R. Rumble (ed.); 102nd ed.). CRC Press/Taylor & Francis.

Rydberg, J., Choppin, G. R., Musikas, C., & Sekine, T. (2004). Solvent extraction equilibria. In J. Rydberg, M. Cox, C. Musikas, & G. R. Choppin (Eds.), *Solvent Extraction Principles and Practice* (2nd ed., p. k). Marcel Dekker, Inc.

Salgado, A. L., Veloso, A. M. O., Pereira, D. D., Gontijo, G. S., Salum, A., & Mansur, M. B. (2003). Recovery of zinc and manganese from spent alkaline batteries by liquid–liquid extraction with Cyanex 272. *Journal of Power Sources*, *115*(2), 367–373. https://doi.org/10.1016/S0378-7753(03)00025-9.

Sandhibigraha, A., Bhaskara Sarma, P. V. R., & Chakravortty, V. (2000). Stripping studies of iron(III) extracted by D2EHPA, PC 88A, and Cyanex 272 from chloride solutions using sulphuric and hydrochloric acids. *Solvent Extraction Research and Development, Japan*, *7*, 93–105.

Shuya, L., Yang, C., Xuefeng, C., Wei, S., Yaqing, W., & Yue, Y. (2020). Separation of lithium and transition metals from leachate of spent lithium-ion batteries by solvent extraction method with Versatic 10. *Separation and Purification Technology*, *250*, 117258. https://doi.org/10.1016/j.seppur.2020.117258.

Sleppy, W. C. (2002). Aluminum compounds, introduction. In *Kirk-Othmer Encyclopedia of Chemical Technology*. Wiley. https://doi.org/10.1002/0471238961.0914201819120516.a01.pub2

Söhnel, O., & Novotný, P. (1985). *Densities of Aqueous Solutions of Inorganic Substances*. Elsevier.

Sole, K. C. (2018). The Evolution of Cobalt–Nickel Separation and Purification Technologies: Fifty Years of Solvent Extraction and Ion Exchange. In *Extraction*

2018. The Minerals, Metals & Materials Series (pp. 1167–1191). Springer, Cham. https://doi.org/10.1007/978-3-319-95022-8_95.

Sorel, C., Baron, P., Dinh, B., Heres, X., Montuir, M., & Pacary, V. (2011). The simple solution modeling implemented in the PAREX code to simulate solvent extraction operations. *Proceedings of GLOBAL 2011, Makuhari, Japan, 11–16 Dec 2011*. 392588. Available from: https://www.researchgate.net/publication/275823548.

Suzuki, T., Nakamura, T., Inoue, Y., Niinae, M., & Shibata, J. (2012). A hydrometallurgical process for the separation of aluminum, cobalt, copper and lithium in acidic sulfate media. *Separation and Purification Technology*, *98*, 396–401. https://doi.org/10.1016/j.seppur.2012.06.034.

Szymanowski, J. (1998). Removal of toxic elements from copper electrolyte by solvent extraction. *Mineral Processing and Extractive Metallurgy Review*, *18*(3–4), 389–418. https://doi.org/10.1080/08827509808914162.

Tanong, K., Tran, L. H., Mercier, G., & Blais, J. F. (2017). Recovery of Zn (II), Mn (II), Cd (II) and Ni (II) from the unsorted spent batteries using solvent extraction, electrodeposition and precipitation methods. *Journal of Cleaner Production*, *148*, 233–244. https://doi.org/10.1016/j.jclepro.2017.01.158.

Thomsen, K. (2005). Modeling electrolyte solutions with the extended universal quasichemical (UNIQUAC) model. *Pure and Applied Chemistry*, *77*(3), 531–542. https://doi.org/10.1351/pac200577030531.

Thornton, J. D. (1992). *Science and Practice of Liquid-Liquid Extraction Volume 1*. Oxford University Press.

Totsuka, T., Sasaki, K., & Nagai, T. (1986). Fundamental studies on purification of copper electrolyte. *Metallurgical Review of MMIJ - Symposium Proceedings*, *3*(2), 146–154.

Travkin, V. F., Glubokov, Y. M., Mironova, E. V., & Yakshin, V. V. (2001). Extraction of arsenic(V) with hexabutylphosphoric triamide. *Russian Journal of Applied Chemistry*, *74*(10), 1664–1667. https://doi.org/10.1023/A:1014801117889.

Travkin, V. F., Kravchenko, A. N., & Miroevsky, G. P. (1993). Extraction of arsenic and antimony from sulfate solutions with organophosphorus reagents (in Russian). *Tsvetnye Metally*, *4*, 14–18.

Vasilyev, F. (2018). *Model-based Design And Optimization Of Hydrometallurgical Liquid-liquid Extraction Processes*. Acta Universitatis Lappeenrantaensis 818. Dissertation, Lappeenranta University of Technology, Lappeenranta.

Vasilyev, F., Virolainen, S., & Sainio, T. (2017). Modeling the phase equilibrium in

liquid–liquid extraction of copper over a wide range of copper and hydroxyoxime extractant concentrations. *Chemical Engineering Science*, *171*, 88–99. https://doi.org/10.1016/j.ces.2017.05.003.

Vasilyev, F., Virolainen, S., & Sainio, T. (2018). Modeling the liquid–liquid extraction equilibrium of iron (III) with hydroxyoxime extractant and equilibrium-based simulation of counter-current copper extraction circuits. *Chemical Engineering Science*, *175*, 267–277. https://doi.org/10.1016/j.ces.2017.10.003.

Vasilyev, F., Virolainen, S., & Sainio, T. (2019). Numerical simulation of counter-current liquid–liquid extraction for recovering Co, Ni and Li from lithium-ion battery leachates of varying composition. *Separation and Purification Technology*, *210*(August 2018), 530–540. https://doi.org/10.1016/j.seppur.2018.08.036.

Vieceli, N., Reinhardt, N., Ekberg, C., & Petranikova, M. (2021). Optimization of manganese recovery from a solution based on lithium-ion batteries by solvent extraction with D2EHPA. *Metals*, *11*(1), 1–20. https://doi.org/10.3390/met11010054.

Virolainen, S., Fallah Fini, M., Laitinen, A., & Sainio, T. (2017). Solvent extraction fractionation of Li-ion battery leachate containing Li, Ni, and Co. *Separation and Purification Technology*, *179*, 274–282. https://doi.org/10.1016/j.seppur.2017.02.010.

Virolainen, S., Wesselborg, T., Kaukinen, A., & Sainio, T. (2021). Removal of iron, aluminium, manganese and copper from leach solutions of lithium-ion battery waste using ion exchange. *Hydrometallurgy*, *202*, 105602. https://doi.org/10.1016/j.hydromet.2021.105602.

Wang, B., Mu, L., Guo, S., & Bi, Y. (2019). Lead leaching mechanism and kinetics in electrolytic manganese anode slime. *Hydrometallurgy*, *183*, 98–105. https://doi.org/10.1016/j.hydromet.2018.11.015.

Wang, F., He, F., Zhao, J., Sui, N., Xu, L., & Liu, H. (2012). Extraction and separation of cobalt(II), copper(II) and manganese(II) by Cyanex272, PC-88A and their mixtures. *Separation and Purification Technology*, *93*, 8–14. https://doi.org/10.1016/j.seppur.2012.03.018.

Wang, S., Li, J., Narita, H., & Tanaka, M. (2021). Solvent extraction equilibrium modeling for the separation of ammonia, nickel(II), and copper(II) from the loaded LIX84-I. *Minerals Engineering*, *172*, 107132. https://doi.org/10.1016/j.mineng.2021.107132.

Wiśniewski, M. (1997). Extraction of arsenic from sulphuric acid solutions by Cyanex 923. *Hydrometallurgy*, *46*(1–2), 235–241. https://doi.org/10.1016/s0304-386x(97)90003-7.

Wiśniewski, M. (1998). Removal of arsenic from sulphuric acid solutions. *Journal of Radioanalytical and Nuclear Chemistry*, *228*(1–2), 105–109. https://doi.org/10.1007/BF02387308.

Wolfram, O., & Krupp, R. E. (1996). Hydrothermal solubility of rhodochrosite, Mn (II) speciation, and equilibrium constants. *Geochimica et Cosmochimica Acta*, *60*(21), 3983–3994. https://doi.org/10.1016/S0016-7037(96)00224-4.

Xun, F., & Golding, J. A. (1987). Solvent extraction of cobalt and nickel in bis(2,4,4-trimethylpentyl) phosphinic acid, "Cyanex 272." *Solvent Extraction and Ion Exchange*, *5*(2), 205–226. https://doi.org/10.1080/07366298708918562.

Yang, Y., Xu, S., & He, Y. (2017). Lithium recycling and cathode material regeneration from acid leach liquor of spent lithium-ion battery via facile co-extraction and co-precipitation processes. *Waste Management*, *64*, 219–227. https://doi.org/10.1016/j.wasman.2017.03.018.

Yun, C. Y., Lee, C., Lee, G. G., Jo, S., & Sung, S. W. (2016). Modeling and simulation of multicomponent solvent extraction processes to purify rare earth metals. *Hydrometallurgy*, *159*, 40–45. https://doi.org/10.1016/j.hydromet.2015.11.001.

Zhang, C., Duan, N., Jiang, L., Xu, F., & Luo, J. (2018). Influence of Mn^{2+} ions on the corrosion mechanism of lead-based anodes and the generation of heavy metal anode slime in zinc sulfate electrolyte. *Environmental Science and Pollution Research*, *25*(12), 11958–11969. https://doi.org/10.1007/s11356-018-1443-2.

Zhang, W., & Cheng, C. Y. (2007). Manganese metallurgy review. Part III: Manganese control in zinc and copper electrolytes. *Hydrometallurgy*, *89*(3–4), 178–188. https://doi.org/10.1016/j.hydromet.2007.08.011.

Zhang, Y., & Muhammed, M. (2001). Critical evaluation of thermodynamics of complex formation of metal ions in aqueous solutions. *Hydrometallurgy*, *60*(3), 215–236. https://doi.org/10.1016/S0304-386X(01)00148-7.

Publication I

Jantunen, N., Virolainen, S., Latostenmaa, P., Salminen, J., Haapalainen, M., and Sainio, T.

Removal and recovery of arsenic from concentrated sulfuric acid by solvent extraction

Reprinted with permission from
Hydrometallurgy
Vol. 187, pp. 101-112, 2019

Hydrometallurgy 187 (2019) 101–112

Contents lists available at ScienceDirect

Hydrometallurgy

journal homepage: www.elsevier.com/locate/hydromet

Removal and recovery of arsenic from concentrated sulfuric acid by solvent extraction

Niklas Jantunen[a], Sami Virolainen[a,*], Petri Latostenmaa[b], Justin Salminen[c], Mika Haapalainen[d], Tuomo Sainio[a]

[a] LUT University, School of Engineering Science, Yliopistonkatu 34, 53850 Lappeenranta, Finland
[b] Boliden Harjavalta Oy, Teollisuuskatu 1, 29200 Harjavalta, Finland
[c] Boliden Kokkola Oy, Sinkkiaukio 1, 67900 Kokkola, Finland
[d] Outotec Oyj, Pori Research Center, Kuparitie 10, 28100 Pori, Finland

ARTICLE INFO

Keywords:
Liquid-liquid extraction
Solvent extraction
Arsenic
Sulfuric acid
Pseudo-countercurrent method
Recycling

ABSTRACT

Arsenic-contaminated sulfuric acid solutions are produced in large quantities as by-product during pyrometallurgical processing of sulfide minerals. Options for re-using such acid solutions are increased if the arsenic is removed and recovered as a product. The performances of tributyl phosphate and a mixture of 6 wt-% 1,2-octanediol in 2-ethylhexanol were studied in liquid-liquid extraction of arsenic from an industrial solution containing 10.4 M H_2SO_4. It was found that, due to the complex phase equilibria, a process design based on conventional batch equilibrium data did not describe the countercurrent processes accurately. A countercurrent flowsheet utilizing undiluted tributyl phosphate was investigated by pseudo-countercurrent extractions. 83.7% extraction of arsenic and 31.4% coextraction of H_2SO_4 was obtained in three-stage countercurrent extraction operated at a solvent-to-feed ratio of 0.79. Two-stage countercurrent scrubbing with pure water at O/A = 4.03 back-extracted 83.6% of H_2SO_4 and 24.9% of arsenic. 100% and 89.7% back-extraction was achieved in four-stage stripping at O/A = 2.01 for H_2SO_4 and arsenic, respectively. The effects of varying the flowsheet and operating parameters on separation efficiency are discussed.

1. Introduction

Utilization of sulfide minerals in the metals refining industry produces by-product H_2SO_4 solutions that contain arsenic and other impurities. In copper production, for instance, pyrometallurgical treatments do not remove the impurities completely, and they thus end up in cast copper anodes. During electrolytic purification of copper, arsenic dissolves in the H_2SO_4 electrolyte from the anodes with other impurities. These impurities decrease the quality of the product cathodes and lower the efficiency of the electrolysis cell. Furthermore, extremely toxic and lethal arsine gas, AsH_3, may form if levels of arsenic get sufficiently high in the electrolyte (Szymanowski, 1998).

Partial replacement of the electrolyte with fresh sulfuric acid solution can alleviate the problems caused by impurities. The electrolyte bleed is then directed to separation processes where the impurities or by-products can be treated and recovered. Copper electrolyte bleeds contain significant amounts of nickel, which can be removed by evaporative crystallization to produce crude nickel sulfate. Evaporation concentrates both H_2SO_4 and arsenic, and the resulting concentrated H_2SO_4 solution can be recycled back to electrolysis or sent for effluent treatment and disposal (Szymanowski, 1998).

Flue gases from copper smelters contain volatilized arsenic. During gas cleaning, the arsenic ends up in electrostatic precipitator (ESP) dust and also into the H_2SO_4 solutions that circulate in wet gas scrubbers. Use of relatively concentrated H_2SO_4 in washing towers is encouraged by the high solubility of arsenic in H_2SO_4 (Dalewski, 1999). Most of the ESP dust is circulated back to the smelter for a more complete recovery of raw materials but a fraction of the dust is leached with H_2SO_4 to prevent accumulation of impurities in the copper refining process (Piret, 1999; Riveros et al., 2001; Opio, 2013; Nazari et al., 2017). The origins of arsenic-contaminated H_2SO_4 solutions are summarized in Fig. 1, which is simplified from the publications by Szymanowski (1998) (Szymanowski, 1998), Dalewski (1999) (Dalewski, 1999) and Nazari et al. (2017) (Piret, 1999). It should be noted that potential sources of arsenic-contaminated acids are not limited to copper refineries.

Arsenic was recently listed in the 'Final List of Critical Minerals 2018' by the US Department of the Interior (DOI) US. Department of the

* Corresponding author.
E-mail address: sami.virolainen@lut.fi (S. Virolainen).

https://doi.org/10.1016/j.hydromet.2019.05.008
Received 5 December 2018; Received in revised form 30 April 2019; Accepted 11 May 2019
Available online 13 May 2019
0304-386X/

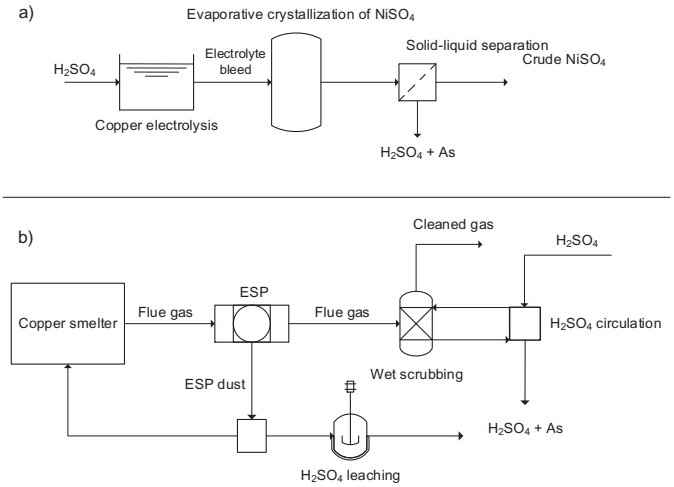

Fig. 1. Schematic diagrams of the formation of arsenic-bearing concentrated H_2SO_4 solutions in copper refineries. a) Copper electrolyte bleed (Szymanowski, 1998) b) Flue gas treatment in a copper smelter (Dalewski, 1999; Nazari et al., 2017).

Interior, 2018. To promote a circular economy, the recovery of arsenic as a product should be considered instead of precipitating arsenic as impure arsenites or arsenates. Concentrated H_2SO_4 solutions, in particular, offer the possibility for producing H_2SO_4 intermediate with significantly less or no arsenic and an arsenic-rich aqueous stream that is suitable for crystallization of As_2O_3.

The applicability of liquid-liquid extraction (LLE) for removal of arsenic from H_2SO_4 solutions has been examined by several authors (Table 1). In purification of copper electrolytes, an arsenic extraction process can be located: 1) directly after copper electrolysis; 2) after decopperizing treatment for the bleed (*e.g.* liberator electrolysis); or 3) after evaporation crystallization of crude $NiSO_4$. If the extraction is done before evaporation, the size of the required extraction equipment will be larger than if the extraction is done after evaporation. On the other hand, highly concentrated H_2SO_4 solutions demand more corrosion-resistant materials (Dermirkiran and Rice, 2002).

In previous research, most authors have focused on extracting arsenic from non-concentrated copper electrolyte bleeds (Table 1). Published results for pre-concentrated copper electrolytes are limited to work reported by De Schepper & Van Peteghem (De Schepper and Van Peteghem, 1977) and Navarro & Alguacil (Navarro and Alguacil, 1996). Demirkiran & Rice (Dermirkiran and Rice, 2002) studied extraction at

Table 1
Literature on liquid-liquid extraction of arsenic from H_2SO_4 solutions.

Extractant(s)	$[As]_0$ [g dm^{-3}]	$[Ni]_0$ [g dm^{-3}]	$[Cu]_0$ [g dm^{-3}]	$[H_2SO_4]_0$ [g dm^{-3}]	Reference
Cyanex 301, 923, 925 Hydroxamic acids 2-ethylhexane-1,3-diol	2.5	–	–	50–200	(Iberhan and Wiśniewski, 2003; Iberhan and Wiśniewski, 2002)
Cyanex 923	0.63–5	–	–	50–200	(Wiśniewski, 1997; Wiśniewski, 1998)
DBBP + D2EHPA	3–7.6	4.6–8.4	30–31.3	160–200	(Ballinas et al., 2003)
TBP	28	34.7	16.6	600	(De Schepper and Van Peteghem, 1977)
TBP	10	16	65	200–600	(Navarro and Alguacil, 1996)
TBP	15	0.4	8.7	200–600	(Dermirkiran and Rice, 2002)
TBP, D2EHPA, TAPO, HBPTA, D2EHMP	6.2	21.7	42.3	< 400	(Travkin et al., 1993)
HBPTA, TBP	4–5	–	–	≤ 300	(Travkin et al., 2001)
Aliphatic alcohols	6–10.5	6–10	40–50	150–300	(Baradel et al., 1986a; Baradel and Guerriero, 1988)
Alkylated polyphenols	5.9	–	45	200	(Baradel et al., 1986b; Baradel et al., 1987)
NMPL	0.075	–	–	137–196	(Avila-Rodriguez et al., 2001)
Trioctylphosphine oxide	2.3	18	28.3	187.2	(Marr et al., 1985)
Hydroxamic acids	10.4–21.5	9.6–21.5	32–54.3	153–225	(Schwab and Kehl, 1989; Kehl et al., 1991)
Mixtures of NOPCs and aliphatic alcohols	90–120	–	30	110–145	(Hiemeleers et al., 1978)
NOPCs, mainly TBP	3.9–11.5	12.3–14.5	8.7–33.1	100–400	(Totsuka et al., 1986)
TBP, DBBP, DPPP, TAPOs	1.4–15.5	–	35–45	140–220	(Dreisinger et al., 1993a; Dreisinger et al., 1993b)

D2EHMP = bis(2-ethylhexyl) methylphosphonate
DBBP = dibutyl butylphosphonate
DPPP = dipentyl pentylphosphonate
HBPTA = hexabutylphosphoric triamide
NMPL = 1-(2,6-dimethylheptyl-4-oxy)-3 methyl-1-oxo-Δ^3-phospholen
NOPC = neutral organophosphorus compound
TAPO = trialkylphosphine oxide

Table 2
Compositions of the feed solutions.

	Shipment #1	Shipment #2
$c(H_2SO_4)$ [g dm^{-3}]	1022.2	963.3
c(As) [g dm^{-3}]	23.9	32.5
$c(As^{3+})$ [%]	9.2	7.1
c(Ni) [g dm^{-3}]	2.1	2.6
c(Cu) [ppm]	2.5	18.9
c(Zn) [ppm]	0.8	< LOD
c(Cd) [ppm]	< LOD	0.1
c(Sb) [ppm]	117.3	187.0
c(Hg) [ppm]	0.7	2.0
c(Pb) [ppm]	1.1	2.0
c(Bi) [ppm]	4.9	43.3

LOD = Limit of detection

600 g dm^{-3} H_2SO_4 feed concentration with synthetic solutions but countercurrent results were reported for non-concentrated copper electrolyte. Concentrating the solution before extraction to H_2SO_4 levels higher than 6 M aims to reduce equipment size further, yield high concentration of arsenic in the stripping raffinate, and enable small volumetric throughput of water and tributyl phosphate (TBP) in the extraction process.

Precise mechanisms and stoichiometry of solvation in extraction of arsenic are not very well known. Travkin et al. (Travkin et al., 1993) have described the extraction of arsenic(V) with Eq. (1)

$$n\mathrm{H_3AsO_4} + h\mathrm{H_2O} + q\bar{\mathrm{S}} \rightleftarrows n\overline{\mathrm{H_3AsO_4 \bullet}h_0\mathrm{H_2O \bullet}q\mathrm{S}} + (h - h_0)\mathrm{H_2O} \quad (1)$$

where S denotes an extractant molecule, and n, h, h_0 and q are stoichiometric constants that depend on the reaction conditions and extractant. When the feed solution contains H_2SO_4, it is co-extracted and associated in the complex (Travkin et al., 1993). TBP is known to extract only arsenic(V) in significant amounts (Giganov et al., 1978) but alcohols and glycols extract also arsenic(III) (Szymanowski, 1998; Baradel et al., 1986a; Baradel and Guerriero, 1988; Baradel et al., 1986b; Baradel et al., 1987). D(As) is known to decrease with several solvating extractants when temperature is increased (Travkin et al., 1993).

It is generally agreed that increasing H_2SO_4 concentration in the feed enhances the extraction of arsenic (Szymanowski, 1998; Iberhan and Wiśniewski, 2003; Iberhan and Wiśniewski, 2002; Wiśniewski, 1997; Wiśniewski, 1998; Ballinas et al., 2003; Navarro and Alguacil, 1996; Dermirkiran and Rice, 2002; Travkin et al., 1993; Travkin et al., 2001; Totsuka et al., 1986). Also, the more H_2SO_4 in the feed, the more aggressive becomes the co-extraction of H_2SO_4. Co-extraction of H_2SO_4 and water causes expansion of the organic phase and simultaneous shrinkage of the aqueous phase, *i.e.* phase ratio changes during extraction. This phenomenon is not significant in extractions with 2–3 M H_2SO_4 solutions, since the absolute amount of co-extracted H_2SO_4 and water are relatively low. Another limitation caused by very high H_2SO_4 concentration in the feed is that neutral organophosphorus compounds (NOPCs) must be used without kerosene-based diluents. Otherwise the system will split into three phases. Third phase formation was also experimentally verified in current study.

To the best of our knowledge, results on extraction of arsenic from extremely concentrated (*i.e.* 10 M or higher) H_2SO_4 solutions have not been published previously and comparisons of TBP and aliphatic alcohols in extraction of arsenic from the same feed solution are missing. Moreover, the performance of alcohols has been reported only for the non-concentrated H_2SO_4 solutions, perhaps due to their reactivity. According to speciation calculations by MEDUSA KTH, Kungliga Tekniska Högskolan, 2019), the fraction of H_3AsO_4 in aqueous H_2SO_4 solution is sensitive to changes in redox-potential (see Section 3, Fig. 10). Design methods and process parameters that are suitable for non-concentrated copper electrolytes are not necessarily applicable with highly concentrated H_2SO_4 solutions. Inconsistencies between McCabe–Thiele analyses and batch countercurrent simulations were reported already at 2 mol dm^{-3} H_2SO_4 (Dermirkiran and Rice, 2002). Process design by McCabe–Thiele or Hunter–Nash methods is challenging, since the apparent D(As) values change with the speciation.

In this work, the separation of arsenic and H_2SO_4 from an industrial 10 M H_2SO_4 solution using undiluted TBP is studied. A flowsheet involving countercurrent extraction, H_2SO_4 scrubbing and arsenic stripping steps (De Schepper and Van Peteghem, 1977) is investigated by pseudo-countercurrent (pseudo-cc) method (Haghighi et al., 2015; Thornton, 1992). Pseudo-cc results are compared with the conventional McCabe-Thiele or Hunter-Nash –type graphical designs that utilize conventionally determined equilibrium curves. Differences in performance of TBP and the mixture of 1,2-octanediol and 2-ethylhexanol are discussed.

2. Experimental

Two shipments of 10.4 M H_2SO_4 solution were received from industry for the extraction studies. Compositions of these acid batches are given in Table 2, and theoretical speciation analysis is shown in Fig. 2, where speciation at $\log([H^+]_{tot}) \approx 1.3$ should approximately represent the feed solution. Only arsenic and nickel were considered in speciation calculation in Fig. 2, and the metals at ppm-levels were neglected. Ionic strength was approximated iteratively in all speciation calculations.

2.1. Chemicals

97% tributyl phosphate (TBP) (M = 266.31 g mol^{-1}), ≥ 90% dibutyl butyl phosphonate (DBBP) (M = 250.31 g mol^{-1}), ≥ 99% 2-ethyl-1-hexanol (M = 130.23 g mol^{-1}) and 98% 1,2-octanediol (M = 146.23 g mol^{-1}) were obtained from Merck KGaA (Sigma-Aldrich). A commercial mixture of trialkylphosphine oxides (Cyanex

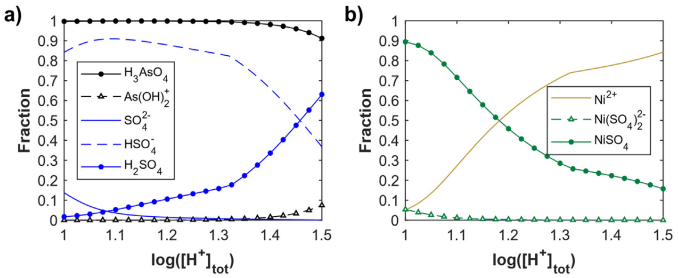

Fig. 2. Effect of proton concentration on speciation of: a) arsenic and H_2SO_4; and b) nickel in the feed solution. Constructed with MEDUSA (KTH, Kungliga Tekniska Högskolan, 2019) using following parameters: $c(SO_4^{2-})_{tot}$ = 10 M, $c(Ni^{2+})_{tot}$ = 0.036 M, $c(AsO_4^{3-})_{tot}$ = 0.32 M, E_h = +0.71 V and T = 25 °C.

923) containing mainly *n*-octyl- and *n*-hexyl hydrocarbon chains was supplied by Cytec (now Solvay). Aliphatic hydrocarbon mixture Exxsol D80 (supplied by Exxon Mobil) was used in preliminary tests with the NOPCs. All chemicals were used as received.

Dilution of TBP, DBBP and Cyanex 923 in Exxsol D80 resulted in third phase formation when extraction from 10.4 M H_2SO_4 solution was attempted. After the observed problem of third phase formations with diluted NOPCs, 97 vol-% TBP was used in the experiments without dilution and it is referred to as undiluted TBP in this text. Cyanex 923 was too viscous in room temperature (21 ± 1 °C) to be used without dilution, and DBBP was not available in sufficient quantities. 6 wt-% solution of 1,2-octanediol in 2-ethylhexanol was prepared for the experiments. The composition of the alcohol mixture was based on works by Baradel & Guerriero (Baradel and Guerriero, 1988) and Szymanowski (Szymanowski, 1998). Deionized and RO-filtered water was used for back-extractions from the loaded extractants.

2.2. Analytical methods

Total concentration of arsenic and metal concentrations were measured from aqueous samples using ICP-MS (Agilent 7900). Samples from the organic phases were back-extracted with pure water at A/O = 30, and concentrations in the back-extraction raffinates were measured to obtain the organic phase equilibrium concentrations. As (III) concentrations in the feed solution were analyzed in an external accredited laboratory. H_2SO_4 concentrations in raffinate samples were determined by acid-base titration with NaOH, and concentrations of H_2SO_4 in the organic phases were calculated from mass balance. Parallel determination of total sulfur with ICP-MS was in good agreement with mass balance calculations in conventional batch extraction experiments. Deviations between the determination by NaOH-titration and ICP-MS analysis were found for samples from scrubbing and stripping experiments. Simultaneous neutralization of H_3AsO_4 became significant as acidity was adequately low in these samples, which affected NaOH consumption in titration. Therefore, ICP-MS data was used in calculation of the pseudo-countercurrent results. Phase densities were measured at 23 °C using an Anton Paar DMA4500 density meter. A Mettler-Toledo LE-150 ORP Ag/AgCl electrode was used for redox potential measurements.

2.3. Experiments

All extraction experiments were performed in glass separation funnels at 21 ± 1 °C. Phases were mixed by using an orbital shaker. Equilibration time of 20 min and shaking rate of 300 min^{-1} were used. The phases were separated by gravity and samples were taken after both phases were considered clear by visual observation. As phase separation problems occurred in certain experiments with the alcohol mixture, phase disengagement was aided by centrifugation for 10 min at 4000 min^{-1}. Loading and stripping isotherms were determined by carrying out several batch extractions with different O/A ratios. In order to quantify the change in phase weights and volumes, separation funnels were weighed before and after each addition or removal of a phase.

2.3.1. Pseudo-countercurrent extractions

Separation of arsenic and sulfuric acid in countercurrent liquid-liquid extraction cascades was experimentally studied by batch extractions according to a pseudo-countercurrent (pseudo-cc) scheme (Fig. 3) described by Haghighi et al. (Haghighi et al., 2015). After several consecutive cycles, the system approaches conditions similar to an actual countercurrent cascade (Fig. 4). Blocks in Fig. 3 represent one batch extraction experiment, and approach to the steady state was monitored by analyzing the cascade outlet streams as reported by Matveev et al. (2018) (Matveev et al., 2018). Steady-state was assumed when concentrations in the outlet streams, *i.e.* $E_{1,n}$ and $R_{3,n}$ in Fig. 3,

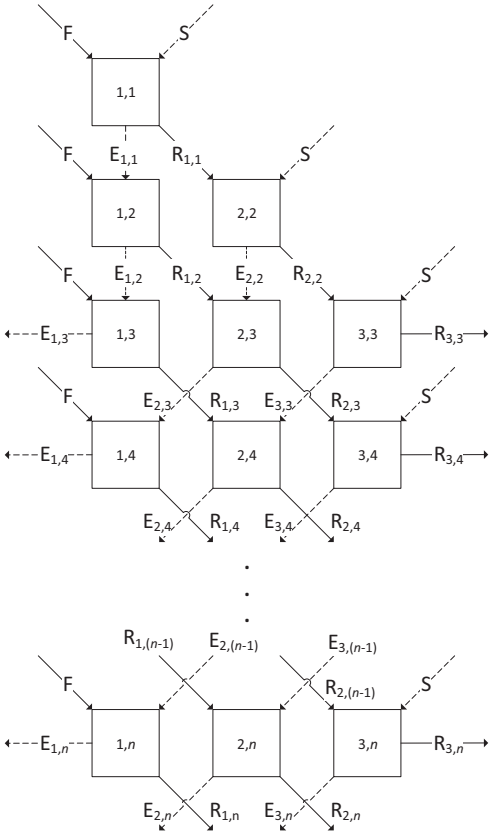

Fig. 3. Pseudo-countercurrent scheme for three extraction stages. *n* is the number of cycles. E = extract, F = feed, R = raffinate, and S = solvent.

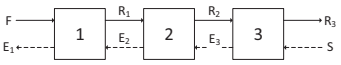

Fig. 4. Schematic diagram of continuous three-stage countercurrent extraction. E = extract, F = feed, R = raffinate, S = solvent.

Table 3
Pseudo-countercurrent extractions.

	Run 1	Run 2	Run 3	Run 4	Run 5
O/A	0.8	4	0.5	2	2
Type	extraction	scrubbing	stripping	stripping	stripping
Stages	3	2	2	2	4
Cycles	9	6	6	6	13
Extractions	24	11	11	11	46

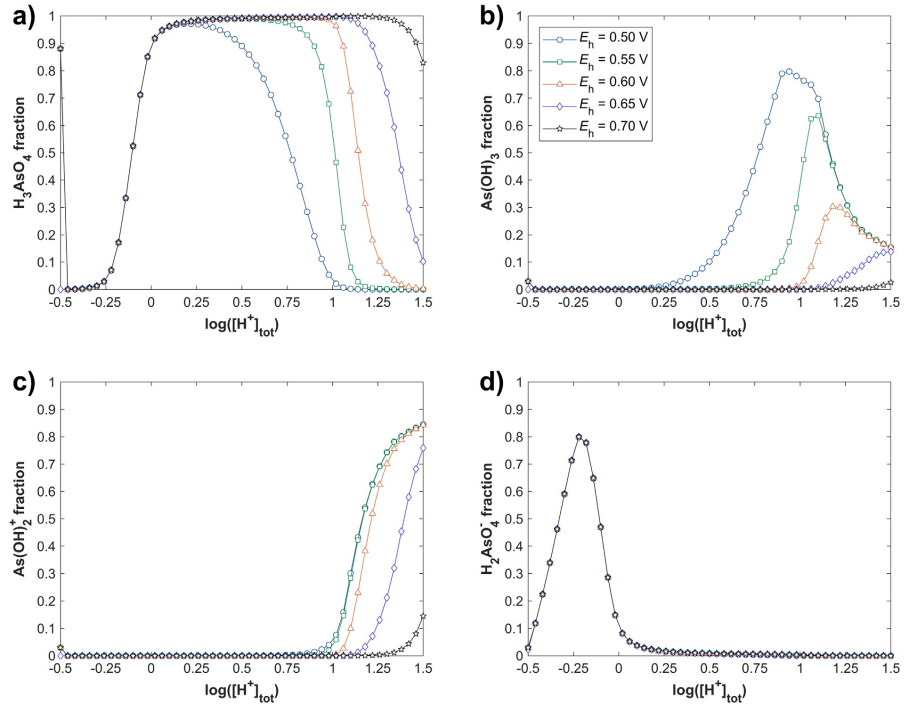

Fig. 5. Effect of redox potential, E_h, on speciation of arsenic in H_2SO_4 solutions at 25 °C. Calculated with MEDUSA (KTH, Kungliga Tekniska Högskolan, 2019) using iterated ionic strength; $c(AsO_4^{3-})_{tot}$ = 0.31 M; $c(SO_4^{2-})_{tot}$ = 10 M.

remained constant in consecutive cycles. Table 3 summarizes the pseudo-cc extractions done in this work.

3. Results and discussion

Speciation calculations (Fig. 5) showed that fractions of H_3AsO_4, $As(OH)_3$ and $As(OH)_2^+$ in concentrated H_2SO_4 solutions are sensitive to changes in redox potential. The fraction of extractable H_3AsO_4 should remain high also in very concentrated H_2SO_4 providing that the redox potential of the solution is +0.65 V or above (Fig. 5a). The fraction of $H_2AsO_4^-$ in mildly acidic solutions seems to be unaffected by changes in redox potential (Fig. 5d). The same observation was made for $HAsO_4^{2-}$ (plot not shown).

3.1. Extraction of arsenic and H_2SO_4

97 vol-% TBP and the mixture of 6 wt-% 1,2-octanediol in 2-ethylhexanol behaved quite similarly in extraction (Table 4, Fig. 6). Percentages of arsenic and H_2SO_4 extracted by TBP and the alcohol mixture were practically the same for both extractants (Fig. 7). However, 22.5 g dm^{-3} peak loading concentration of arsenic in the alcohol mixture is slightly lower than the 26.4 g dm^{-3} measured for TBP (Fig. 6).

Mass balance calculations showed a 1:2:1 ratio of H_2SO_4:H_2O:TBP in the loaded organic phase, when $c(H_2SO_4)_{org}$ was 200–300 g dm^{-3}. When $c(H_2SO_4)_{org}$ decreased below 15 g dm^{-3} in stripping, the stoichiometric ratio H_2O:TBP was 7:1. Respectively, H_2O:alcohol ratio was 1:1 when there was 200–370 g dm^{-3} H_2SO_4 in the loaded alcohol phase, but H_2SO_4:alcohol ratio varied between 0.4 and 0.9. Loading isotherms for H_2SO_4 (Fig. 6b) are linear, and the slopes of the isotherms are quite similar to those reported by Gromov et al. for 2-ethyl-1-hexanol (Gromov et al., 2018).

Arsenic was more selectively extracted by TBP at O/A between 0.1 and 1, whereas at O/A ratios 2 and 3.5 the alcohol mixture was more selective to arsenic. D(As) of approximately 2.7 published by Navarro & Alguacil (Navarro and Alguacil, 1996) is probably the highest reported for undiluted TBP. It was obtained with a feed containing 18 g dm^{-3} arsenic and 600 g dm^{-3} H_2SO_4 (Navarro and Alguacil, 1996). Typical D(As) values for TBP have ranged between 0.4 and 1.7 for feed solutions

Table 4
Comparison of TBP and alcohol mixture in extraction of arsenic and H_2SO_4 from feed solution containing 23.9 g dm^{-3} of arsenic and 1022.2 g dm^{-3} of H_2SO_4.

O/A	TBP			6 wt-% 1,2-octanediol in 2-ethylhexanol		
	D(As)	$D(H_2SO_4)$	ß(As/H_2SO_4)	D(As)	$D(H_2SO_4)$	ß(As/H_2SO_4)
0.1	1.22	0.34	3.54	1.01	0.37	2.74
0.125	1.27	0.36	3.50	1.07	0.38	2.79
0.25	1.24	0.34	3.68	1.02	0.37	2.72
0.5	1.28	0.33	3.92	1.03	0.36	2.88
0.8	1.31	0.32	4.07	0.93	0.35	2.64
1	1.22	0.31	3.92	1.14	0.35	3.26
2	1.04	0.30	3.41	1.31	0.31	4.20
3.5	0.74	0.30	2.46	1.52	0.29	5.19

ß(As/H_2SO_4) = D(As)/$D(H_2SO_4)$.

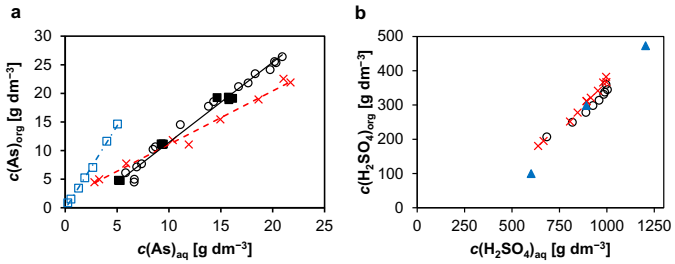

Fig. 6. Loading isotherms for extraction of arsenic (a) and H_2SO_4 (b) from feed solution containing 23.9 g dm^{-3} arsenic and 1022.2 g dm^{-3} H_2SO_4. Undiluted TBP (circles), undiluted TBP in pseudo-cc extraction (filled squares), 6 wt-% 1,2-octanediol in 2-ethylhexanol (crosses), undiluted TBP & 600 g dm^{-3} H_2SO_4 in the feed (Navarro and Alguacil, 1996) (hollow squares), 2-ethylhexanol (Gromov et al., 2018) (triangles).

with 1–3 M H_2SO_4 (Navarro and Alguacil, 1996; Dermirkiran and Rice, 2002; Travkin et al., 1993; Travkin et al., 2001; Dreisinger et al., 1993b). For 10.4 M H_2SO_4 solution containing 23.9 g dm^{-3} arsenic, the highest *D*(As) in the current experiments was 1.31 (Table 4). The probable reason for lower *D*(As) compared with Navarro's & Alguacil's (Navarro and Alguacil, 1996) results is that the feed in current study contained higher amount of undissociated H_2SO_4 (Fig. 2a). The higher amount of undissociated H_2SO_4 makes competition between H_2SO_4 and H_3AsO_4 more aggressive. Together with possible differences in redox potential, the greater amount of undissociated H_2SO_4 explains the lower *D*(As) in the current study (Fig. 5).

D(As) values of aliphatic alcohols are available in the literature only for 150–200 g dm^{-3} H_2SO_4 solutions (Szymanowski, 1998; Iberhan and Wiśniewski, 2003; Baradel et al., 1987). Iberhan & Wiśniewski (Iberhan and Wiśniewski, 2003) published a *D*(As(V)) value of approximately 0.4 for 2-ethylhexane-1,3-diol with 150 g dm^{-3} H_2SO_4. In the current study *D*(As) ranged from 0.9 to 1.5 for 6 wt-% 1,2-octanediol in 2-ethylhexanol. As with TBP, the overall distribution coefficients of arsenic are very dependent on the feed composition.

3.1.1. Phase behavior

Change in phase ratio, Δ(O/A), with alcohol mixture at initial O/A ratios between 0.1 and 1.5 is slightly more extensive than Δ(O/A) for TBP (Fig. 8a). The more extensive Δ(O/A) can explain the slightly more gradual loading isotherm (Fig. 6a). Because of the changes in phase ratios, percentages of extraction are not precisely deducible from distribution coefficients alone.

The feed acid became completely miscible with TBP at initial O/A = 6.5. With complete or near-complete uptake of feed acid into the organic phase there would be little or no raffinate stream coming from the extraction stages. Therefore, O/A ratios above 4 were not tested with the alcohol mixture after miscibility observations with TBP. In general, phase behavior at room temperature favors the use of TBP. Samples from backextraction analyses (A/O = 30) of the alcohol mixture had to be centrifuged, since the backextracted samples were still hazy four days after shaking. In the case of TBP, backextracted organic samples were separated by gravity and no centrifugation was required. Baradel et al. (Baradel et al., 1986b) reported that raising the temperature provides faster phase separation, which could improve phase behavior of the alcohol mixture. On the other hand, increasing the temperature would also increase the reactivity of the alcohols (see Section 3.2.1).

3.1.2. Extraction performance in countercurrent operation

McCabe–Thiele interpolation with linear operating lines has been used by several authors (Wiśniewski, 1998; Navarro and Alguacil, 1996; Dermirkiran and Rice, 2002) in evaluation and development of LLE flowsheets for separating arsenic and H_2SO_4 from dilute to moderately concentrated H_2SO_4. The requirement for a linear operating line would be that O/A ratios remain constant between the stages and no speciation changes take place in the system (Wankat, 2009). Demirkiran & Rice (Dermirkiran and Rice, 2002) have already reported inconsistencies between McCabe–Thiele constructions and experimental results. Therefore, pseudo-cc extractions by TBP were used to study the distributions in countercurrent cascades. Due to the unpredictable phase behavior of 1,2-octanediol and 2-ethylhexanol in back-extraction and better phase separation observed with TBP, the alcohol mixture was not investigated by pseudo-cc method.

Three stages with O/A = 0.8 (higher $ß(As/H_2SO_4)$ for TBP, see Table 4) was selected to study countercurrent extraction, since 95% extraction of arsenic with three countercurrent extraction stages operating at O/A = 1.17 was reported earlier by Navarro & Alguacil (Navarro and Alguacil, 1996). Even such a low number of stages is enough to reveal possible curvature in an operating line. Initial O/A = 0.8 produced an equilibrium O/A of 1.38 in conventional batch experiments (Fig. 8a), and thus using O/A = 0.8 does not lower the volume of the raffinate too much.

Concentration profiles for arsenic and H_2SO_4 in three-stage pseudo-

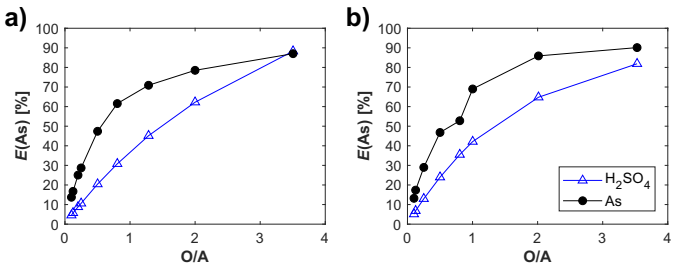

Fig. 7. Percentages of arsenic and H_2SO_4 extracted from feed solution containing 23.9 g dm^{-3} of arsenic and 1022.2 g dm^{-3} of H_2SO_4: a) 97 vol-% TBP; b) 6 wt-% 1,2-octanediol in 2-ethylhexanol.

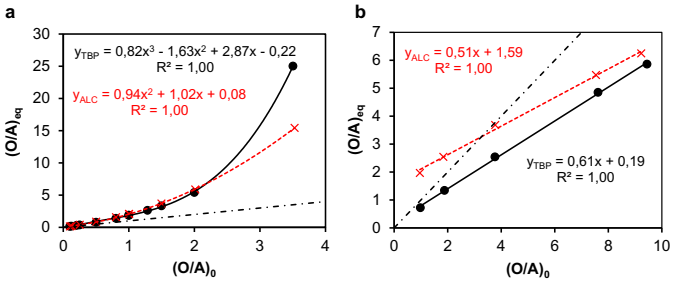

Fig. 8. Changes in O/A ratios in extraction (a) and scrubbing (b) of arsenic and H_2SO_4 from feed solution Shipment #1. 97 vol-% TBP (circles), 6 wt-% 1,2-octanediol in 2-ethylhexanol (crosses). Dash-dot line represents constant phase ratio.

Table 5
Results of three-stage pseudo-cc extraction. The feed solution contained 23.9 g dm^{-3} arsenic and 1022.2 g dm^{-3} H_2SO_4. O/A = 0.79 (in); E/R = 1.43 (out).

Stage	1	2	3
$V_{0,aq}$ [cm^3]	124.7	121.8	111.5
$V_{0,org}$ [cm^3]	124.7	125.3	99.0
$V_{0,tot}$ [cm^3]	249.5	244.8	213.6
O/A	1.00	1.03	0.89
$V_{t,aq}$ [cm^3]	123.6	118.2	87.6
$V_{t,org}$ [cm^3]	125.7	129.0	121.3
$V_{t,tot}$ [cm^3]	249.6	245.2	214.3
E/R	1.02	1.09	1.38
D(As)	1.31	1.20	0.93
$D(H_2SO_4)$	0.29	0.29	0.28
$ß(As/H_2SO_4)$	4.56	4.09	3.31
$c(As)_{aq}$ [g dm^{-3}]	14.65	9.26	5.14
$c(As)_{org}$ [g dm^{-3}]	19.24	11.14	4.78
$c(H_2SO_4)_{aq}$ [g dm^{-3}]	1015.0	994.4	904.9
$c(H_2SO_4)_{org}$ [g dm^{-3}]	292.1	292.9	254.2

cc extraction are given in Table 5 and Fig. 9b. In Table 5 the feed solution entered at stage 1, and TBP at stage 3, respectively. V_0 values indicate the initial phase volumes of the stages and V_t is used to describe the volumes at equilibrium. 83.7% of the arsenic and 31.4% of the H_2SO_4 were extracted at O/A = 0.79. The percentage of arsenic extracted is somewhat lower than reported in (Navarro and Alguacil, 1996) for O/A = 1.17. Arsenic is significantly extracted in all stages, but the concentration profiles of the cascade show that most of the H_2SO_4 extraction occurs in stage 3 where TBP is fed (Table 5). Additional extraction stages should therefore enhance the separation and increase E(As), since cumulative $E(H_2SO_4)$ remains practically constant in the stages that follow the TBP feeding stage. Enhancement in separation is seen also from the increase in $ß(As/H_2SO_4)$ and D(As) from stage 3 to stage 1. After three-stage extraction, TBP contained 19.24 g dm^{-3} arsenic and 292 g dm^{-3} H_2SO_4. Respectively, the raffinate composition was 5.14 g dm^{-3} arsenic and 905 g dm^{-3} H_2SO_4.

Simplified McCabe–Thiele analysis suggests that five stages are required to extract 83.7% of the arsenic at O/A = 0.79 (Fig. 9a). The pseudo-cc steady-state compositions indicate that such extraction results could be achieved in only three countercurrent stages (Fig. 9b). The McCabe–Thiele analysis in Fig. 9a was constructed by utilizing conventional batch experiment data and assuming constant phase ratio. The percentage of extraction was set to 83.7%, which was achieved in real pseudo-cc experiments. There were probably no significant changes in the aqueous speciation during extraction, as the equilibrium line remained fixed in the pseudo-cc experiments (Fig. 6a and Fig. 9). Theoretical McCabe–Thiele diagram (Fig. 9a) predicted a higher number of stages because curvature in the operating line was not considered.

3.2. Back-extraction

Separation of arsenic and H_2SO_4 in back-extraction is based on the different strength of the acids. As a stronger acid H_2SO_4 dissociates at higher proton concentration than H_3AsO_4 (Fig. 10). Protons and anions which are formed by dissociation have much stronger affinity to water, and they are back-extracted more aggressively than the undissociated acids. According to theoretical calculations (Fig. 10), the first dissociation of H_3AsO_4 starts approximately when $\log([H^+]) = 0.5$ in the raffinate. At this proton concentration there is no undissociated H_2SO_4 in the aqueous solution.

Theoretically it would be favorable to increase O/A ratio stage by

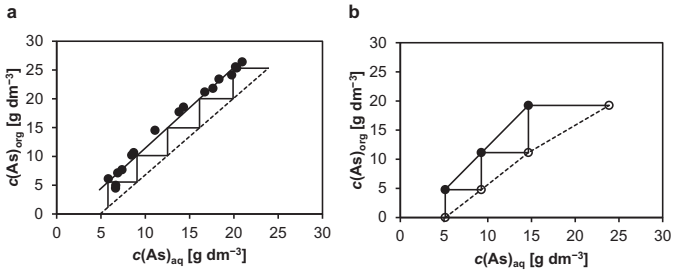

Fig. 9. Comparison of theoretical McCabe-Thiele analysis (a) with the experimental results (b). O/A = 0.79 and 83.7% removal of arsenic. $c_0(As)_{aq}$ = 23.9 g dm^{-3} and $c_0(As)_{org}$ = 0.

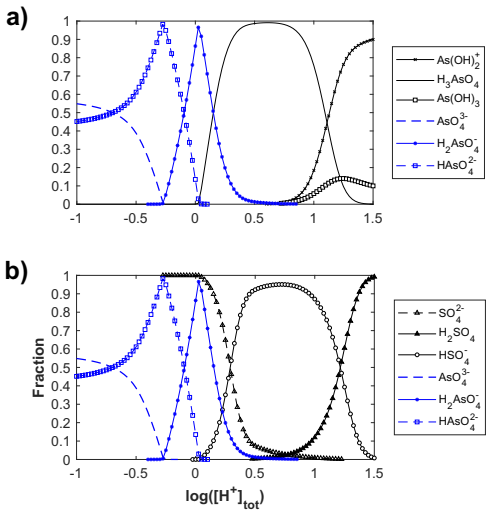

Fig. 10. Effect of proton concentration on speciation of H_3AsO_4 and H_2SO_4. Calculated by MEDUSA (KTH, Kungliga Tekniska Högskolan, 2019). Input parameters for MEDUSA are the same as were measured for stripping raffinate in the pseudo-cc experiments (Section 3.2.2): $E_h = +649$ mV; $c(AsO_4^{3-})_{tot} = 0.536$ M; $c(SO_4^{2-})_{tot} = 0.653$ M; $T = 25$ °C; iterated ionic strength.

stage in H_2SO_4 scrubbing so that $0.5 \leq \log([H^+]) \leq 1$ in the back-extraction raffinates. This type of fractional extraction could be attempted to separate the acids completely. If the fractional extraction approach turns out to be non-feasible in practice, at least bulk separation can be done by solvent extraction to produce a relatively low volume of arsenic-rich solution whose total concentration of SO_4^{2-} is significantly lower. It can be concluded from Fig. 5a and Fig. 10 that co-extraction of H_2SO_4 does not lower the separation efficiency as long as the redox potential is sufficiently high in the initial feed solution.

3.2.1. Scrubbing

Organic phases were prepared for the batch scrubbing experiments by loading both extractants with the feed solution from Shipment #1 at O/A = 0.1. Water scrubbing of loaded TBP exhibited very similar behavior to that reported by Navarro & Alguacil (Navarro and Alguacil, 1996). 17.2% of arsenic and 59.3% of H_2SO_4 were back-extracted at O/A = 3.77 (Fig. 11). Selectivity towards H_2SO_4 with O/A ≈ 4 and above was maintained in consecutive scrubbing treatment. Back-extraction with water is more selective to H_2SO_4 until the acidity of the system gets sufficiently low (Fig. 10). Separation of arsenic and H_2SO_4 by TBP is clearly better than by the mixture of 1,2-octanediol and 2-ethylhexanol. Moreover, phase separation times were longer for the alcohol mixture.

Another issue with using the mixture of 1,2-octanediol in 2-ethylhexanol is the reactivity of the alcohols. Etherification of 2-ethylhexanol is likely to occur, especially at slightly elevated temperatures (Hendrickson et al., 1970). The redox potential of the feed solution was approximately +710 mV *vs.* SHE at +21 °C and it is questionable whether the oxidation reactions of alcohols are negligible under such conditions. Coupled with possible reactions of the diol, the resulting mixture has practically an unknown composition. The reaction products themselves probably have extractive properties but their mutual solubilities with water are likely different compared with the original alcohol constituents (Kislik, 2012). Water-miscible reaction products would explain the observed difficulties in back-extraction of the organic samples (Section 3.1.1).

In scrubbing of the loaded TBP, O/A ratios decreased as expected, due to back-extraction of H_2SO_4 (Fig. 8b). However, in scrubbing of the loaded alcohol mixture with initial O/A ratios of 1 and 2, the O/A ratios increased, suggesting that some H_2O was still extracted to the organic phase. The scrubbing raffinates were quite concentrated H_2SO_4 solutions up to 750 g dm^{-3} but they also contained significant amounts of arsenic, especially the raffinates from scrubbing of the alcohol mixture (Table 6). Scrubbing raffinates can be recycled back to extraction stages.

As the literature (Szymanowski, 1998; Iberhan and Wiśniewski, 2003; Dermirkiran and Rice, 2002; Travkin et al., 1993) suggests, if the As(V) species are predominant and in an extractable form of H_3AsO_4 in the solution, arsenic can be extracted to the organic phase with co-extraction of H_2SO_4. More complete separation can be achieved in subsequent scrubbing and stripping stages (Fig. 10). However, if extraction is performed from H_2SO_4 solutions in which As(III) species are dominant, in principle H_2SO_4 should be more selectively extracted by TBP. SO_2 absorption can be used to reduce As(V) species to As(III) (Szymanowski, 1998; Dermirkiran and Rice, 2002; Totsuka et al., 1986), which is what happens in certain types of gas scrubbing.

TBP was loaded for the pseudo-cc scrubbing and stripping experiments by contacting it with the feed acid from Shipment #2 at O/A = 0.1. TBP prepared in this way contained initially 35.3 g dm^{-3} of arsenic and 284.2 g dm^{-3} of H_2SO_4 (Table 7). Two-stage scrubbing with an O/A ratio of 4.03 back-extracted 24.9% of arsenic and 83.6% of H_2SO_4. Concentrations in the scrubbed TBP were 30.5 g dm^{-3} and 53.5 g dm^{-3} for arsenic and H_2SO_4, respectively. The composition of the scrubbed TBP is promising for producing an arsenic-rich stripping raffinate, although the scrubbing could be optimized further. The

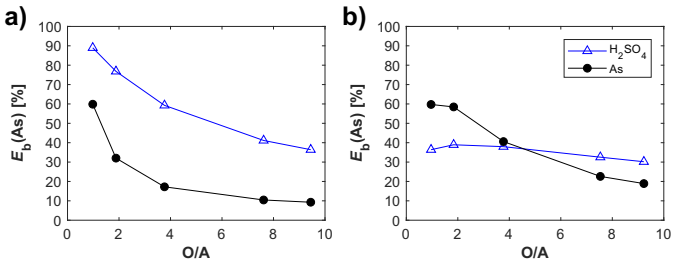

Fig. 11. Back-extraction percentages in scrubbing of the loaded extractants. a) 97 vol-% TBP with 25.3 g dm^{-3} arsenic and 330 g dm^{-3} H_2SO_4. b) 6 wt-% 1,2-octanediol in 2-ethylhexanol with 21.9 g dm^{-3} arsenic and 390 g dm^{-3} H_2SO_4.

Table 6
Distribution of arsenic and H_2SO_4 in water scrubbing of loaded TBP (25.3 g dm^{-3} arsenic and 330 g dm^{-3} H_2SO_4) and a mixture of 1,2-octanediol and 2-ethylhexanol (21.9 g dm^{-3} arsenic and 390 g dm^{-3} H_2SO_4).

O/A	TBP				6 wt-% 1,2-octanediol in 2-ethylhexanol			
	$[As]_{aq}$ [g dm^{-3}]	$[As]_{org}$ [g dm^{-3}]	$[H_2SO_4]_{aq}$ [g dm^{-3}]	$[H_2SO_4]_{org}$ [g dm^{-3}]	$[As]_{aq}$ [g dm^{-3}]	$[As]_{org}$ [g dm^{-3}]	$[H_2SO_4]_{aq}$ [g dm^{-3}]	$[H_2SO_4]_{org}$ [g dm^{-3}]
1	13.08	12.2	253.7	43.8	19.3	6.6	196.8	174.9
2	12.58	20.0	393.5	88.8	29.8	8.3	331.8	204.7
4	12.38	23.4	555.3	150.3	33.3	13.2	521.0	231.4
8	13.81	24.4	710.3	209.4	28.5	17.9	688.0	260.8
10	14.71	24.5	752.4	224.4	27.3	18.8	730.8	270.7

addition of a third scrubbing stage would enhance the separation. With three scrubbing stages, there could also be room for increasing the O/A while maintaining near-complete scrubbing of H_2SO_4. In the two-stage scrubbing, the volume of the aqueous phase expanded from 19.6 cm^3 to 29.2 cm^3, and it contained 21.6 g dm^{-3} of arsenic and 670.4 g dm^{-3} of H_2SO_4. Increase in O/A would result in a smaller volume of more concentrated scrubbing raffinate, which would make smaller change to the extraction stage feed when recycled.

3.2.2. Pseudo-countercurrent stripping of loaded and scrubbed TBP

The organic phase for the stripping experiments was prepared by scrubbing loaded TBP twice with an aliquot of pure water equivalent to O/A = 4 in single contact. TBP produced by this method contained 25 g dm^{-3} and 35 g dm^{-3} of arsenic and H_2SO_4, respectively.

Results from pseudo-cc back-extraction experiments are summarized in Table 7. 89.7% of arsenic was stripped in four countercurrent stages at O/A = 2, yielding a raffinate with 40 g dm^{-3} arsenic and 64 g dm^{-3} H_2SO_4. Total sulfur in stripped TBP was below the detection limit of the back-extraction-ICP-MS determination (Table 7), and hence it was assumed that all H_2SO_4 was stripped. Arsenic concentration in stripped TBP was 2.7 g dm^{-3}.

Two-stage stripping with pure water is enough to back-extract arsenic almost completely (98.6%) at O/A = 0.5. The resulting stripping raffinate at O/A = 0.5 contained 11.7 g dm^{-3} of arsenic and 14.1 g dm^{-3} of H_2SO_4, whereas with O/A = 2 the concentrations in stripping raffinate were 32.3 g dm^{-3} and 66 g dm^{-3} for arsenic and H_2SO_4, respectively. However, with O/A = 2, back-extraction of arsenic was lowered to 75%. Complete stripping of arsenic requires either the deployment of a sufficient number of stages or decreasing O/A, but a decrease in O/A dilutes the raffinate.

Stripping efficiency and phase separation could be further improved by increasing temperature. Travkin et al. (Travkin et al., 1993) reported a significant decrease in D(As(V)) from over 0.9 at 20 °C to approximately 0.4 at 65 °C. In this work, phase separation by gravity was successful in the experiments at room temperature but overnight settling was required to get rid of haziness in the aqueous phase. Instead of using pure water, dilute saline solution containing *e.g.* Na_2SO_4, Na_2CO_3 or dilute H_2SO_4 can be used for stripping to facilitate phase separation (Szymanowski, 1998; Dermirkiran and Rice, 2002).

3.2.3. Comparison of batch equilibrium data with pseudo-countercurrent data

Concentration of arsenic peaked 29 g dm^{-3} in the conventional stripping isotherm, which was determined by batch stripping by pure water and varying the O/A ratio (Fig. 12a). This stripping isotherm did not reveal the possibility of producing an aqueous stripping raffinate with over 30 g dm^{-3} of arsenic. A linear operating line drawn on the basis of 89% back-extraction for arsenic and O/A = 2 intersects with both equilibrium lines. However, over-the-isotherm performance was observed in four-stage stripping at O/A = 2 as both the isotherm and operating line relocated in the $c(As)_{aq}$ *vs.* $c(As)_{org}$ plot. (Fig. 12c & Fig. 12d).

Two-dimensional graphical constructions (*e.g.* McCabe–Thiele and Hunter–Nash) based on the measured c(As) values fail to describe the separation cascades accurately. The deviations are highlighted especially at back-extraction stages, which can be explained by dissociation

Table 7
Results from pseudo-countercurrent back-extraction experiments.

Target	Scrubbing		Stripping		Stripping		Stripping			
$c_0(H_2SO_4)_{org}$ [g dm^{-3}]	284.2		35.0		35.0		35.0			
$c_0(As)_{org}$ [g dm^{-3}]	35.3		25.0		25.0		25.0			
O/A (in)	4.03		0.5		2.01		2.01			
E/R	2.33		0.45		1.87		1.83			
E(As) [%]	24.9		98.6		75.0		89.7			
$E(H_2SO_4)$ [%]	83.6		100		99.6		100			
Stage	1	2	1	2	1	2	1	2	3	4
$V_{0,aq}$ [cm^3]	19.6	24.4	99.7	97.5	29.6	30.6	29.8	30.0	29.9	30.3
$V_{0,org}$ [cm^3]	72.8	79.2	47.4	49.4	58.1	59.7	57.4	58.2	58.2	59.8
$V_{0,tot}$ [cm^3]	92.4	103.6	147.0	146.9	87.7	90.3	87.1	88.1	88.1	90.1
O/A (stagewise)	3.71	3.24	0.48	0.51	1.96	1.95	1.93	1.94	1.95	1.98
$V_{eq,aq}$ [cm^3]	24.1	29.2	97.5	103.9	30.1	31.6	30.2	30.4	30.2	31.2
$V_{eq,org}$ [cm^3]	68.1	73.5	46.9	47.5	59.1	56.3	57.0	57.7	57.9	58.8
$V_{eq,tot}$ [cm^3]	92.2	102.8	144.3	151.4	89.2	87.9	87.1	88.1	88.1	90.0
E/R (stagewise)	2.83	2.52	0.48	0.46	1.96	1.78	1.89	1.89	1.91	1.88
D(As)	1.31	1.64	0.21	0.34	0.37	0.57	0.27	0.35	0.43	0.58
$D(H_2SO_4)$	0.16	0.25	–	–	–	–	–	–	–	0.03
$ß(As/H_2SO_4)$	8.23	6.68	–	–	–	–	–	–	–	17.35
$c(As)_{aq}$ [g dm^{-3}]	23.33	21.59	1.79	11.72	17.74	32.28	9.84	23.22	35.67	40.13
$c(As)_{org}$ [g dm^{-3}]	30.47	35.43	0.37	4.03	6.51	18.42	2.68	8.20	15.18	23.19
$c(H_2SO_4)_{aq}$ [g dm^{-3}]	337.2	670.4	< 1.7[a]	14.1	3.2	66.0	< 1.3[a]	< 1.3[a]	3.1	64.0
$c(H_2SO_4)_{org}$ [g dm^{-3}]	53.5	164.8	< 5[a]	< 5[a]	< 5[a]	< 5[a]	< 2[a]	< 2[a]	< 2[a]	2.1

[a] Limit of detection

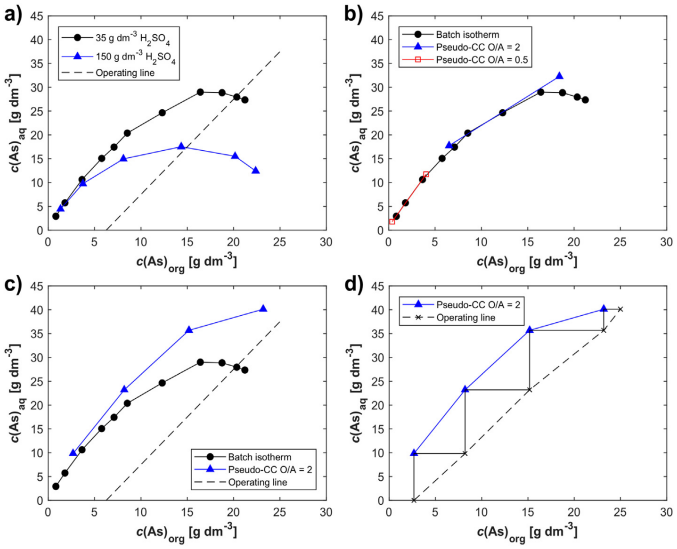

Fig. 12. Arsenic distributions in batch and pseudo-cc experiments: a) influence of H_2SO_4 concentration on batch stripping isotherms; b) comparison of two-stage pseudo-cc equilibrium lines with batch isotherm; c) comparison of four-stage pseudo-cc equilibrium line with batch isotherm; d) McCabe–Thiele plot based on data from four-stage pseudo-cc stripping.

of H_3AsO_4 at low acidity (Fig. 10). Sharply decreasing D(As) in the back-extraction stages (Table 6) is in agreement with this explanation.

No established model describes the chemical equilibria of the system, and thus rigorous mass balance iterations are currently impossible. Furthermore, McCabe–Thiele and Hunter–Nash diagrams or mass balance iterations as such provide only theoretical prediction and can only serve as tools to give initial estimates for piloting studies. Pseudo-cc extraction provides information also about the practical feasibility of a process, and the equilibrium compositions of the streams can be experimentally verified. Drawbacks of the pseudo-cc method are that completing the schemes requires a lot of manual labor and recycle streams are hard to embed in the design by pseudo-cc method. The number of extractions increases rapidly when the number of counter-current stages increases and the schemes must be replicated in order to carry out sensitivity analyses for process parameters. Despite these weaknesses it is a cost-effective intermediate design method for continuous processes involving hazardous materials or processes that require instrumentation with expensive materials.

3.3. Process scheme

Pseudo-cc experiments showed that with certain adjustments and considerations, a similar flowsheet to the one patented by De Schepper & Van Peteghem (De Schepper and Van Peteghem, 1977) is suitable also for treating 10 M H_2SO_4 solutions. Calculation of the flowsheet in Fig. 13 was based on percentages of extraction and phase volume changes that were determined by pseudo-cc experiments. Recycling of expanded TBP, scrubbing raffinate and stripping raffinate bleed was not taken into account. Recycling water-containing stripped TBP and scrubbing raffinate back to extraction might lower *E*(As) slightly. 261.4 dm^3 per time unit less water would be required if scrubbing was carried out by stripping raffinate. Use of stripping raffinate in scrubbing would also help with back-extraction loss of arsenic during scrubbing. If only 5% loss of arsenic is assumed in scrubbing, stripping raffinate would contain 47.6 g dm^{-3} of arsenic, which is close to the 50 g dm^{-3} presented by De Schepper & Van Peteghem (De Schepper and Van Peteghem, 1977). However, the back-extraction percentage of H_2SO_4 would then be lower in scrubbing and it would end in the stripping raffinate without a third scrubbing stage. Treating 1000 dm^3/t of feed acid with 790 dm^3/t of undiluted TBP and 720 dm^3/t of water yielded 737 dm^3/t of raffinate with significantly lowered arsenic concentration, and 487 dm^3/t of arsenic-rich stripping raffinate. Flow rates of stripping raffinate, inlet water and feed acid will be reduced once the recycle streams are connected.

Increasing O/A in extraction would provide higher *E*(As) assuming the same number of stages but it would also decrease the throughput of the process and the $c(H_2SO_4)$ in the raffinate, as the larger amount of fed TBP would extract more H_2SO_4 and H_2O. The throughput would be lower also because higher volume of scrubbing liquor should be recycled to the extraction stages. If higher loading of H_2SO_4 was compensated by decreasing O/A in scrubbing, the throughput of the process would again be decreased due to increased circulation to the feed.

The solvent extraction circuit discussed here aims at bulk recovery of arsenic. Raffinates of the process are classified as hazardous waste not only because of the arsenic but also because of other heavy metals (EUR-Lex, 2019). The environmental limits for heavy metals in aqueous waste in the European Union are 0.15 ppm, 0.03 ppm and 0.2 ppm for arsenic, mercury and lead, respectively. For copper and nickel the limit is 0.5 ppm (EUR-Lex, 2019).

TBP extracts arsenic and H_2SO_4 in significant amounts but partial extraction of mercury was also noticeable in the ICP-MS results. The concentration of mercury was 4.5–8 ppm in the extracts, and it was partially back-extracted in stripping, resulting in 2–3 ppm of mercury in the stripping raffinate. Stripping raffinate requires further SO_4^{2-} removal if As_2O_3 crystallization at high purity is intended, and the mercury must be removed in possible plant operation. Raffinate from the extraction stages could be re-used in applications where the impurities can be tolerated at the levels found, *e.g.* in leaching.

4. Conclusions

Liquid-liquid extraction of arsenic and H_2SO_4 by undiluted TBP (97 vol-%) and mixture of 1,2-octanediol and 2-ethylhexanol was investigated experimentally for treating a 10.4 M industrial H_2SO_4

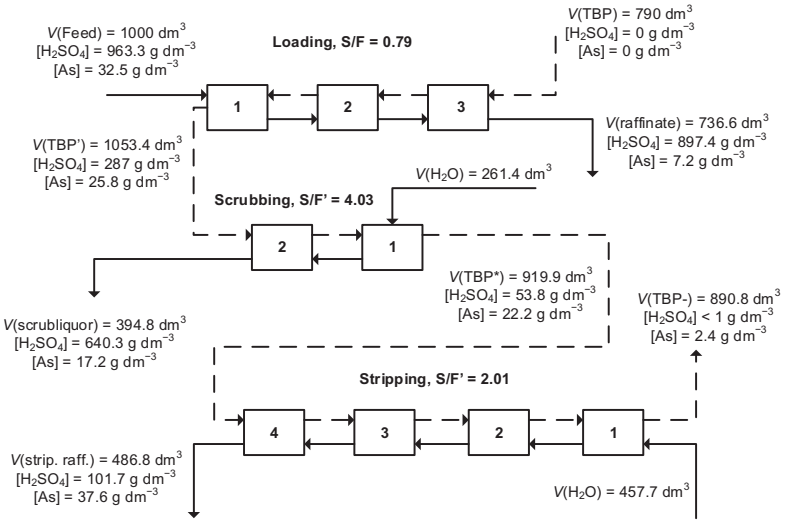

Fig. 13. Flowsheet for separating arsenic and H_2SO_4 as investigated by pseudo-countercurrent experiments.

solution containing 32.5 g dm^{-3} arsenic. If neutral organophosphorus extractants are used, they must be used in undiluted form for such concentrated H_2SO_4 to maintain the system in two phases. Phase behavior of TBP was superior to the mixture of 1,2-octanediol and 2-ethylhexanol in back-extraction of the loaded extractants at room temperature. Moreover, TBP offered better separation of arsenic and H_2SO_4, and the difference in separation efficiency was highlighted in scrubbing.

McCabe–Thiele analyses were shown to be inaccurate in design of liquid-liquid extraction cascades for the system at hand. The Hunter–Nash method could predict H_2SO_4 transfer with reasonable accuracy but the distribution of arsenic is more complicated to describe. Performances of the countercurrent cascades were experimentally determined by a pseudo-countercurrent batch extraction scheme. It was shown that significantly better performance can be achieved in the stripping cascade than could be predicted from a stripping isotherm determined by conventional methods, most probably due to significant changes in aqueous speciation.

A conventional solvent extraction flowsheet utilizing TBP can also be used for very concentrated H_2SO_4 solutions. 83.7% of arsenic was removed by undiluted TBP in three countercurrent stages with a solvent-to-feed ratio of 0.79 from a 10.4 M (1022.2 g dm^{-3}) H_2SO_4 solution containing initially 23.9 g dm^{-3} arsenic. The results show that arsenic concentrations of 40–50 g dm^{-3} in the stripping raffinate can be obtained with the proposed non-optimized flowsheet.

Acknowledgements

Russian-English translations given by Mr. Fedor Vasilyev and experimental assistance provided by Mr. Tommi Huhtanen are gratefully acknowledged.

Funding

This work was supported by Business Finland and industrial partners of the Circular Metal Ecosystems (CMEco) project consortium.

References

Avila-Rodriguez, M., Barron-Zambrano, J.A., Navarro-Mendoza, R., Saucedo-Medina, T.I., 2001. Thermodynamic study of liquid-liquid extraction of arsenic(V) by NMPL from H_2SO_4 medium. Solvent Extr. Ion Exc. 19 (3), 457–472. https://doi.org/10.1081/SEI-100103280.

Ballinas, M.L., San Miguel, E.R., Muños, M., Gyves, J., 2003. Arsenic(V) extraction from sulfuric acid media using DBBP-D2EHPA organic mixtures. Ind. Eng. Chem. Res. 42, 574–581. https://doi.org/10.1021/ie020402a.

Baradel, A., Guerriero, R., Process for Separating Arsenic from Acid Solutions which Contain it, US Patent No. 4737350, 1988, (April 12).

Baradel, A., Guerriero, R., Meregalli, L., Vittadini, I., 1986a. Extraction of As from from copper refining electrolyte. JOM 38 (32), 32–37. https://doi.org/10.1007/BF03257918.

Baradel, A., Guerriero, R., Meregalli, L., Vittadini, I., 1986b. New extractant for arsenic separation from industrial solutions. In: ISEC '86 International Solvent Extraction Conference: Preprints, Volume II, Dechema, Frankfurt, pp. 401–407.

Baradel, A., Guerriero, R., Veronese, G., Process for Separating Arsenic from Acid Solutions Containing it, US Patent No. 4701311, 1987, (October 20).

Dalewski, F., 1999. Removing arsenic from copper smelter gases. JOM 51 (9), 24–26. https://doi.org/10.1007/s11837-999-0153-0.

De Schepper, A., Van Peteghem, A., Treatment of Solutions Containing Impure Metals, US Patent No. 4061564, 1977, (December 6).

Dermirkiran, A., Rice, N.M., 2002. The extraction of arsenic (V) from copper refinery electrolytes with tri-n-butyl phosphate: II – Flowsheet development. In: Sole, K.C., Cole, P.M., Preston, J.S., Robinson, D.J. (Eds.), Proceedings of the International Solvent Extraction Conference, ISEC 2002. SAIMM, Johannesburg, pp. 890–895.

Dreisinger, D.B., Leong, B.J.Y., Balint, B.J., Beyad, M.H., 1993a. The solvent extraction of as, Sb and bi from copper refining electrolytes using organophosphorus reagents. In: Logsdail, D.H., Slater, M.J. (Eds.), Solvent Extraction in the Process Industries Volume 3 – Proceedings of ISEC '93. Elsevier Science Publishers Ltd., Barking, pp. 1271–1278.

Dreisinger, D.B., Leong, B.J.Y., Saito, B.R., West-Sells, P.G., 1993b. The solvent extraction and ion-exchange removal of As, Sb and Bi from copper sulphate-sulphuric acid solutions. In: Hiskey, J.B., Warren, G. (Eds.), Hydrometallurgy: Fundamentals, Technology and Innovations, Society for Mining, Metallurgy and Exploration, pp. 801–815.

EUR-Lex, 2019. Directive 2010/75/EU of the European Parliament and of the Council of 24 November 2010 on industrial emissions (integrated pollution prevention and control). https://eur-lex.europa.eu/eli/dir/2010/75/oj (Accessed: 1 February 2019).

Giganov, G.P., Travkin, V.F., Ankina, N.P., 1978. Extraction of arsenic from acidic solutions with tributylphosphate. Tsvet. Met. 8, 27–29.

Gromov, P.B., Kasikov, A.G., Shchelokova, E.A., Petrova, A.M., 2018. Regeneration of sulfuric acid from electrolyte waste of the copper - smelting plant using solvent extraction. Hydrometallurgy 175, 187–192. https://doi.org/10.1016/j.hydromet.2017.11.008.

Haghighi, H.K., Moradkhani, D., Salarirad, M.M., 2015. Separation of zinc from manganese, magnesium, calcium and cadmium using batch countercurrent extraction

simulation followed by scrubbing and stripping. Hydrometallurgy 154, 9–16. https://doi.org/10.1016/j.hydromet.2015.03.007.
Hendrickson, J.B., Cram, D.J., Hammond, G.S., 1970. Organic Chemistry, 3 ed. McGraw-Hill, New York.
Hiemeleers, J., De Schepper, A., Van Peteghem, A., Treatment of Ores and Metallic by-Products Containing Arsenic and Antimony, US Patent No. 4102976, 1978, (July 25).
Iberhan, L., Wiśniewski, M., 2002. Removal of arsenic(III) and arsenic(V) with Cyanex 925, Cyanex 301 and their mixtures. Hydrometallurgy 63, 23–30. https://doi.org/10.1016/S0304-386X(01)00198-0.
Iberhan, L., Wiśniewski, M., 2003. Removal of arsenic(III) and arsenic(V) from sulfuric acid solution by liquid–liquid extraction. J. Chem. Technol. Biotechnol. 78, 659–665. https://doi.org/10.1002/jctb.843.
Kehl, R., Schwab, W., Sudderth, R.B., Korkosky, G.A., Process for Selective Extraction of Contaminant Elements from Mixtures of Electrolytes in Solution, US Patent No. 5039496, August 13, 1991.
Kislik, V.S., 2012. Solvent Extraction – Classical and Novel Approaches, 1st ed. Elsevier, Oxford.
KTH, Kungliga Tekniska Högskolan, 2019. School of Chemical Science and Engineering, MEDUSA, Chemical Equilibrium Diagrams. https://www.kth.se/che/medusa/) Updated: 26.04.2013, Accessed: 1 February 2019).
Marr, R., Bart, H-J., Wachter, R., Method of Removing Arsenic from Copper Electrolyte, US Patent No. 4503015, 1985, (March 5).
Matveev, P.I., Petrov, V.G., Egorova, B.V., Senik, N.N., Semenkova, A.S., Dubovava, O.V., Valkov, A.V., Kalmkov, S.N., 2018. Solvent extraction of rare earth elements by tri-*n*-butyl phosphate and tri-iso-amyl phosphate in the presence of $Ca(NO_3)_2$. Hydrometallurgy 175, 218–223. https://doi.org/10.1016/j.hydromet.2017.12.007.
Navarro, P., Alguacil, F.J., 1996. Removal of arsenic from copper electrolytes by solvent extraction with tributylphosphate. Can. Metall. Q. 35, 133–141. https://doi.org/10.1016/0008-4433(95)00044-5.
Nazari, A.M., Radzinski, R., Ghahreman, A., 2017. Review of arsenic metallurgy: treatment of arsenical minerals and immobilization of arsenic. Hydrometallurgy 174, 258–281. https://doi.org/10.1016/j.hydromet.2016.10.011.
Opio, F.K., 2013. Investigation of Fe(III)–As(III) Phases and their Potential for Arsenic Disposal. Queen's University, Kingston, Canada.
Piret, N.L., 1999. Removal and safe disposal of arsenic in copper processing. JOM 51 (9), 16–17. https://doi.org/10.1007/s11837-999-0150-3.
Riveros, P.A., Dutrizac, J.E., Spencer, P., 2001. Arsenic disposal practices in the metallurgical industry. Can. Metall. Q. 40, 395–420. https://doi.org/10.1179/cmq.2001.40.4.395.
Schwab, W., Kehl, R., Common separation of Contaminating Elements from Electrolyte Solutions of Valuable Metals, US Patent No. 4834951, 1989, (May 30).
Szymanowski, J., 1998. Removal of toxic elements from copper electrolyte by solvent extraction. Miner. Process. Extr. Metall. Rev. 18, 389–418. https://doi.org/10.1080/08827509808914162.
Thornton, J.D., 1992. Science and Practice of Liquid-liquid Extraction. vol. 1 Oxford University Press, New York.
Totsuka, T., Sasaki, K., Nagai, K., 1986. Fundamental studies on purification of copper electrolyte. Metall. Rev. MMIJ 3 (2), 146–154.
Travkin, V.F., Kravchenko, A.N., Miroevsky, G.P., 1993. Extraction of arsenic and antimony from sulfate solutions with organophosphorus reagents. Tsvet. Met. 4, 14–18.
Travkin, V.F., Glubokov, Y.M., Mironova, E.V., Yakshin, V.V., 2001. Extraction of arsenic (V) with hexabutylphosphoric triamide. Russ. J. Appl. Chem. 74, 1664–1667. https://doi.org/10.1023/A:1014801117889.
US. Department of the Interior, 2018. Final List of Critical Minerals. https://www.federalregister.gov/documents/2018/05/18/2018-10667/final-list-of-critical-minerals-2018 (Accessed: 5 October 2018).
Wankat, P.C. (Ed.), 2009. Separation Process Engineering, 2nd ed. Prentice Hall, Westford.
Wiśniewski, M., 1997. Extraction of arsenic from sulphuric acid solutions by Cyanex 923. Hydrometallurgy 46, 235–241. https://doi.org/10.1016/S0304-386X(97)90003-7.
Wiśniewski, M., 1998. Removal of arsenic from sulphuric acid solutions. J. Radioanal. Nucl. Chem. 228, 105–108. https://doi.org/10.1007/BF02387308.

Publication II

Jantunen, N., Kauppinen, T., Salminen, J., Virolainen, S., Lassi, U., and Sainio, T.
Separation of zinc and iron from secondary manganese sulfate leachate by solvent extraction

Reprinted with permission from
Minerals Engineering
Vol. 173, p. 107200, 2021

Minerals Engineering 173 (2021) 107200

Contents lists available at ScienceDirect

Minerals Engineering

journal homepage: www.elsevier.com/locate/mineng

Separation of zinc and iron from secondary manganese sulfate leachate by solvent extraction

Niklas Jantunen [a], Toni Kauppinen [b], Justin Salminen [c], Sami Virolainen [a,*], Ulla Lassi [b], Tuomo Sainio [d]

[a] LUT University, School of Engineering Science, Yliopistonkatu 34, 53850 Lappeenranta, Finland
[b] University of Oulu, Pentti Kaiteran katu 1, 90014 Oulu, Finland
[c] Boliden Kokkola Oy, Sinkkiaukio 1, 67900 Kokkola, Finland
[d] LUT University, School of Engineering Science, Mukkulankatu 19, 15210 Lahti, Finland

ARTICLE INFO

Keywords:
Continuous solvent extraction
Countercurrent extraction
Anode sludge
Manganese
Zinc
Iron

ABSTRACT

Purification of concentrated manganese sulfate solution by solvent extraction is discussed in this paper. The use of bis(2-ethylhexyl) hydrogen phosphate (D2EHPA) and bis(2,4,4-trimethylpentyl)phosphinic acid (BTMPPA) was studied in removal of impurities from zinc electrowinning anode sludge leachates. Over 99 % of zinc and iron were removed by both extractants at around pH 3 in two mixer-settlers operating in continuous countercurrent mode at a solvent-to-feed (S/F) ratio of 0.43 and $T = 22 \pm 1$ °C. BTMPPA had higher selectivity for zinc and iron over manganese than D2EHPA under all experimental conditions. Extraction of manganese was typically below 10 % and can be limited by crowding the extractants, since the fraction of manganese in both loaded extractants was decreased by decreasing organic to aqueous volumetric ratio (O/A). A significant amount of the co-extracted Mn was recovered by selective stripping with 0.5 M sulfuric acid. Extraction by BTMPPA was more sensitive to pH adjustment than extraction by D2EHPA. Increasing the mean residence time in mixer from 3.6 min to 6.0 min improved the removal of zinc and iron with BTMPPA but the change in residence time had little or no effect on zinc and iron removal with D2EHPA.

1. Introduction

Manganese and zinc are widely used elements in the metallurgical industry. Most of the Mn is used in steelmaking (Matricardi et al., 1995) but it is also a key element in the production of Ni–Mn–Co (NMC) cathode active materials for lithium-ion batteries (LIBs). The global demand for battery chemicals is currently increasing due to the trends of digitization and electrification of vehicles. Zn is also used in battery manufacturing although its primary uses are in corrosion protection, manufacturing of die castings and in the production of brass (Goodwin et al., 1998; Brodd et al., 1992). Anode sludges from Zn electrowinning usually contain around 40 wt% Mn and 6–10 wt% Pb on a dry basis (Kauppinen et al., 2020; Ayala and Fernández, 2013; Zhang et al., 2018). The presence of Zn, Ca, Mg, Na, K and Sr in the sludges at lower than 10 wt% total concentration has been reported; there may also be other base metals in tiny amounts (0.1 % or less each) (Kauppinen et al., 2020; Ayala and Fernández, 2013; Zhang et al., 2018). Aside from Zn electrowinning, Mn-bearing anode sludges are also formed during electrolytic refining of Cu and Mn (Zhang and Cheng, 2007; Wang et al., 2019). Because of their significant Mn content, the anode sludges are acknowledged as secondary sources of Mn.

Zhang and Cheng (2007) have published a comprehensive review of the leaching methods for Mn-containing ores and secondary raw materials. Recently, Kauppinen et al. (2020) applied reductive H_2SO_4 leaching for Zn electrowinning sludges to liberate Mn. The recovery of Mn is high (98.5 %) but leaching of the impurities from such heterogeneous raw materials can rarely be completely avoided. Therefore, the leachates usually require further purification using methods such as solvent extraction, precipitation, adsorption or ion exchange. The impurity levels in the recovered Mn should be as low as possible for re-use applications such as battery manufacturing or the production of metallic Mn. Impurities may be allowed at ppm levels but the tolerable ranges are process- and element-specific (Qina et al., 2015; Krüger et al., 2014; Eilers-Rethwisch et al., 2018; Zhao et al., 2015; Lu et al., 2014; Louis et al., 1859).

The literature on the separation of Mn and Zn in sulfate solutions by

* Corresponding author.
E-mail address: sami.virolainen@lut.fi (S. Virolainen).

https://doi.org/10.1016/j.mineng.2021.107200
Received 14 May 2021; Received in revised form 16 August 2021; Accepted 9 September 2021
Available online 24 September 2021

solvent extraction (Ibiapina et al., 2018; Chen et al., ; Tanong et al., 2017; Biswas et al., 2016; Mishra et al., 2016; Haghighi et al., 2015; Falco et al., 2014; Nayl et al., 2014; Innocenzi and Veglio, 2012; Ahmadipour et al., 2011; Hosseini et al., 2011; Hosseini et al., 2010; Cheng et al., 2010; Lee et al., 2010; Pereira et al., 2007; El-Nadi et al., 2007; Nathsarma and Devi, 2006; Salgado et al., 2003; Cheng, 2000; Devi et al., 1997; Steiner et al., 1992) is summarized in a table that can be found in the electronic supplementary material (ESM). Bis(2,4,4-trimethylpentyl)phosphinic acid (BTMPPA, Cyanex 272) and bis-2-ethylhexyl hydrogen phosphate (D2EHPA) and their Na-salts are the most widely applied reagents (Lee et al., 2010; Pereira et al., 2007; Chen et al., ; Tanong et al., 2017; Biswas et al., 2016; Mishra et al., 2016; Haghighi et al., 2015; Falco et al., 2014; Nayl et al., 2014; Innocenzi and Veglio, 2012; Ahmadipour et al., 2011; Hosseini et al., 2011; Hosseini et al., 2010; Nathsarma and Devi, 2006; Salgado et al., 2003; Cheng, 2000; Devi et al., 1997). 2-ethylhexoxy(2-ethylhexyl)phosphinic acid (PC88-A, Ionquest 801, P-507) is structurally similar to BTMPPA and has qualitatively similar separation characteristics in the extraction of Mn and Zn (Biswas et al., 2016; Nathsarma and Devi, 2006). The use of bis(2,4,4-trimethylpentyl)thiophosphinic acid (Cyanex 302) (Biswas et al., 2016; Hosseini et al., 2011; Hosseini et al., 2010) and bis(2,4,4-trimethylpentyl)dithiophosphinic acid (Cyanex 301) (Biswas et al., 2016; El-Nadi et al., 2007; Steiner et al., 1992) has also been studied for Mn–Zn separation but their industrial use is limited by their tendency to decompose (Flett, 2005). Furthermore, Cyanex 301 is known for its irreversible extraction of Fe and Cu (Steiner et al., 1992; Flett, 2005). Additionally, the complete stripping of Zn from loaded Cyanex 301 is cumbersome since it requires multiple contacts with concentrated acids (*e.g.* 5 N HCl or 30 % H_2SO_4) (Nayl et al., 2014; Steiner et al., 1992). A synergistic mixture of 0.5 M neodecanoic acid (Versatic 10) and 0.4 M 5,8-diethyl-7-hydroxydodecan-6-oxime (LIX 63) was suggested by Cheng et al. (2010) for the separation of Co and Zn from Mn, Mg, and Ca. However, extraction of Zn using Versatic 10, or the synergistic mixture requires significantly higher pH than D2EHPA or BTMPPA. The pH_{50} value for the extraction of Zn with the synergistic mixture was 3.8 (Cheng et al., 2010) whereas the corresponding pH_{50} is usually below 2.5 with both D2EHPA and BTMPPA at similar extractant concentrations (Biswas et al., 2016; Ahmadipour et al., 2011; Hosseini et al., 2010; Lee et al., 2010; Pereira et al., 2007; Salgado et al., 2003). Tri-*n*-butyl phosphate (TBP) and trialkyl phosphine oxides (*e.g.* Cyanex 923) can be used to extract Zn from H_2SO_4 solutions when the free acidity in the aqueous phase is sufficiently high, *e.g.* free $[H^+] = 5$ M or higher for extraction with TBP or between 0.1 and 1 M with Cyanex 923, respectively (Ibiapina et al., 2018). On the other hand, H_2SO_4 acts as an antisolvent for concentrated $MnSO_4$ solutions, such as the anode sludge leachates obtained by reductive H_2SO_4 leaching (Taylor, 1952). Therefore, NOPCs can be recommended only as phase modifiers or synergists in the treatment of very concentrated $MnSO_4$ solutions by solvent extraction.

Sulfate solutions with less than 45 g L^{-1} Mn have been widely studied in earlier solvent extraction research on Zn–Mn separation (Ibiapina et al., 2018; Chen et al., ; Tanong et al., 2017; Biswas et al., 2016; Mishra et al., 2016; Haghighi et al., 2015; Falco et al., 2014; Nayl et al., 2014; Innocenzi and Veglio, 2012; Ahmadipour et al., 2011; Hosseini et al., 2011; Hosseini et al., 2010; Cheng et al., 2010; Lee et al., 2010; Pereira et al., 2007; El-Nadi et al., 2007; Nathsarma and Devi, 2006; Salgado et al., 2003; Cheng, 2000; Devi et al., 1997; Steiner et al., 1992; Flett, 2005; Pakarinen and Paatero, 2011; MOHAPATRA et al., 2007; Principe and Demopoulos, 2004). Extraction of Mn to the organic phase, followed by stripping of a Mn-rich product (Pakarinen and Paatero, 2011) is a viable process scheme for solutions with low or moderate Mn content. However, a different approach was investigated in this study for the highly concentrated ([Mn] > 150 g L^{-1}) $MnSO_4$ solutions. The aim was to extract Al, Ca, Fe and Zn to the organic phase while minimizing the extraction of Mn. Usually, Al, Ca, Fe and Zn are extracted by D2EHPA at a lower pH than Mn (Lee et al., 2010; Pereira et al., 2007; Cheng, 2000; Pakarinen and Paatero, 2011; MOHAPATRA et al., 2007; Principe and Demopoulos, 2004). Since the impurity metals (here, metals other than Mn) are present in the anode sludge leachate at much smaller concentration than Mn, extraction of the impurities should be possible with smaller chemical consumption than extraction and stripping of Mn. However, changes in temperature or composition of the feed solutions affect the distribution coefficients and might even change the extraction order of the metals for D2EHPA (Lee et al., 2010; Pereira et al., 2007; Cheng, 2000). BTMPPA also extracts Al, Fe, and Zn ahead of Mn (Flett, 2005; Pakarinen and Paatero, 2011; MOHAPATRA et al., 2007), but extraction of Ca is negligible at pH values below 5; Mn is extracted ahead of Ca (Pakarinen and Paatero, 2011). Besides the differences in chemical equilibria with chemically different solutions, the physical behavior of the phases at high ionic strength is different than at low or moderate ionic strength. Adjusting the pH of concentrated $MnSO_4$ solutions is restricted, since addition of alkali metal hydroxides or NH_3 in large quantities may result in the formation of Tutton's salts (Montgomery et al., 1966).

Based on the literature discussed above, D2EHPA and BTMPPA were selected as extractants for removal of Zn and Fe from concentrated $MnSO_4$ solution in this study. Results from the separation of Mn and Zn by continuous multi-stage extraction have been published earlier by only a few authors. Haghighi et al. (2015) and Nathsarma and Devi (2006) have simulated the countercurrent extraction of Mn- and Zn-bearing solutions by batch experiments. Salgado et al. (2003) included two-stage crosscurrent extraction in their studies. Also, Pereira et al. (2007) have published results from continuous countercurrent separation of Mn and Zn. This paper contributes to the topic by presenting new extraction equilibria and results of the purification of Mn-rich anode sludge leachate by continuous countercurrent solvent extraction in laboratory-scale mixer-settlers.

2. Materials and methods

2.1. Production of the $MnSO_4$ solutions

$MnSO_4$ solutions were prepared for the solvent extraction studies by leaching anode sludge from Zn electrowinning by the method described by Kauppinen et al. (2020). The leaching procedure was scaled up for a 50 dm^3 glass reactor with a mixer and baffles made of acid-resistant steel (AISI 316) to produce enough feed solution for the continuous experiments. The sludge was first mixed for 1 h with 0.5 M H_2SO_4 (reagent grade 95–98 wt%, Merck KGaA) solution to wash most of the Mg, Al, Fe and Zn before liberation of Mn by reductive leaching. S/L of 500 g L^{-1} was used in the preliminary washing step, and water was pre-heated to 65–70 °C before introducing the sludge and acid into the reactor. The acidic wash liquor was separated from the sludge by gravity settling. After removing most of the acidic overflow, the sludge was rinsed with pure water and the suspension was vacuum filtered in 5 dm^3 Büchner funnels to yield the washed anode sludge. The moisture content of the sludge was 34 wt% after filtration.

In the reductive leaching step pure water and part of the washed anode sludge were pre-loaded into the reactor. 95 wt% H_2SO_4 (Orikem Oy, Kangasala, Finland) and 30 wt% H_2O_2 (VWR Chemicals) were continuously fed into the reactor by peristaltic pumps. The flowrates were 22.8 mL min^{-1} and 41.3 mL min^{-1} for H_2SO_4 and H_2O_2, respectively. To maintain the S/L ratio at 450 g L^{-1} during the leaching process, the rest of the wet sludge was intermittently fed into the reactor at a rate of 5.4 kg h^{-1}. A few drops of anionic polyacrylamide flocculant (1 g L^{-1} solution of Kemira Superfloc A-100) were added into 40 dm^3 of suspension to aid the solid–liquid separation after the reductive leaching. The preliminary wash and leaching before solvent extraction are depicted in Fig. 1.

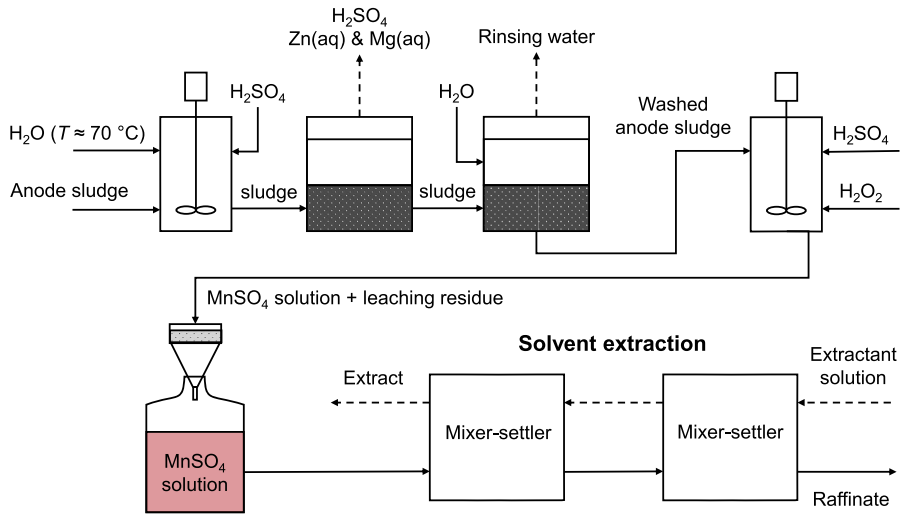

Fig. 1. Schematics showing the processing of the anode sludge in this study.

2.2. Batch extraction experiments

D2EHPA (97 % bis(2-ethylhexyl) hydrogen phosphate, Merck KGaA) and BTMPPA (85–90 % bis(2,4,4-trimethylpentyl)phosphinic acid, trade name Cyanex 272, Solvay) were diluted in Exxsol D80 (Exxon Mobil) aliphatic hydrocarbon mixture, and the solutions were used without pre-treatments. The metal concentrations of the anode sludge leachate used in the batch experiments are given in Table 1. The total concentration of Co, Ni and Cu together was 5.4 mg L^{-1}. The pH of the solution was 0.6 and the redox potential was + 800 mV (vs. SHE) at 22 ± 1 °C. This solution is referred as the "Pregnant leach solution 1 (PLS 1)."

Batch extractions were carried out in a 1 dm^3 jacketed glass reactor. The pH was adjusted by bubbling gaseous NH_3 into the reaction mixture via a submerged PTFE tube. The temperature was controlled by an external thermostat. Volumetric phase ratio O/A = 1 was used in determination of the pH isotherms. Loading isotherms were determined in a similar manner, but the O/A ratio was varied, whereas the pH was maintained constant. Back-extraction performance was studied by stripping loaded 0.8 M extractants with 0.5 M H_2SO_4 at various O/A ratios without other pH adjustment. The equilibration time was 15 min.

2.3. Continuous experiments

Composition of the feed solution in the continuous experiments (Table 2) was slightly different from PLS 1 due to the scale-up of the reductive leaching and subsequent solid–liquid separation. The leachate used in the continuous experiments (PLS 2) was more acidic (pH < 0), and the total concentration of Co, Ni and Cu together in the solution was 12.1 mg L^{-1}. The redox potential of the second leachate (PLS 2) was + 760 mV (vs. SHE) at 22 ± 1 °C after pH adjustment to 1.2.

MEAB MSU0,5 mixer-settler units (MEAB) made of PTFE and PFA were used in the continuous extraction experiments. The mixer volume of a single MSU0,5 unit is 120 mL; the volume of the settler is 460 mL. The horizontal cross-sectional area of the settler is 55 cm^2. PLS 2 and the extractant solutions were fed by PTFE diaphragm pumps (ProMinent DLTA). A dual-channel syringe pump (Gemini 88, KD Scientific) was used for pH adjustment with NaOH or H_2SO_4. Additionally, a Consort C3060 was used for pH logging. All continuous experiments were done at room temperature (22 ± 1 °C). A minimum of five cascade volumes of liquid were processed in each experiment as suggested by the conventional theory on residence time distributions. 3.6 min mean residence time in mixer (τ_{mix}) was near the lower operating limit determined by the linear settling velocity and horizontal cross-sectional area of the settlers. D2EHPA and BTMPPA solutions were prepared with 0.8 M nominal concentration of the active component. The proton capacities of the D2EHPA and BTMPPA solutions were 0.779 mol L^{-1} and 0.755 mol L^{-1}, respectively, as determined by titrating the extractant solutions in 75 vol-% isopropanol against 0.1 M NaOH standard solution. The 0.8 M extractant solutions were pre-neutralized using 5 M NaOH at O/A =

Table 1
Metal concentrations in the first anode sludge leachate (PLS 1) as determined from ten different analyses of parallel samples.

Element	Unit	Average	Standard deviation
Mn	g L^{-1}	**179.8**	11.3
Al	mg L^{-1}	**82.7**	29.3
K	mg L^{-1}	**4121.4**	168.3
Ca	mg L^{-1}	**290.8**	127.1
Fe	mg L^{-1}	**37.5**	5.4
Zn	mg L^{-1}	**448.6**	13.6

Table 2
Metal concentrations in the second anode sludge leachate (PLS 2) as determined from nine different analyses of parallel samples.

Element	Unit	Average	Standard deviation
Mn	g L^{-1}	**161**	9.1
Na	g L^{-1}	**17.7**	2.4
Mg	mg L^{-1}	**215.1**	9.6
Al	mg L^{-1}	**63**	45.7
K	mg L^{-1}	**2997**	280.9
Ca	mg L^{-1}	**203.7**	42.9
Fe	mg L^{-1}	**134.9**	12.4
Zn	mg L^{-1}	**999.4**	41.5

10 before extraction. The prepared Na-BTMPPA was a completely transparent single phase microemulsion, whereas the D2EHPA solution and 5 M NaOH formed a milky dispersion, which was continuously mixed in the feed tank to maintain homogeneousness. The solvent-to-feed flow ratios (S/F) reported here are given for the volumetric flow-rates of the pre-neutralized extractants. Nominal concentrations (0.8 M) of the active component are used in discussion of the pre-neutralized extractant solutions.

2.4. Analyses of the liquid samples

The organic samples were backextracted at A/O = 20 with HCl (GPR RECTAPUR, VWR). The HCl raffinates from backextraction were analyzed using ICP-MS (Agilent 7900). 3 N HCl was used for the organic samples from the batch experiments, while 5 N HCl was used for the samples from the continuous experiments. It was realized during the experimental work that stripping of Fe from loaded D2EHPA would be most efficient by 5 N HCl, whereas 3–5 M H_2SO_4 should be used for the stripping of BTMPPA (Sandhibigraha et al., 2000). To get reliable information about the Fe loading in the continuous extraction, certain organic steady-state samples were dissolved in super-pure HNO_3 (67–69 wt%, ROMIL) by wet digestion (Milestone UltraWAVE) under 250 °C and 130 bar for 10 min after a 70 min heating ramp. Metal concentrations in the aqueous samples were analyzed using ICP-MS.

2.5. Data treatment

The selectivity of Zn and Fe over Mn was evaluated by comparing the molar concentration of Mn in the organic phase against the total molar concentration of metals in the organic phase. The total concentration of metals in the organic phase was approximated as the sum of $[Fe]_{org}$, $[Zn]_{org}$, and $[Mn]_{org}$, since the concentrations of other metals in the organic samples were negligible with respect to $[Fe]_{org}$, $[Zn]_{org}$ and $[Mn]_{org}$. The formal mole fraction of Mn in the organic phase was defined using Eq. (1),

$$f^{*}_{Mn,org} = \frac{[Mn]_{org}}{[M]_{org,tot}} \cong \frac{[Mn]_{org}}{[Fe]_{org} + [Zn]_{org} + [Mn]_{org}} \quad (1)$$

where $f^{*}_{Mn,org}$ is the mole fraction of Mn in the organic phase with respect to the total concentration of metals in the organic phase and $[M]_{org,tot}$ is the total concentration of metals in the organic phase [mol L^{-1}].

The crowding plots, where quantity $f^{*}_{Mn,org}$ is plotted against $[M]_{org,tot}$ or O/A were convenient for selectivity evaluations because, in this case, [Fe] in the aqueous phase was lowered below the detection limit and distribution coefficients or separation factors could not be calculated for Fe. Furthermore, the raffinates from backextraction analyses (see chapter 2.5) of the organic samples were less prone to interference-related analytical errors due to their much lower salinity compared to the aqueous samples with [Mn] ≥ 150 g L^{-1}.

The relative purity of Mn was calculated using Eq. (2),

$$P_R(Mn) = \frac{w_{Mn}}{\sum_j w_j} \quad (2)$$

where P_R(Mn) is the relative purity of Mn [wt%], w is the mass concentration [g L^{-1}] and the summation in the denominator goes through all metals in the solution.

The reported average pH values for the continuous experiments were determined from the pH logger data by taking the average of the pH values from the end half of an experiment (Fig. 2) to exclude the fluctuations in the startup-phase. Similarly, the reported extract and raffinate concentrations (Table 3) are the average concentration from the last three samples.

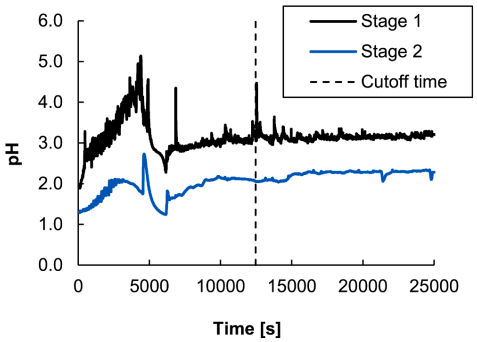

Fig. 2. Stagewise pH profiles from two-stage continuous countercurrent extraction of the anode sludge leachate (PLS 2) with 0.8 M Na-D2EHPA as an example to illustrate the determination of the average pH values.

3. Results and discussion

3.1. Comparison of the performances of D2EHPA and BTMPPA in batch extractions

3.1.1. Effect of pH and extractant concentration on extraction of Fe, Zn and Mn

Fe and Zn were efficiently removed from the concentrated $MnSO_4$ leachate (Fig. 3) at pH 3.0 and above. As a more acidic reagent, D2EHPA can extract the metals at lower pH values than BTMPPA (Pakarinen and Paatero, 2011). Over 80 % of Fe was extracted by 0.2 M D2EHPA at pH 0.8, whereas a pH > 1.5 was required with 0.2 M BTMPPA. The interpolated pH_{50} values of Zn extraction were 1.48 and 2.12 for 0.2 M D2EHPA and 0.2 M BTMPPA, respectively. The effect of pH on the extraction of Zn (Fig. 3) was qualitatively similar with earlier results published in the literature (Chen et al.; Biswas et al., 2016; Innocenzi and Veglio, 2012; Pereira et al., 2007; Salgado et al., 2003; Cheng, 2000). An increase in extractant concentration decreased the pH required to achieve a specific degree of Zn extraction (Fig. 3), in accordance with Pereira's et al. (2007) observations. Extraction of Mn by 0.8 M BTMPPA was 1.9–5.8 % and 3.3–11.4 % by 0.8 M D2EHPA as determined from the raffinate phase concentrations (Fig. 3). The extraction of Co, Ni and Cu could not be verified from the analytical results, likely due to their very low initial concentration (below 5 mg L^{-1} each) in PLS 1 (Table 1). The concentration of Al in the organic samples throughout this study was below 20 mg L^{-1}, meaning that Al was only weakly extracted (E(Al) < 30 %) by both extractants.

3.1.2. Extraction of Ca

The extraction of Ca by both BTMPPA and D2EHPA was negligible between pH 0.5 and 6 (Fig. 4). The concentration of Ca was below the detection limit (approximately 25 mg L^{-1}) in almost all the organic samples from determination of the loading isotherms (Fig. 5). For D2EHPA, this is an unexpected result when compared to earlier studies for different solutions containing Ca. Haghighi et al. (2015) reported significant extraction of Ca by 30 vol-% D2EHPA for various O/A ratios at 45 °C, Cheng (2000) obtained over 1 g L^{-1} loading of Ca with 10 vol-% D2EHPA with around 250 mg L^{-1} of Ca in the aqueous phase in equilibrium. Additionally, Pakarinen and Paatero (2011) reported over 80 % extraction of Ca by 25 vol-% D2EHPA at pH ≥ 2.5 and 25 °C from 200 mg L^{-1} initial concentration. Extractions with 0.2 M extractant solutions were repeated at 15 °C, since Pakarinen and Paatero (2011) have observed an increase in the extraction of Ca at lowered temperature.

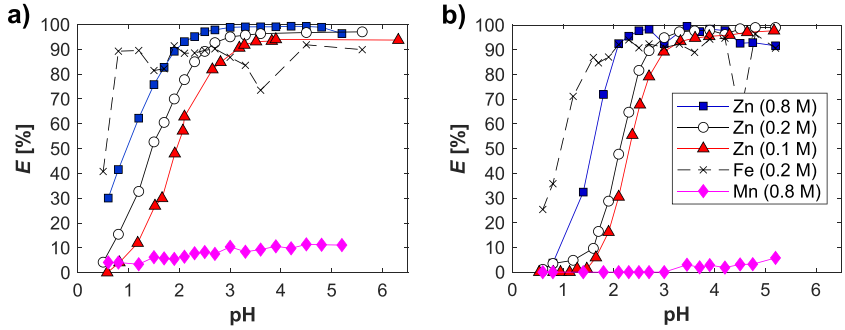

Fig. 3. Effect of pH on extraction of Zn, Fe and Mn at various extractant concentrations at 25 ± 1 °C by a) D2EHPA and b) BTMPPA from the anode sludge leachate. Concentration of the extractant is given in brackets. $[Zn]_0$ = 450 mg L^{-1}, $[Fe]_0$ = 40 mg L^{-1}, $[Ca]_0$ = 320–350 mg L^{-1} and $[Mn]_0$ = 180 g L^{-1}.

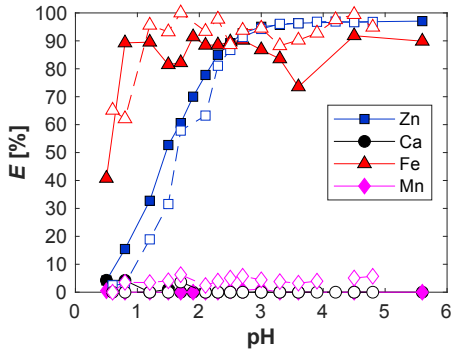

Fig. 4. Extraction of Zn, Fe, Ca and Mn by 0.2 M D2EHPA at 25 °C (filled symbols) and 15 °C (hollow symbols) from the anode sludge leachate. $[Zn]_0$ = 450 mg L^{-1}, $[Fe]_0$ = 40 mg L^{-1}, $[Ca]_0$ = 320–350 mg L^{-1} and $[Mn]_0$ = 180 g L^{-1}.

Here Ca was not extracted, even at 15 °C. Lowering the temperature from 25 °C to 15 °C did not have a significant effect on the extraction of Zn, Fe and Mn, either (Fig. 4). The reason behind the poor Ca extraction by D2EHPA was not studied further, but it seems to be associated with the high amount of Mn and/or SO_4^{2-} in the system.

3.1.3. Effect of metal loading in the organic phase on Zn/Mn and Fe/Mn selectivity

The fraction of Mn in the organic phase decreased with both extractants when the metal loading in the organic phase increased (Fig. 6 a) regardless of the pH or temperature used in the experiment. Selectivity towards Zn and Fe was higher with BTMPPA than with D2EHPA. The lowest $f^*_{Mn,org}$ was 28.9 mol-% for crowded D2EHPA at 0.2 M extractant concentration and pH 2.7, whereas with crowded 0.2 M BTMPPA the $f^*_{Mn,org}$ was 10.0 mol-%, respectively. The Mn-selectivity of D2EHPA was affected by pH (Fig. 6). Crowding of 0.8 M D2EHPA at pH 3.0 lowered the $f^*_{Mn,org}$ to 35 mol-%. But, at pH 1.7, the $f^*_{Mn,org}$ in loaded D2EHPA did not decrease below 65 mol-%. On the other hand, $f^*_{Mn,org}$ in the crowded 0.8 M BTMPPA lowered below 10 mol-% at pH 1.7. Co-extraction of Mn can thus be limited by crowding the extractants (Fig. 6 b). Mn ions that occupy the deprotonated organic ligands are replaced by Zn and Fe ions; the separation can also be carried out using low pH and high excess of BTMPPA. The aqueous solution can then be maintained at low pH, and the risk of precipitation due to pH elevation will be lower. However, choosing the extractant and operating conditions is not unequivocal since, at low pH, D2EHPA extracts higher overall amounts of Zn and Fe than BTMPPA does.

3.1.4. Separation of the co-extracted Mn from Zn and Fe during backextraction

The co-extracted Mn was recovered at 99.5–99.8 wt% relative purity by stripping the loaded 0.8 M extractants with 0.5 M H_2SO_4 at high O/A ratios (Fig. 7). The Mn-rich fractions of the stripping raffinates contained 29.4–33.9 g L^{-1} Mn, 13–16 mg L^{-1} Al, 1.5–5.2 mg L^{-1} Zn and < 1 mg L^{-1} Fe. 55.7 % of the co-extracted Mn could be selectively stripped at P_R(Mn) > 99.5 wt% from D2EHPA and 71.5 % from BTMPPA, respectively. Increasing the amount of stripping acid (i.e. lowering O/A and/or increasing the concentration of H_2SO_4) lowers the pH so that Zn and Fe are also stripped according to the pH isotherms (Fig. 3). Thus, the relative purity of Mn was lowered with decreasing O/A (Fig. 7). Zn and Mn can be completely stripped from BTMPPA and D2EHPA with adequate amounts of H_2SO_4 or HCl (Biswas et al., 2016). However, stripping Fe from BTMPPA and D2EHPA requires special attention. Fe (III) is only partially stripped from loaded D2EHPA by H_2SO_4, but 99 % of the loaded Fe can be stripped by 5 N HCl (Sandhibigraha et al., 2000). Moreover, stripping by 7.5 % oxalic acid at 60 °C (Singh et al., 2013) or a mixture of H_2SO_4 and a reducing agent (Liu et al., 2014) has been suggested for a complete Fe stripping from D2EHPA. Fe is more efficiently stripped from BTMPPA by H_2SO_4 than by HCl; 98–100 % Fe stripping can be obtained with 8–10 N H_2SO_4 (Sandhibigraha et al., 2000). Stripping of Fe with HCl from BTMPPA is inefficient with over 3 N concentrations (Sandhibigraha et al., 2000). Fe can be removed from the solution by hydroxide precipitation before extraction, or a bleed stream for Fe removal could be employed to the solvent extraction process.

3.2. Extraction performance in continuous counter-current extraction

3.2.1. Removal rates of Zn, Fe and Mn

Table 3 summarizes the removal percentages of Zn, Fe and Mn from

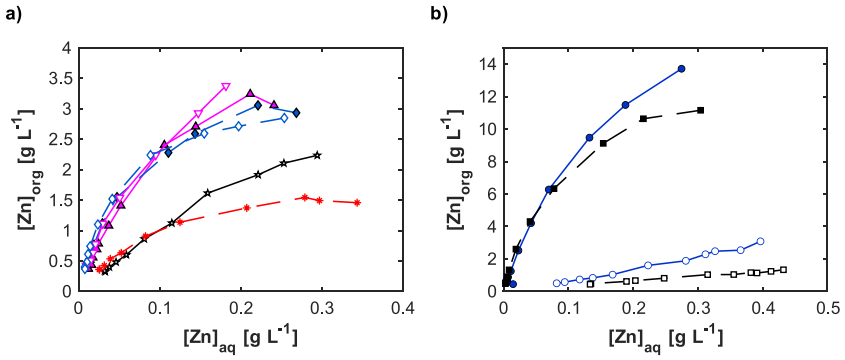

Symbol	HL	pH	*T* [°C]
△	D2EHPA	3.7	25
▽	D2EHPA	3.7	15
☆	D2EHPA	2.7	25
◆	BTMPPA	3.7	25
◇	BTMPPA	3.7	15
✱	BTMPPA	2.7	25

Symbol	HL	pH	*T* [°C]
●	D2EHPA	3.0	25
○	D2EHPA	1.7	25
■	BTMPPA	3.0	25
□	BTMPPA	1.7	25

Fig. 5. The determined Zn loading isotherms for a) 0.2 M and b) 0.8 M extractants. $[Zn]_0$ = 450 mg L^{-1}, $[Fe]_0$ = 40 mg L^{-1}, $[Ca]_0$ = 320–350 mg L^{-1} and $[Mn]_0$ = 180 g L^{-1}; HL denotes extractant.

the anode sludge leachate in the continuous experiments. D2EHPA removed Zn and Fe more efficiently than BTMPPA did, but it co-extracted more Mn. Single-stage extraction with 0.8 M Na-D2EHPA at 22 ± 1 °C with a 3.6 min mean residence time (τ_{mix}) and S/F = 1 removed 97 % of the Fe, 96 % of the Zn and 16.6 % of the Mn. In similar conditions, 0.8 M Na-BTMPPA removed 77.1 % of the Fe, 93.1 % of the Zn and 8.4 % of the Mn. The addition of another extraction stage as well as lowering the S/F ratio to 0.43 increased the removal of Zn and Fe by D2EHPA and decreased the removal of Mn. Two-stage extraction by BTMPPA was more sensitive to pH adjustment. When pH was adjusted in the aqueous feed stage (stage 1) only, the raffinate from two-stage extraction (S/F = 0.43; τ_{mix} = 3.6 min) by 0.8 M Na-BTMPPA had a higher Zn concentration (96.3 mg L^{-1}) than the raffinate from single-stage extraction (S/F = 1) (69.8 mg L^{-1}). Introducing the pH adjustment in both extraction stages resulted in 99.5 % Zn removal and 98.7 % Fe removal by 0.8 M Na-BTMPPA; also, the Mn loading in the organic phase increased (Table 3). However, the concentration of Mn in loaded BTMPPA (<4 g L^{-1}) was still significantly lower than that in loaded D2EHPA (>9 g L^{-1}) although the extraction efficiencies of Zn and Fe were similar.

3.2.2. *Comparison of the experimental results against theoretical predictions*

The experimental results are in relatively good agreement with the McCabe–Thiele predictions (Fig. 8 a–d) of the extraction of Zn. Loading isotherms of 0.8 M BTMPPA and 0.8 M D2EHPA at pH = 3 are so similar that there is no significant difference between the predictions (Fig. 8 a & c). Moreover, the Zn extraction equilibria and the McCabe–Thiele diagrams (Fig. 8 e–f) suggest that 2 stages operating at O/A = 0.4 and pH = 3 would be sufficient for the treatment of a more concentrated solution with *e.g.* 4 g L^{-1} Zn without significant loss of purification performance. However, relatively large errors to the predicted stagewise concentrations can be introduced by fitting, interpolation or extrapolation of steep equilibrium curves. Even a small difference in raffinate concentration corresponds to a relatively large change in extract concentration. The average concentrations given in Table 3 are not in complete agreement with mass balance; the errors can be explained by the deviations in the ICP-MS analyses, precipitation and fluctuation in the feed flowrates.

3.2.3. *Effect of the mean residence time on process performance*

Increasing mean residence time from 3.6 min to 6.0 min in the two-stage countercurrent extraction increased the Zn/Mn and Fe/Mn selectivities for 0.8 M Na-BTMPPA considerably (Table 4). The increase in τ_{mix} from 3.6 min to 6.0 min had marginal—if any—effect on the extraction performance of D2EHPA. Higher Zn and Fe loading was obtained with τ_{mix} = 6.0 min than with τ_{mix} = 3.6 min. However, the pH differed slightly between these experiments, which could explain the observed difference in extraction performance. Adjusting the pH on both stages in the two-stage extraction by 0.8 M Na-D2EHPA increased the extraction of Mn but had very little effect on removal of Zn and Fe.

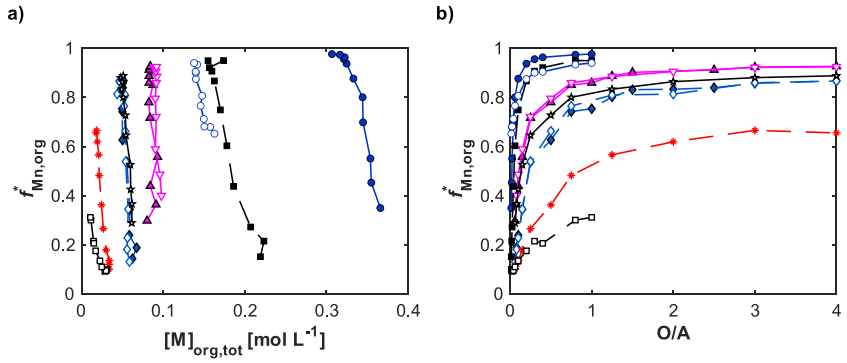

Symbol	HL	[HL], [mol L^{-1}]	pH	T [°C]
	D2EHPA	0.2	3.7	25
	D2EHPA	0.2	3.7	15
	D2EHPA	0.2	2.7	25
	BTMPPA	0.2	3.7	25
	BTMPPA	0.2	3.7	15
	BTMPPA	0.2	2.7	25
	D2EHPA	0.8	3.0	25
	D2EHPA	0.8	1.7	25
	BTMPPA	0.8	3.0	25
	BTMPPA	0.8	1.7	25

Fig. 6. Effect of crowding on the mole fraction of Mn in the organic phase. $[Zn]_0 = 450$ mg L^{-1}, $[Fe]_0 = 40$ mg L^{-1}, $[Ca]_0 = 320–350$ mg L^{-1} and $[Mn]_0 = 180$ g L^{-1}. HL denotes extractant and $f^*_{Mn,org}$ is defined in Eq. (1).

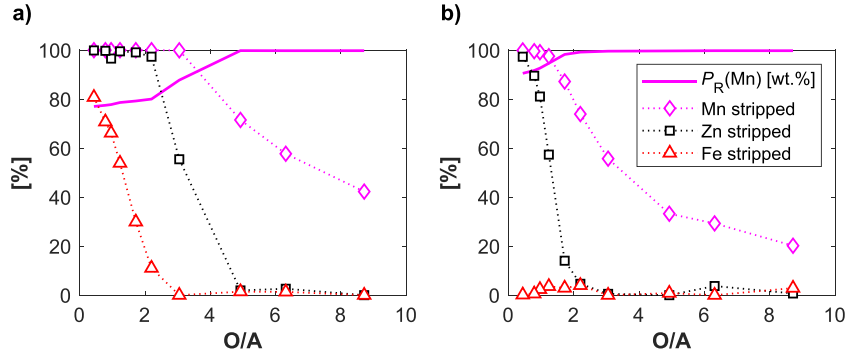

Fig. 7. Effect of phase ratio on stripping of Mn, Zn and Fe from loaded 0.8 M BTMPPA (a) and 0.8 M D2EHPA (b) at 25 ± 1 °C with 0.5 M H_2SO_4. Initial metal loadings: $[Mn]_{BTMPPA} = 8.2$ g L^{-1}, $[Zn]_{BTMPPA} = 1.09$ g L^{-1}, $[Fe]_{BTMPPA} = 79.9$ mg L^{-1}; $[Mn]_{D2EHPA} = 16.8$ g L^{-1}, $[Zn]_{D2EHPA} = 1.09$ g L^{-1}, $[Fe]_{D2EHPA} = 76.4$ mg L^{-1}.

Therefore, with 0.8 M D2EHPA the second extraction stage can operate at pH ≈ 2 and almost complete removal of Zn and Fe is obtained for the anode sludge leachates studied (Table 3). High extraction of Zn is typical for both D2EHPA and BTMPPA. The Zn removal reported here for D2EHPA is similar to the results of Pereira et al. (2007): they obtained over 98 % Zn removal by 20 wt% D2EHPA in three countercurrent extraction stages at pH = 2.5 and 28 ± 1 °C. However, a significant difference in the extraction of Fe between this study and Pereira et al. (2007) can be observed. The concentration of Fe has decreased from 240.6 mg L^{-1} to 115.5 mg L^{-1} in the three-stage extraction with S/F = 1 in Pereira et al. (2007), whereas, in the current study, [Fe] was lowered from 135 mg L^{-1} to below 2 mg L^{-1} in two extraction stages with S/F = 0.43. Moreover, the results of Pereira et al. (2007) show a 22 % and an 11.3 % decrease in concentrations of Ca and Mg, respectively. However, the concentrations of Ca and Mg in their feed solution were roughly 2.5 and 10 times higher, respectively, than in the PLS 2 solution studied here (Table 2). Ca could not be detected in the organic samples during this work. Mg was not detected in loaded BTMPPA, either. The concentration of Mg in all D2EHPA samples from the countercurrent extractions was below 2 mg L^{-1}. The 7–9 % removal of Mn reported in this study (Table 3) for two-stage extraction by 0.8 M Na-D2EHPA is similar to the 8.3 % Mn removal obtained by Pereira et al. (2007), although the concentration of Mn in the aqueous feed solution was much lower (<1 g L^{-1}) in Pereira et al. (2007).

3.2.4. Formation of solids

Solid precipitates were formed during the countercurrent extractions. These precipitates caused gelation in the settlers. However, no precipitates were visually observed in the extract and raffinate samples or during the batch extraction experiments. The precipitates were likely Mn and Fe hydroxides, but the formation of Tutton's salts is also possible. Operation of the solvent extraction process discussed here is recommended with a high excess of extractant. Thus, the active amount of extractant would be sufficiently high for the desired extraction efficiency at the lowest possible pH (Fig. 3). The precipitation can perhaps be completely avoided at low pH. On the other hand, an increase in extractant concentration or S/F ratio likely increases co-extraction of Mn. However, avoiding precipitation is a priority over avoiding extraction of Mn because a significant amount of the co-extracted Mn can be selectively recovered in stripping (see chapter 3.1). The estimated Mn losses to the impure stripping fractions due to co-extraction were 0.1–0.3 % for BTMPPA and 1.2–2.1 % for D2EHPA (28.5 % and 44.3 % of the loaded Mn, respectively, Table 3).

Table 4
Selectivity ratios and total molar concentration of metals in the extracts from continuous countercurrent solvent extraction of Mn-rich sulfate leachate with 0.8 M Na-BTMPPA and 0.8 M Na-D2EHPA at 22 ± 1 °C. Total molar concentration of metals was approximated with $[M]_{org,tot} \approx [Zn]_{org} + [Fe]_{org} + [Mn]_{org}$.

Extractant	*N*	S/F	τ_{mix} min	$\frac{[Zn]_{org} + [Fe]_{org}}{[Mn]_{org}}$	$\frac{[Mn]_{org}}{[M]_{org,tot}}$	$[M]_{org,tot}$ mol L^{-1}
Na-BTMPPA	1	1	3.6	0.42	0.7	0.04
	2	0.43	3.6	1.27	0.44	0.06
	2*	0.43	3.6	0.61	0.62	0.11
	2	0.43	6.0	1.77	0.36	0.06
Na-D2EHPA	1	1	3.6	0.07	0.93	0.24
	2	0.43	3.6	0.23	0.82	0.21
	2*	0.43	3.6	0.15	0.87	0.33
	2	0.43	6.0	0.27	0.79	0.21

*pH adjustment in both stages.

3.3. Composition of the purified leachate

The average composition of the raffinates (Table 3) where $[Zn]_{aq} \leq 5$ mg L^{-1} is given in Table 5. The purified anode sludge leachate is proposed for use in the co-precipitation synthesis of NMC cathode precursors. The diluted concentrations for NMC622 and NMC811 in Table 5 are calculated for a solution in which the total concentration of Ni, Mn and Co is 2 mol L^{-1}, which is suitable for the hydroxide co-precipitation synthesis (Eilers-Rethwisch et al., 2018). Na and K are usually soluble in alkaline media. Therefore, Al, Mg, and Ca would be the most significant impurities for the co-precipitation synthesis at concentrations of 5.8–11.5 mg L^{-1}, 15–30 mg L^{-1} and 13–30 mg L^{-1}, respectively. The concentration of Zn and Fe will be lower than 1 mg L^{-1} after dilution, so they are unlikely to complicate the precursor synthesis. Concentration of Ni and Co can be adjusted by salt addition. Further performance evaluation of an NMC cathode material produced from the purified anode

Table 3
Removal percentages of Zn, Fe and Mn and their average concentrations in the extracts and raffinates in continuous countercurrent solvent extraction of Mn-rich sulfate leachate with 0.8 M Na-BTMPPA and 0.8 M Na-D2EHPA at 22 ± 1 °C. Stages were numbered starting from the organic feed stage and ending in the aqueous feed stage. Average concentrations in the aqueous feed solutions are given in bold font.

Extractant	S/F	τ_{mix} min	pH_{avg} stage 1	pH_{avg} stage 2	$[Mn]_{aq}$ g L^{-1}	$[Zn]_{aq}$ mg L^{-1}	$[Fe]_{aq}$ mg L^{-1}	$[Mn]_{org}$ g L^{-1}	$[Zn]_{org}$ mg L^{-1}	$[Fe]_{org}$ mg L^{-1}	R(Mn) %	R(Zn) %	R(Fe) %
Na-BTMPPA	–	–	–	–	**156.6**	**1005.4**	**133.7**	–	–	–	–	–	–
	1	3.6	3.12[a] (0.09*)	–	143.3	69.8	30.6	1.6	756.7	29.7	8.4	93.1	77.1
	0.43	3.6	3.65[a] (0.06*)	2.15[u] (0.05*)	147.8	96.3	9.9	1.6	2114.1	218.9	5.6	90.4	92.6
	0.43	3.6	3.07[a] (0.14*)	2.91[a] (0.29*)	148.4	5	1.7	3.8	2381	312.2	5.2	99.5	98.7
	0.43	6	3.18[a] (0.03*)	1.97[u] (0.07*)	147.4	50.7	< 0.5	1.3	2330.8	298.5	5.8	95	100
Na-D2EHPA	–	–	–	–	**167.9**	**977.4**	**135.6**	–	–	–	–	–	–
	1	3.6	2.85[a] (0.02*)	–	140.1	39.2	4.1	12.3	948	85.1	16.6	96	97
	0.43	3.6	3.05[a] (0.20*)	1.99[u] (0.26*)	152.9	5.5	< 0.5	9.2	2217.8	229	8.9	99.4	100
	0.43	3.6	3.12[a] (0.05*)	3.07[a] (0.08*)	155.6	2.7	2.2	15.8	2481	306.2	7.3	99.7	98.4
	0.43	6	3.14[a] (0.07*)	2.24[u] (0.09*)	155.7	1.4	< 0.5	9.3	2559.8	311.1	7.3	99.9	100

*Standard deviation.
[a)] adjusted pH.
[u)] unadjusted pH.

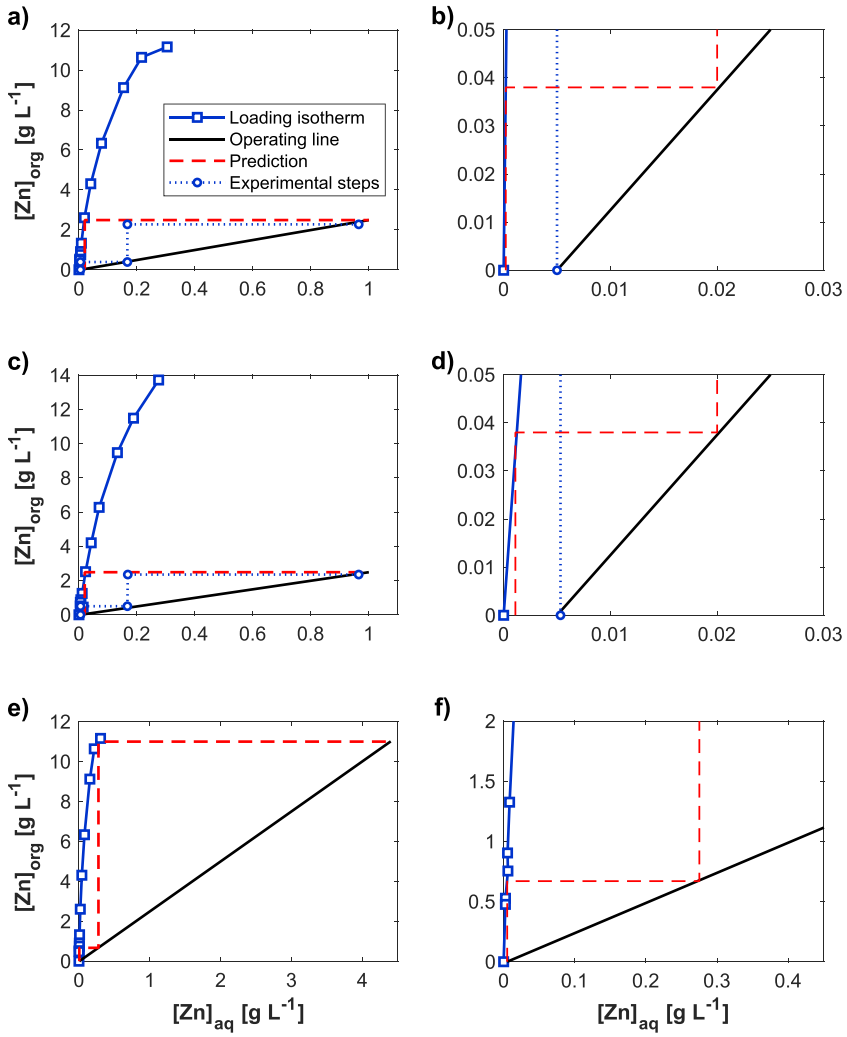

Fig. 8. McCabe–Thiele analysis of the countercurrent extraction of Zn at pH = 3.0 by 0.8 M BTMPPA (a & b) and 0.8 M D2EHPA (c & d) from the anode sludge leachate in comparison with the experimental results. Subfigures e) and f) show the construction for 0.8 M BTMPPA and an aqueous feed solution with $[Zn]_{0,aq}$ = 4.4 g L^{-1}.

sludge leachate (Table 5) involves precursor synthesis, battery manufacturing, and voltammetric testing that have been made but are not in the scope of this paper. Ni, Co, Cu, Zn and Fe are also in the tolerable range for the Mn electrolysis (Lu et al., 2014; Louis et al., 1859). According to our knowledge, no deteriorating effects of Al, Ca, Mg and Na on Mn electrolysis have been reported in the literature. Al, Ca, Mg and Na have lower standard reduction potentials than Mn (Electrochemical series, 2020), so it is assumed that they are not deposited on the Mn cathodes. Not all impurities were extracted by D2EHPA or BTMPPA from the anode sludge leachates in this work. Therefore, another approach or additional treatment must be applied if the purity of the $MnSO_4$ solution must be higher than presented in Table 5.

Table 5
Approximate composition of the purified anode sludge leachate (i.e. raffinate from solvent extraction) and concentrations of the diluted raffinate in potential re-use applications.

	Unit	Raffinate from solvent extraction	Electrolytic Mn	NMC622 co-precipitation	NMC811 co-precipitation
Mn	g L^{-1}	153.1	45	22	11
Na	g L^{-1}	24	7.1	3.4	1.7
Mg	mg L^{-1}	208.4	61.3	29.9	15
Al	mg L^{-1}	80.3	23.6	11.5	5.8
K	mg L^{-1}	2926.6	860	420	210
Ca	mg L^{-1}	188.3	55.3	27	13.5
Fe	mg L^{-1}	1	0.3	0.1	0.1
Co	mg L^{-1}	4.2	1.2	0.6	0.3
Ni	mg L^{-1}	2.2	0.6	0.3	0.2
Cu	mg L^{-1}	4.9	1.4	0.7	0.4
Zn	mg L^{-1}	3.7	1.1	0.5	0.3

4. Conclusions

Purification of Mn-rich anode sludge leachates by solvent extraction with D2EHPA and BTMPPA was studied. Both extractants can be used to remove Zn and Fe from a concentrated $MnSO_4$ solution. BTMPPA had higher selectivity for Zn and Fe over Mn than D2EHPA in all studied conditions. Over 99.5 % removal of Zn and Fe was obtained with 0.8 M Na-D2EHPA and 0.8 M Na-BTMPPA in two countercurrent extraction stages operating at S/F = 0.43 under 22 ± 1 °C. The concentration of Zn was decreased from approximately 1000 mg L^{-1} to below 10 mg L^{-1}. Additionally, the concentration of Fe decreased from 135 mg L^{-1} to 2 mg L^{-1} or below. Extraction by 0.8 M Na-BTMPPA lowered Zn and Fe concentrations in the raffinate below 10 mg L^{-1} only when both countercurrent extraction stages operated at pH = 3. With 0.8 M Na-D2EHPA, concentrations of Zn and Fe in the raffinate were lowered below 10 mg L^{-1}, also when the pH was adjusted to 3 only in the organic feed stage; with the aqueous feed stage operating around pH = 2. Increasing the mean residence time in the mixer from 3.6 min to 6.0 min improved the removal of Zn and Fe with BTMPPA, but with D2EHPA the change in extraction performance was marginal. The mole fraction of Mn in the organic phase ($f^*_{Mn,org}$) decreased with increasing metal loading with both D2EHPA and BTMPPA, so the co-extraction of Mn can be significantly limited by crowding the extractants. $f^*_{Mn,org}$ in crowded BTMPPA solutions was between 9 and 15 mol-% and remained in this range in crowded BTMPPA at all studied pH values. Proton activity has a considerable effect on the crowding characteristics of D2EHPA. The $f^*_{Mn,org}$ in crowded 0.8 M D2EHPA was 65.3 mol-% at pH 1.7 but only 34.9 mol-% at pH 3.7. 55.7 % of the co-extracted Mn was selectively stripped (P_R(Mn) > 99.5 wt%) by 0.5 M H_2SO_4 from loaded D2EHPA, whereas 71.5 % of the co-extracted Mn could be stripped from BTMPPA, respectively. Ca and Mg were not significantly extracted by either 0.8 M Na-D2EHPA or 0.8 M Na-BTMPPA at pH = 3. The Zn- and Fe-barren $MnSO_4$ raffinate contained over 145 g L^{-1} Mn, around 50–100 mg L^{-1} Al, 200 mg L^{-1} Ca and 200 mg L^{-1} Mg. Precipitation and gelation was encountered in the mixer-settlers in continuous runs when pH increased to 3.0 or above, but solids were not observed in the extract and raffinate outlets or in the batch extraction experiments. The purified $MnSO_4$ leachate and the Mn-rich fraction of the stripping raffinates are proposed for use in the synthesis of NMC-cathode precursors or for manufacturing electrolytic manganese metal.

CRediT authorship contribution statement

Niklas Jantunen: Methodology, Investigation, Data curation, Formal analysis, Writing – original draft, Visualization. **Toni Kauppinen:** Methodology, Investigation, Data curation, Formal analysis, Writing – review & editing. **Justin Salminen:** Conceptualization, Resources, Project administration, Writing – review & editing, Supervision, Funding acquisition. **Sami Virolainen:** Conceptualization, Methodology, Validation, Formal analysis, Data curation, Writing – review & editing, Supervision. **Ulla Lassi:** Conceptualization, Resources, Project administration, Writing – review & editing, Supervision, Funding acquisition. **Tuomo Sainio:** Conceptualization, Resources, Project administration, Writing – review & editing, Supervision, Funding acquisition.

Declaration of Competing Interest

The authors declare that they have no known competing financial interests or personal relationships that could have appeared to influence the work reported in this paper.

Acknowledgements

The funding provided by Business Finland (decision numbers 4236/31/2018 and 4300/31/2018) as a part of SYMMET (Symbiosis of metals production and nature) consortium is gratefully acknowledged.

Appendix A. Supplementary material

Supplementary data to this article can be found online at https://doi.org/10.1016/j.mineng.2021.107200.

References

Ahmadipour, M., Rashchi, F., Ghafarizadeh, B., Mostoufi, N., 2011. Synergistic effect of D2EHPA and Cyanex 272 on separation of zinc and manganese by solvent extraction. Separat. Sci. Technol. 46 (15), 2305–2312. https://doi.org/10.1080/01496395.2011.594848.

Ayala, J., Fernández, B., 2013. Reuse of anode sludge generated by the zinc industry to obtain a liquor for manufacturing electrolytic manganese. JOM 65, 1007–1014. https://doi.org/10.1007/s11837-013-0667-3.

Biswas, R.K., Habib, M.A., Karmakar, A.K., Tanzin, S., Recovery of manganese and zinc from waste Zn–C cell powder: Mutual separation of Mn(II) and Zn(II) from leach liquor by solvent extraction technique, Waste Management 51, 2016, 149–156. 10.1016/j.wasman.2015.09.041.

Brodd, R., Batteries (Introduction), in: Kroschwitz, J.I., Howe-Grant, M., (ed.), Kirk–Othmer Encyclopedia of Chemical Technology, 4th ed., Vol. 3, John Wiley & Sons, Inc., New York, 1992, 963–991.

Chen, W–S., Liao, C–T., Chang, C–H., Recovery of Zinc and Manganese from Spent Zn-Mn Batteries Using Solvent Extraction, Key Engineering Materials 775, 2018, 427–433. 10.4028/www.scientific.net/KEM.775.427.

Cheng, C.Y., 2000. Purification of synthetic laterite leach solution by solvent extraction using D2EHPA. Hydrometallurgy 56 (3), 369–386. https://doi.org/10.1016/S0304-386X(00)00095-5.

Cheng, C.Y., Zhang, W., Pranolo, Y., 2010. Separation of cobalt and zinc from manganese, magnesium, and calcium using a synergistic solvent extraction system consisting of Versatic 10 and LIX 63. Solvent Extraction and Ion Exchange 28 (5), 608–624. https://doi.org/10.1080/07366299.2010.499299.

Devi, N.B., Nathsarma, K.C., Chakravortty, V., 1997. Extraction and separation of Mn(II) and Zn(II) from sulphate solutions by sodium salt of Cyanex 272. Hydrometallurgy 45 (1–2), 169–179. https://doi.org/10.1016/S0304-386X(96)00076-X.

Eilers-Rethwisch, M., Winter, M., Schappacher, F.M., Synthesis, electrochemical investigation and structural analysis of doped Li[Ni0.6Mn0.2Co0.2-xMx]O2 (x = 0, 0.05; M = Al, Fe, Sn) cathode materials, Journal of Power Sources 387, 2018, 101–107. 10.1016/j.jpowsour.2018.02.080.

"Electrochemical series" in CRC Handbook of Chemistry and Physics, 101st Edition (Internet Version 2020), John R. Rumble, ed., CRC Press/Taylor & Francis, Boca Raton, FL.

El-Nadi, Y.A., Daoud, J.A., Aly, H.F., 2007. Leaching and separation of zinc from the black paste of spent MnO2-Zn dry cell batteries. J. Hazardous Mater. 143 (1-2), 328–334. https://doi.org/10.1016/j.jhazmat.2006.09.027.

Falco, L., Quina, M.J., Gando-Ferreira, L.M., Thomas, H., Curutchet, G., 2014. Solvent extraction studies for separation of Zn(II) and Mn(II) from spent batteries leach solutions. Separat. Sci. Technol. 49 (3), 398–409. https://doi.org/10.1080/01496395.2013.850510.

Flett, D.S., 2005. Solvent extraction in hydrometallurgy: the role of organophosphorus extractants. J. Organometall. Chem. 690 (10), 2426–2438. https://doi.org/10.1016/j.jorganchem.2004.11.037.

Goodwin, F.E., Zinc and Zinc Alloys, in Kroschwitz, J.I., Howe-Grant, M., (ed.), Kirk–Othmer Encyclopedia of Chemical Technology, 4th ed., Vol. 25, John Wiley & Sons, Inc., New York, 1998, 789–839.

Haghighi, H.K., Moradkhani, D., Salarirad, M.M., 2015. Separation of zinc from manganese, magnesium, calcium and cadmium using batch countercurrent extraction simulation followed by scrubbing and stripping. Hydrometallurgy 154, 9–16. https://doi.org/10.1016/j.hydromet.2015.03.007.

Hosseini, T., Rashchi, F., Vahidi, E., Mostoufi, N., 2010. Investigating the synergistic effect of D2EHPA and Cyanex 302 on zinc and manganese separation. Separat. Sci. Technol. 45 (8), 1158–1164. https://doi.org/10.1080/01496391003727908.

Hosseini, T., Mostoufi, N., Daneshpayeh, M., Rashchi, F., 2011. Modeling and optimization of synergistic effect of Cyanex 302 and D2EHPA on separation of zinc and manganese. Hydrometallurgy 105 (3–4), 277–283. https://doi.org/10.1016/j.hydromet.2010.10.015.

Ibiapina, V.F., Afonso, J.C., da Silva, R.S., Vianna, C.A., Mantovano, J.L., Separation of zinc from manganese by solvent extraction from acidic leachates of spent zinc-MnO2 dry cells using neutral organophosphorus extractants, Química Nova 41(7), 2018, 770–777. 10.21577/0100-4042.20170249.

Innocenzi, V., Veglio, F., 2012. Separation of manganese, zinc and nickel from leaching solution of nickel-metal hydride spent batteries by solvent extraction. Hydrometallurgy 129–130, 50–58. https://doi.org/10.1016/j.hydromet.2012.08.003.

Kauppinen, T., Vielma, T., Salminen, J., Lassi, U., 2020. Selective recovery of manganese from anode sludge residue by reductive leaching. ChemEngineering 4 (2), 40. https://doi.org/10.3390/chemengineering4020040.

Krüger, S., Hanisch, C., Kwade, A, Winter, W., Nowak, S., Effect of impurities caused by a recycling process on the electrochemical performance of Li[Ni0.33Co0.33Mn0.33]O2, Journal of Electroanalytical Chemistry 726, 2014, 91–96. 10.1016/j.jelechem.2014.05.017.

Lee, J.Y., Pranolo, Y., Cheng, C.Y., 2010. The recovery of zinc and manganese from synthetic spent-battery leach solutions by solvent extraction, Solvent Extraction and Ion Exchange 28(1), 2010, 73–84. 10.1080/07366290903409043.

Liu, Yang, Nam, Sang-Ho, Lee, Manseung, 2014. Stripping of Fe(III) from the loaded mixture of D2EHPA and TBP with sulfuric acid containing reducing agents. Bul. Korean Chem. Soc. 35 (7), 2109–2113. https://doi.org/10.5012/bkcs.2014.35.7.2109.

Louis, P. Martin, J.P., Increased current efficiency during the electrodeposition of manganese from sulphate electrolytes, Report 1859, 1976, National Institute for Metallurgy, Republic of South Africa.

Lu, J., Dreisinger, D., Glück, T., 2014. Manganese electrodeposition – a literature review. Hydrometallurgy 141, 105–116. https://doi.org/10.1016/j.hydromet.2013.11.002.

Matricardi, L.R., Downing, J., Manganese and manganese alloys, in: Kroschwitz, J.I., Howe-Grant, M., (ed.), Kirk–Othmer Encyclopedia of Chemical Technology, 4th ed., Vol. 15, John Wiley & Sons, Inc., New York, 1995, 963–990.

MEAB Metallextraction AB, Datavägen 51, 436 32 Askim, Sweden. https://www.meab-mx.se/products.htmlhttps://www.meab-mx.se/products.html.

Mishra, R.K., Rout, P.C., Sarangi, K., Nathsarma, K.C., 2016. Solvent extraction of zinc, manganese, cobalt and nickel from nickel laterite bacterial leach liquor using sodium salts of TOPS-99 and Cyanex 272. Trans. Nonferrous Met. Soc. China 26 (1), 301–309. https://doi.org/10.1016/S1003-6326(16)64119-5.

Mohapatra, D., Hong-in, K., Nam, C–W., Park, K–H., Liquid–liquid extraction of aluminium(III) from mixed sulphate solutions using sodium salts of Cyanex 272 and D2EHPA, Separation and Purification Technology 56(3), 2007, 311–318. https://www.sciencedirect.com/science/article/abs/pii/S1383586607001220.z.

Montgomery, H., Chastain, R.V., Lingafelter, E.C., The crystal structure of Tutton's Salts. V. Manganese ammonium sulfate hexahydrate, Acta Crystallographica 20, 1966, 731–733. 10.1107/S0365110X66001762.

Nathsarma, K.C., Devi, N., 2006. Separation of Zn(II) and Mn(II) from sulphate solutions using sodium salts of D2EHPA, PC88A and Cyanex 272. Hydrometallurgy 84 (3–4), 149–154. https://doi.org/10.1016/j.hydromet.2006.05.004.

Nayl, A.A., Ahmed, I.M., Aly, M.I., 2014. Liquid-liquid extraction and separation of divalent manganese and zinc by Na-CYANEX 272 from sulfate solution. Separat. Sci. Technol. 49 (2), 290–297. https://doi.org/10.1080/01496395.2013.818037.

Pakarinen, J., Paatero, E., 2011. Effect of temperature on Mn–Ca selectivity with organophosphorus acid extractants. Hydrometallurgy 106 (3–4), 159–164. https://doi.org/10.1016/j.hydromet.2011.01.003.

Pereira, D.D., Rocha, S.D.F., Mansur, M.B., 2007. Recovery of zinc sulphate from industrial effluents by liquid–liquid extraction using D2EHPA (di-2-ethylhexyl phosphoric acid). Separat. Purificat. Technol. 53 (1), 89–96. https://doi.org/10.1016/j.seppur.2006.06.013.

Principe, F., Demopoulos, G.P., 2004. Comparative study of iron(III) separation from zinc sulphate–sulphuric acid solutions using the organophosphorus extractants, OPAP and D2EHPA: Part I: Extraction. Hydrometallurgy 74 (1–2), 93–102. https://doi.org/10.1016/j.hydromet.2004.01.004.

Qina, S., Heelan, J.A., Lu, Y., Apelian, D., Wang, Y., Copper Impurity Effects on LiNi1/3Mn1/3Co1/3O2 Cathode Material, ACS Applied Materials & Interfaces 7(37), 2015, 20585–20590. 10.1021/acsami.5b04426.

Salgado, A.L., Veloso, A.M.O., Pereira, D.D., Gontijo, G.S., Salum, A., Mansur, M.B., 2003. Recovery of zinc and manganese from spent alkaline batteries by liquid–liquid extraction with Cyanex 272. J. Power Sources 115, 367–373. https://doi.org/10.1016/S0378-7753(03)00025-9.

Sandhibigraha, A., Bhaskara Sarma, P.V.R., Chakravortty, V., 2000. Stripping studies of Iron(III) extracted by D2EHPA, PC88A, and CYANEX272 from chloride solutions using sulphuric and hydrochloric acids. Solvent Extraction Res. Dev. Japan 7 (7), 93–105.

Singh, D.K., Yadav, K.K., Singh, H., Extraction and Stripping Behavior of Iron (III) from Phosphoric Acid Medium by D2EHPA Alone and Its Mixtures with TBP/TOPO, Separation Science and Technology 48, 2013, 1556–1564. 10.1080/01496395.2012.753084.

Steiner, L., Miaolin, X., Hartland, S., Recovery of zinc and manganese from waste batteries by liquid-liquid extraction, in Sekine, T. (ed.), Solvent Extraction 1990 – Proceedings of the International Solvent Extraction Conference (ISEC '90), Part B, Elsevier, Amsterdam, Netherlands, 1992, 1175–1180. 10.1016/B978-0-444-88677-4.50015-5.

Tanong, K., Tran, L–H., Mercier, G., Blais, J–F., Recovery of Zn (II), Mn (II), Cd (II) and Ni (II) from the unsorted spent batteries using solvent extraction, electrodeposition and precipitation methods, Journal of Cleaner Production 148, 2017, 233–244. 10.1016/j.jclepro.2017.01.158.

Taylor, D., The system MnSO4–H2SO4–H2O, Journal of the Chemical Society 8, 1952, 2370–2375. 10.1039/JR9520002370.

Wang, B., Mu, L., Guo, S., Bi, Y., 2019. Lead leaching mechanism and kinetics in electrolytic manganese anode sludge. Hydrometallurgy 183, 98–105. https://doi.org/10.1016/j.hydromet.2018.11.015.

Zhang, W., Cheng, C.Y., Manganese metallurgy review. Part I: Leaching of ores/secondary materials and recovery of electrolytic/chemical manganese dioxide, Hydrometallurgy 89(3–4), 137–159. 10.1016/j.hydromet.2007.08.010.

Zhang, W., Cheng, C.Y., 2007. Manganese metallurgy review Part III: Manganese control in zinc and copper electrolytes. Hydrometallurgy 89 (3–4), 178–188. https://doi.org/10.1016/j.hydromet.2007.08.011.

Zhang, C., Duan, N., Jiang, L., Xu, F., Luo, J., 2018. Influence of Mn^{2+} ions on the corrosion mechanism of lead-based anodes and the generation of heavy metal anode sludge in zinc sulfate electrolyte. Environ. Sci. Pollut. Res. 25, 11958–11969. https://doi.org/10.1007/s11356-018-1443-2.

Zhao, J., Wang, Z., Guo, H., Li, X., He, Z., Li, T., Synthesis and electrochemical characterization of Zn-doped Li-rich layered Li[Li0.2Mn0.54Ni0.13Co0.13]O2 cathode material, Ceramics International 41(9), 2015, 11396–11401. 10.1016/j.ceramint.2015.05.102.

Publication III

Jantunen, N., Virolainen, S., and Sainio, T.

Direct production of Ni–Co–Mn mixtures for cathode precursors from cobalt-rich lithium-ion battery leachates by solvent extraction

Reprinted with permission from
Metals
Vol. 12, p. 1445, 2022

metals

MDPI

Article

Direct Production of Ni–Co–Mn Mixtures for Cathode Precursors from Cobalt-Rich Lithium-Ion Battery Leachates by Solvent Extraction

Niklas Jantunen [1,*], Sami Virolainen [1] and Tuomo Sainio [2]

[1] School of Engineering Science, LUT University, Yliopistonkatu 34, 53850 Lappeenranta, Finland
[2] School of Engineering Science, LUT University, Mukkulankatu 19, 15210 Lahti, Finland
* Correspondence: niklas.jantunen@lut.fi

Abstract: A novel solvent extraction scheme was developed for the processing of Co-rich lithium-ion battery (LIB) leachate to a Ni–Co–Mn (NCM) sulfate mixture that can be directly used in the precursor synthesis of LIB cathodes. Conventional hydrometallurgical recycling of spent LIBs usually aims at separation of Li, Ni, Co, and Mn into pure fractions, which is simplified here. Operating pH and the number of extraction stages for each separation were evaluated from batch equilibrium experiments. Two continuous countercurrent extractions with bis(2-ethylhexyl) hydrogen phosphate (D2EHPA) and one with Cyanex 272 were studied in bench-scale mixer-settler equipment, and a Ni–Co–Mn solution with n(Ni):n(Co) = 14.16 and n(Ni):n(Mn) = 8.06 was obtained. The Ni:Co:Mn molar ratio in the NCM mixture can be adjusted to, for example, 8:1:1 using a Co-rich raffinate from the same process, and no additional transition metal salts are required for tuning the composition. Stripping raffinate containing 102.7 g L^{-1} Co at 99.8% relative purity was obtained from Cyanex 272 extraction. The main benefit of the process concept is that the solvent extraction separations can be operated with less stringent requirements than when producing pure metal salts.

Keywords: continuous solvent extraction; flowsheet development; battery recycling; lithium; nickel; manganese; cobalt

Citation: Jantunen, N.; Virolainen, S.; Sainio, T. Direct Production of Ni–Co–Mn Mixtures for Cathode Precursors from Cobalt-Rich Lithium-Ion Battery Leachates by Solvent Extraction. *Metals* **2022**, *12*, 1445. https://doi.org/10.3390/met12091445

Academic Editors: Alexandre Chagnes and Kerstin Forsberg

Received: 18 July 2022
Accepted: 26 August 2022
Published: 30 August 2022

1. Introduction

Recycling of lithium-ion batteries (LIBs) has recently gained a lot of attention due to rapidly increasing use of battery-powered devices and vehicles. The larger demand for LIBs will not only increase the consumption of raw materials but the growth in LIB sales will also result in an increasing number of end-of-life batteries in the future. Sustainability imposes recovery of the spent raw materials, especially metals. Chagnes and Pospiech (2013) [1], Li et al. (2018) [2], and Meshram et al. (2014) [3] have published extensive reviews on recycling of spent LIBs. Metals are recovered from the spent LIBs using combinations of mechanical, pyrometallurgical, and hydrometallurgical processes.

The hydrometallurgical recycling of LIBs involves the liberation of metals from the spent cathode powders by reductive acid leaching. Many different mineral- and carboxylic acids can be used for leaching [1–3] but H_2SO_4 with H_2O_2 as a reductant can be recommended due to high leaching recoveries and economical advantage [4]. Hence, the discussion in this paper is focused on sulfate solutions. The LIB leachates contain the key cathode metals (Li, Co, Ni, and Mn), and the presence of Al, Fe, and Cu in small quantities is common [2,3]. Since the metal concentrations in the leachates vary depending on the composition of the utilized battery waste, the heterogeneous solutions require further processing before the recovery of the valuable metal fractions as products or intermediates. Solvent extraction, precipitation and/or ion exchange are well-known methods for the separation and purification of metals from battery leachates [1–3,5]. Especially solvent

extraction is advantageous, because the equilibrium chemistry and kinetics with commercial extractants enable the processing of large volumes of solutions at a low temperature (e.g., 20–50 °C) in a relatively short time. Furthermore, high recoveries and separation efficiencies can be achieved.

Solvent extraction processes often aim at the isolation of the metals into their own fractions from where they can be precipitated or crystallized as pure metal salts or electrowon [4–11]. However, due to the growing battery markets and shift towards Ni-rich NCM cathodes in LIB manufacturing, a multi-metal solution with specific amounts of Ni, Co, and Mn (NCM-solution) can also be one product of the solvent extraction process [12–14]. Recently, Liu et al. (2021) [12] used bis-(2-ethylhexyl)phosphinic acid (P227) to co-extract Ni, Co, and Mn from chloride leachates of NCM622 and NCM811 cathode powders. The loaded Ni, Co, and Mn were stripped and co-precipitated as oxalates, which were further processed to NCM111 and NCM622 cathode materials. A similar co-extraction approach has been studied in sulfate media by Shuya et al. (2020) [13] and Yang et al. (2017) [14]. Shuya et al. (2020) [13] used Versatic 10 (neodecanoic acid) for the co-extraction of Ni, Co, and Mn from Ni-rich sulfate leachate, whereas Yang et al. (2017) [14] used bis(2-ethylhexyl) hydrogen phosphate (D2EHPA) for NCM111 leachate.

On the other hand, the LIB leachates may be rich in Co [15,16], or otherwise not matching any commercial NCM cathode composition. In these cases, the composition of the co-precipitation synthesis mixture must be adjusted using additional transition metal salts, as Yang et al. (2017) [14] have suggested, or the excess metal content must be separated from the leachate. This paper presents a solvent extraction flowsheet that separates most of the Li, Co, and Mn from a Co-rich LIB leachate and produces a Ni-rich NCM synthesis mixture with desired composition as another product. Here, the compositional tuning and pre-concentration of the NCM synthesis mixture is done by solvent extraction alone, without using additional transition metal salts.

The processing of the LIB leachates begins with the removal of impurities (here Al, Fe, and Cu), which can be accomplished by NaOH precipitation [17], ion exchange [18], or solvent extraction [19]. The extractive method is recommended because of the potential loss of Co during the hydroxide precipitation [8,20] and part of the Mn may be lost together with the impurity metals during ion exchange [18]. Once the impurities are removed, Ni, Co, and Mn are extracted to the organic phase by suitable extractants, while at least most of the Li remains in the raffinate. Acidic organophosphorus extractants D2EHPA, Cyanex 272 (bis(2,4,4-trimethylpentyl)phosphinic acid), and PC88-A (2-ethylhexoxy(2-ethylhexyl)phosphinic acid) are well-known extractants for this kind of metal separation. Mn can be separated from Li, Co, and Ni using D2EHPA, but the separation of Co and Ni by D2EHPA is difficult [21,22]. On the other hand, Cyanex 272 has excellent Co/Ni selectivity but weak Mn/Co selectivity [22]. The Co/Ni selectivity of PC88-A is not as good as Cyanex 272 [23], and PC88-A does not exhibit phenomenal Mn/Co selectivity, either [11,24]. Instead of using a single extractant, Chen and Ho (2018) [4] suggested the separation of Li, Ni, Co, and Mn by separate Cyanex 272 and D2EHPA circuits. Mn and Co were separated from Li and Ni by Cyanex 272, and Ni was selectively precipitated from the raffinate (containing Li and Ni) using dimethylglyoxime. Mn and Co were separated by D2EHPA from the mixture of $MnSO_4$ and $CoSO_4$, which was obtained by stripping of the loaded Cyanex 272. Weak extraction of Li by D2EHPA, Cyanex 272, and PC88-A has been typically reported (<10%) at pH $\leq$ 6 [4–6,10,20,24], but the extraction of Li becomes significant when there are plenty of free extractant ligands [14,25]. D2EHPA and Cyanex 272 were selected as the extractants for this work because it was recognized that the overall material efficiency could be improved with the industry-proven extractants by an improved flowsheet. The key extraction steps of the flowsheet were studied by batch equilibrium experiments, and the numbers of required extraction stages for countercurrent extractions were evaluated by the McCabe–Thiele method. The key steps within the presented process concept were experimentally validated by continuous countercurrent experiments in mixer-settlers.

2. Materials and Methods

2.1. Chemicals

A synthetic aqueous solution (Table 1) was prepared to simulate a purified LIB leachate by dissolving appropriate amounts of $Li_2SO_4 \cdot H_2O$ (≥99%, Acros Organics, Thermo Fisher (Kandel) GmbH, Kandel, Germany), $NiSO_4 \cdot 6H_2O$ (99%, GPR RECTAPUR®, VWR Chemicals, VWR International, Leuven, Belgium), $CoSO_4 \cdot 7H_2O$ (≥97%, VWR Chemicals, VWR International, Leuven, Belgium), $MnSO_4 \cdot H_2O$ (99.8%, AnalaR NORMAPUR® ACS, Reag. Ph. Eur., VWR Chemicals, VWR International, Leuven, Belgium), and H_2SO_4 (95–97%, GPR RECTAPUR®, VWR Chemicals, VWR International, Leuven, Belgium) in pure water (de-ionized and purified by reverse osmosis). Redox potential of the solution was +590 ± 15 mV vs. SHE, and its pH was 1.0. Al, Fe, and Cu were not included here in the simulated leachate because effective methods for their removal have been reported earlier [17–19], and the removal of impurities was not in the scope of the current work. Na_2SO_4 (99.5%, AnalaR NORMAPUR® ACS, Reag. Ph. Eur., VWR Chemicals, VWR International, Leuven, Belgium) was used for ionic strength adjustment when metal solutions with experimentally determined raffinate compositions were prepared for subsequent extraction experiments.

Table 1. Composition of the simulated LIB leachate. Metal concentrations adopted from [26].

	Li	Ni	Co	Mn	H_2SO_4	*I* (Ionic Strength)
c [g L^{-1}]	2.50	2.00	16.8	2.10	15.0	–
c [mmol L^{-1}]	360	34.1	285	38.2	306	2430

0.8 M D2EHPA solution with 5 vol-% TBP as a phase modifier was prepared by dissolving bis(2-ethylhexyl) hydrogen phosphate (97%, Merck KGaA, Darmstadt, Germany) and tri-*n*-butyl phosphate (98%, Alfa Aesar, Thermo Fisher (Kandel) GmbH, Germany) in Exxsol D80 (ExxonMobil, Irving, TX, USA) aliphatic hydrocarbon mixture. Third phase formation will occur with D2EHPA and Exxsol D80 under heavy Na loading if a phase modifier is not used [27]. Cyanex 272 (85.3%, bis(2,4,4-trimethylpentyl)phosphinic acid, Solvay, Brussels, Belgium) was dissolved in Exxsol D80 without a separate phase modifier because Cyanex 272 contains 10–15% tris(2,4,4-trimethylpentyl)phosphine oxide. The Cyanex 272 solution was prepared at 0.8 M concentration. D2EHPA, Cyanex 272, TBP, and Exxsol D80 were used as received without pre-conditioning, except when stripping of metals from the loaded extractants was studied.

2.2. Batch Experiments

Batch extractions were carried out in a 1.0 dm^3 jacketed glass reactor. The pH was adjusted using aqueous NaOH solutions. Temperature was controlled by an external thermostat. O/A = 1 was used in determination of the pH isotherms, unless specifically stated otherwise. Loading isotherms were determined in a similar manner but the O/A ratio was varied, whereas pH was maintained constant. Back-extraction performance was studied by stripping the loaded extractants with H_2SO_4 at various O/A ratios without other pH adjustment. Equilibration time was 15 min.

2.3. Continuous Experiments

MEAB MSU0,5 mixer-settler units (MEAB Metallextraktion AB, Askim, Sweden) made of PTFE and PFA were used in the continuous extraction experiments. The mixer volume of a single MSU0,5 unit is 120 cm^3 and the volume of the settler is 460 cm^3. The horizontal cross-section area of the settler is 55 cm^2. The aqueous sulfate solutions and the extractant solutions were fed by PTFE diaphragm pumps (ProMinent DLTA), and a dual-channel syringe pump (Gemini 88) was used for injecting NaOH solution to control pH. Mettler-Toledo InLab® Semi-Micro-L electrodes and Consort C3060 were used for measuring and logging the pH values. All continuous experiments were done at room

temperature (21 ± 1 °C) and a minimum of five cascade volumes of liquid was processed in each experiment, as suggested by the conventional well-known theory on residence time distributions.

2.4. Analytical Methods

The samples were centrifuged to minimize entrainments before further analytical procedures. Metal concentrations were determined from both phases using ICP-MS (Agilent 7900). D2EHPA extract samples were backextracted at A/O = 20 with 5 N HCl, and the HCl raffinates from backextraction were analyzed. Similar backextraction analysis was done for the Cyanex 272 extracts, but 3 M H_2SO_4 was used instead of HCl for stripping of the metals.

2.5. Data Treatment

The percentage of extraction was calculated using Equation (1)

$$E = \frac{100D}{D + \frac{V_{aq}}{V_{org}}} \quad (1)$$

where E is the percentage of extraction [%], D is the distribution ratio ($D = [M]_{org}/[M]_{aq}$ where M denotes a metal), V_{aq} is the volume of the aqueous phase, and V_{org} is the volume of the organic phase.

The relative purity was calculated using Equation (2)

$$P_R(M) = 100\% \cdot \frac{w_M}{\sum_i w_i} \quad (2)$$

where $P_R(M)$ is the relative purity of metal M [wt.%], w is weight concentration [g L^{-1}], and the summation in the denominator includes all metals in the solution.

3. Results and Discussion

A solvent extraction process (Figure 1) for producing Li_2SO_4, $CoSO_4$, $MnSO_4$, and NCM synthesis mixtures from LIB leachates was conceptualized based on the existing knowledge on solvent extraction (see Introduction) and the requirements set by hydroxide co-precipitation synthesis of NCM cathode precursors.

The hydroxide co-precipitation syntheses are often carried out from solutions that contain Ni, Co, and Mn at a specific molar ratio (e.g., 8:1:1) at 2 mol L^{-1} total concentration of Ni, Co, and Mn [28–31]. Here, the concentrated NCM sulfate mixture is obtained via solvent extraction by stripping a metal-bearing extractant solution with moderately concentrated acid at a high solvent-to-feed (S/F) ratio. To produce an NCM sulfate mixture for the co-precipitation synthesis of, e.g., NCM811, Ni:Co, and Ni:Mn, molar ratios in the organic phase must be 8. If one or both of the ratios are higher than 8, the composition in the final NCM mixture is adjusted to the desired stoichiometric ratio using the concentrated $CoSO_4$ and $MnSO_4$ products from the same process. Here (Figure 1), a loaded D2EHPA solution with suitable amounts of Ni, Co, and Mn (NCM-D2EHPA) is obtained by mixing the NiSX extract with an extract bleed from MnSX. Alternatively, the partially loaded D2EHPA from the MnSX circuit could be used for the extraction of Ni. Co can be delivered to the NCM-D2EHPA within the NiSX extract and/or within the MnSX extract bleed because of the co-extraction of Co in both MnSX and NiSX. Therefore, a small amount of Co can be allowed in the CoSX raffinate (Figure 1) and one extraction stage is likely sufficient for the partial separation of Co. Design of the extraction and stripping stages in the process scheme was studied experimentally and will be discussed in the following sections.

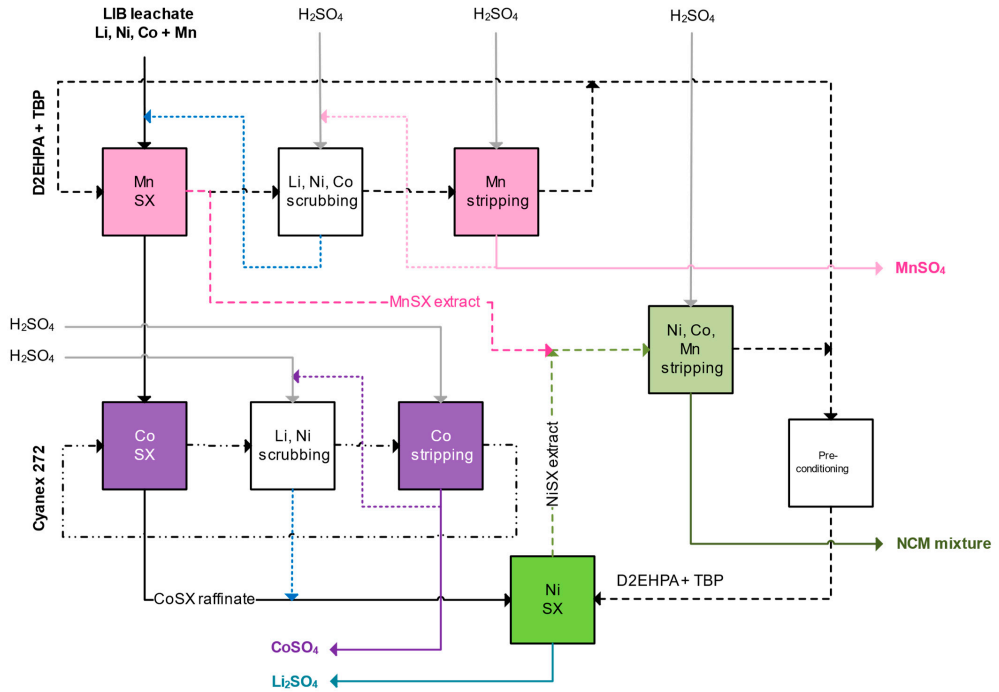

Figure 1. A simplified diagram of a solvent extraction process for the processing of lithium-ion battery leachates. The blocks studied in this work are colored. Dashed line = D2EHPA stream (organic), dashdot line = Cyanex 272 stream (organic), solid line = aqueous stream, dotted line = bleed-off from stripping raffinate (aqueous).

3.1. Selecting the pH for Mn, Co, and Ni Extraction Stages

Mn is the most easily extracted metal by D2EHPA among the metals in the simulated leachate (Table 1), and over 95% Mn was extracted from the simulated leachate by 0.8 M D2EHPA at pH $\geq$ 3.14 (Figure 2a). The pH_{50} values in extraction by 0.8 M D2EHPA were approximately 1.98 for Mn, 3.95 for Co, and 4.70 for Ni as determined by graphical interpolation. These pH_{50} values agree reasonably well with those given by Sole (2018) [22] and further emphasize why the Co–Ni separation by D2EHPA is more challenging than Mn–Co and Mn–Ni separations. Na^+ ions were introduced into the Li–Ni–Co–Mn sulfate system due to pH adjustment (Figure 2a), hence the extraction of Na. The extraction of Co and Ni was incomplete likely because of the extractant saturation. According to the ICP-MS analysis, the loaded 0.8 M D2EHPA contained 0.11 mol L^{-1} Li, 0.18 mol L^{-1} Na, 0.03 mol L^{-1} Ni, 0.26 mol L^{-1} Co, and 0.04 mol L^{-1} Mn in equilibrium at pH = 7.7. These concentrations seem to suggest over-stoichiometric extraction when assuming 2:1 ligand-to-metal stoichiometry for the extraction of Ni, Co, and Mn; and 1:1 extraction stoichiometry for Li and Na, respectively. This may be explained by surfactant effects, such as formation of reversed micelles or microemulsions [27].

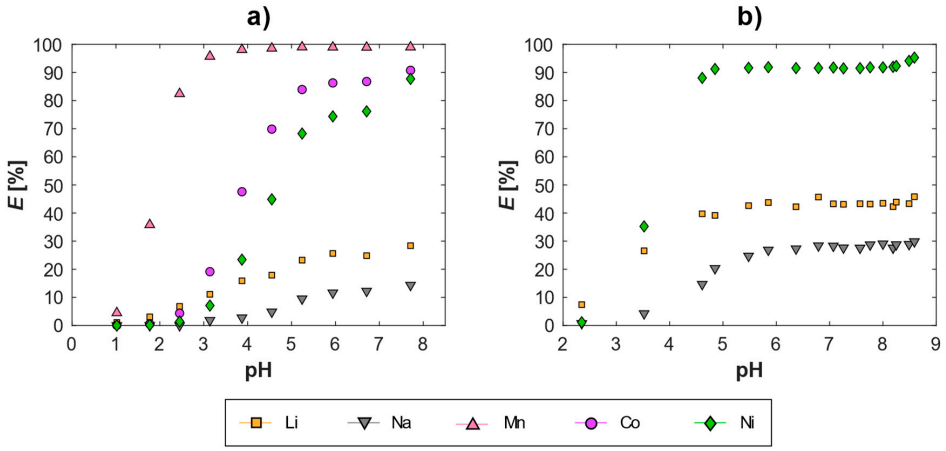

Figure 2. The effect of pH on the extraction of Li, Ni, Co, Mn, and Na by 0.8 M D2EHPA (modified by 5 vol-% TBP and diluted in Exxsol D80). $T = 25 \pm 1$ °C; $t_{eq} = 15$ min; O/A = 1. Initial aqueous concentrations [g L^{-1}]: (**a**) Li: 2.52; Ni: 2.05; Co: 16.5; Mn: 2.09; (**b**) Li: 2.29; Na: 26.2; Ni: 1.94.

To study the effect of pH on extraction of Ni and Li by 0.8 M D2EHPA, an aqueous solution containing Li_2SO_4, $NiSO_4$, and Na_2SO_4 was used in extraction experiments to simulate Mn- and Co-free raffinate. Instead of H_2SO_4, Na_2SO_4 was used to adjust the ionic strength to a similar level with the simulated leachate (Table 1) because Na^+ will be introduced into the system if NaOH is used for pH adjustment during the extraction of Mn and Co (Figure 1). A total of 91.2% Ni was extracted at pH = 4.85 but further increases in pH had a limited effect in increasing the extraction of Ni and Li (Figure 2b). The pH isotherms of Ni and Li were shifted toward lower pH values in the absence of Mn and Co (Figure 2), and much higher amounts of Ni, Li, and Na were extracted from the Li_2SO_4–$NiSO_4$–Na_2SO_4 system than the simulated leachate. Increases in pH above 4.85 mostly increased the extraction of Na, and an increase in $[Na]_{org}$ from 8.0 to 13.3 g L^{-1} was observed due to addition of NaOH. At pH $\geq$ 4.85 there was 1.6–1.7 g L^{-1} Ni and 0.9–1.1 g L^{-1} Li in the organic phase, meaning that most of the extractant was in the form of Na-D2EHPA.

Cyanex 272 requires a higher pH than D2EHPA for extracting the metals since bis(2,4,4-trimethylpentyl)phosphinic acid is a weaker acid than D2EHPA. The pH_{50} values in extraction by 0.8 M Cyanex 272 were 3.82 for Mn and 4.44 for Co. The pH_{50} value (Figure 3a) for Co is in close agreement with the pH isotherm reported by Virolainen et al. (2017) [10] for 1 M Cyanex 272, and the minor difference is explained by different extractant concentration. Extraction of Li, Ni, or Na by 0.8 M Cyanex 272 was minimal at O/A = 1 (Figure 3a). However, the extraction of Co was incomplete (96.6%) at O/A = 1 and pH = 6.35 because there was more than enough Mn and Co to load the extractant near its practical maximum capacity. Cyanex 272 turns into an extremely viscous gel under heavy Co loading, and the rheology would not allow operation above pH = 6.35 at O/A = 1. The viscosity increase is related to polymerization of the Co-loaded Cyanex 272 when the loading of Co reaches 70–75% of the theoretical extractant capacity [32]. Since Cyanex 272 cannot be used in practice under high Co loading, the pH isotherms for 0.8 M Cyanex 272 were determined also using O/A = 2.5 (Figure 3b). An increase in the amount of extractant enables a higher amount of metals to be extracted and shifts the pH isotherms towards lower pH values (Figure 3b). In total, 99.8% Mn and 99.0% Co were extracted by Cyanex 272 at pH = 5.27 and O/A = 2.5, whereas 13.9% Ni and 3.6% Li were co-extracted (Figure 3b). Both Cyanex

272 and D2EHPA extract Li and Na when there are not enough more extractable cations (such as H^+ and Mn^{2+}) to occupy the extractant ligands (Figures 2 and 3). This observation is consistent with [14,25] and similar behavior has also been reported with Versatic 10 [13].

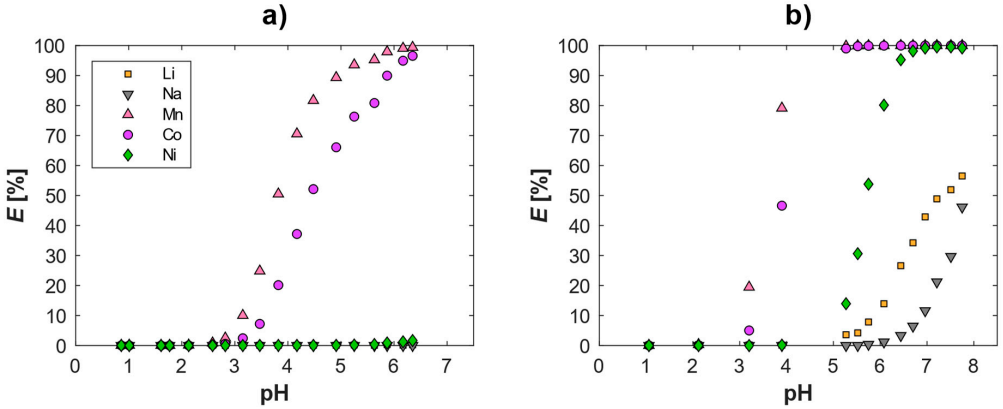

Figure 3. The effect of pH on the extraction of Li, Ni, Co, Mn, and Na by 0.8 M Cyanex 272 (diluted in Exxsol D80). $T = 25 \pm 1$ °C; $t_{eq} = 15$ min. Initial aqueous concentrations [g L^{-1}]: Li: 2.52; Ni: 2.05; Co: 16.5; Mn: 2.09. Subfigures: (**a**) O/A = 1; (**b**) O/A = 2.5.

3.2. Separation of Mn from Li, Ni, and Co by 0.8 M D2EHPA

All the Mn was extracted by 0.8 M D2EHPA, but co-extraction of the other metals increased as the number of metal-free extractant ligands increased (Figures 2a and 4). The relative purity of Mn in the organic phase is increased when O/A is lowered, but a high recovery of Mn cannot be obtained by single extraction using small O/A (Figure 4b). Therefore, multiple extraction stages will be required to achieve both a high percentage of extraction and a good selectivity for Mn. McCabe–Thiele analysis suggested that 99.5% of the Mn could be removed by 0.8 M D2EHPA in three ideal countercurrent extraction stages operating with S/F = 0.8 at pH = 2.50 (Figure 5). A total of 94.2% Mn was extracted from the simulated leachate in three countercurrent stages (Table 2) and the raffinate contained 0.12 g L^{-1} Mn. The experimental results (Table 2) are different from the theoretical prediction (Figure 5) likely because the raffinate exit stage operated at pH = 2.08, whereas the prediction assumes pH = 2.50 for all stages. Moreover, chemical equilibrium is often not achieved in continuous extractors, i.e., the stage efficiency is below 100%. The separation of Mn from Li, Ni, Co, and Na can be further improved by lowering S/F and increasing the number of extraction stages. Considering the process concept in Figure 1, complete removal of Mn is more important than minimizing the co-extraction of Li, Ni, and Co. Any Mn remaining in the raffinate will be extracted in the next process step by Cyanex 272 during the extraction of Co and will negatively impact the purity of the $CoSO_4$ product (Figure 1, see Section 3.3).

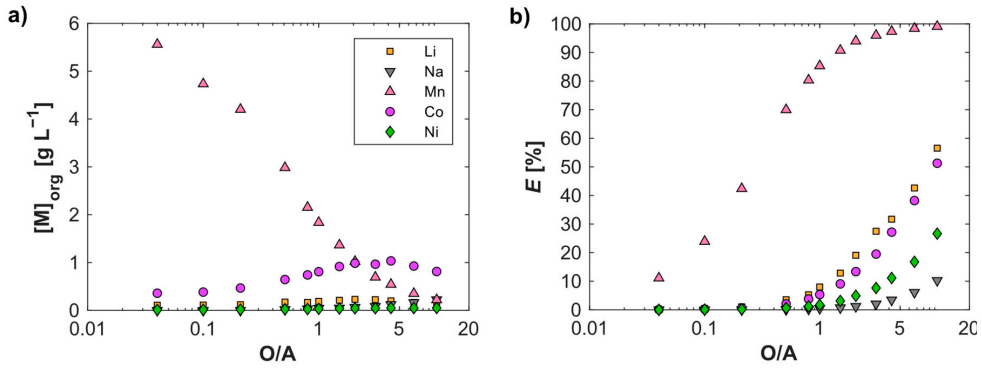

Figure 4. Effect of volumetric phase ratio on (**a**) metal concentrations in the organic phase and (**b**) the percentage of Li, Ni, Co, Mn, and Na extracted by 0.8 M D2EHPA (modified by 5 vol-% TBP and diluted in Exxsol D80). $T = 25 \pm 1$ °C; pH = 2.5; t_{eq} = 15 min. Initial aqueous concentrations [g L^{-1}]: Li: 2.63; Ni: 1.98; Co: 16.2; Mn: 2.07. Note the logarithmic O/A-axis.

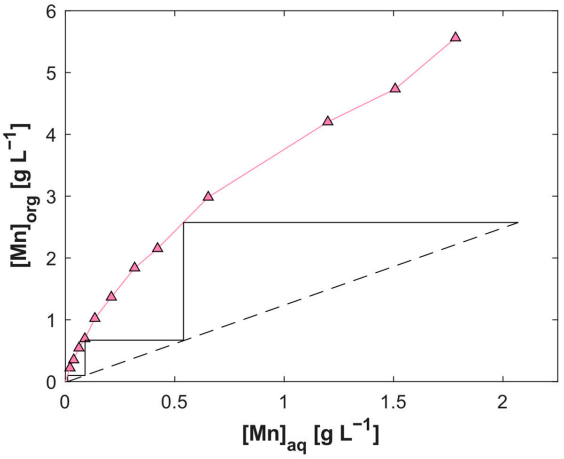

Figure 5. A McCabe–Thiele analysis applied on the equilibrium distribution of Mn between 0.8 M D2EHPA (modified by 5 vol-% TBP and diluted in Exxsol D80) and simulated LIB leachate. $T = 25 \pm 1$ °C; pH = 2.5; t_{eq} = 15 min. Initial aqueous concentrations [g L^{-1}]: Li: 2.63; Ni: 1.98; Co: 16.2; Mn: 2.07. The operating line was calculated with S/F = 0.8 and 99.5% Mn removal.

Table 2. Compositions of the extract and raffinate in three-stage countercurrent extraction of Mn from a simulated LIB leachate by 0.8 M D2EHPA. S/F = 0.8; $T = 21 \pm 1$ °C; τ_{mix} = 4 min. Concentrations in [mg L^{-1}]. Numbering of the stages is started from the organic feed stage.

	[Li]	[Na]	[Mn]	[Co]	[Ni]	pH_{avg}
Simulated leachate	2340	6930	2070	16,200	1820	Stage 1: 2.08 ± 0.03
Raffinate	2180	8300	115	15,700	1790	Stage 2: 2.52 ± 0.06
Extract	151	21.2	2970	541	17.7	Stage 3: 2.49 ± 0.02

Co, Ni, and Li were co-extracted during the extraction of Mn from the simulated leachate (Table 2). Small amounts of co-extracted Li, Ni, and Co in D2EHPA (Figure 4; Table 2) are not a concern considering the production of NCM mixtures but scrubbing of the Mn-rich extract with dilute H_2SO_4 and/or $MnSO_4$ solution is recommended so that a purified $MnSO_4$ solution can be obtained (Figure 6). Li, Ni, Co, and Mn will be completely stripped when the amount of H_2SO_4 is sufficiently high (Figure 6b,d), but the separation of Mn is enhanced when the amount of H_2SO_4 is limited with respect to the stoichiometric amount of Mn. In total, 41.3% Li, 96.2% Ni, 79.9% Co, and 3.9% Mn were backextracted from the loaded 0.8 M D2EHPA by 0.5 M H_2SO_4 at O/A = 50 (Figure 6b). A concentrated $MnSO_4$ solution can be obtained by stripping the Mn-D2EHPA with moderately concentrated H_2SO_4 (Figure 6c) at large O/A ratio, and a bleed from the concentrated $MnSO_4$ raffinate can be used for scrubbing (Figure 1). Then, the raffinate from scrubbing can be blended in the LIB leachate, which enters the Mn extraction stages (Figure 1).

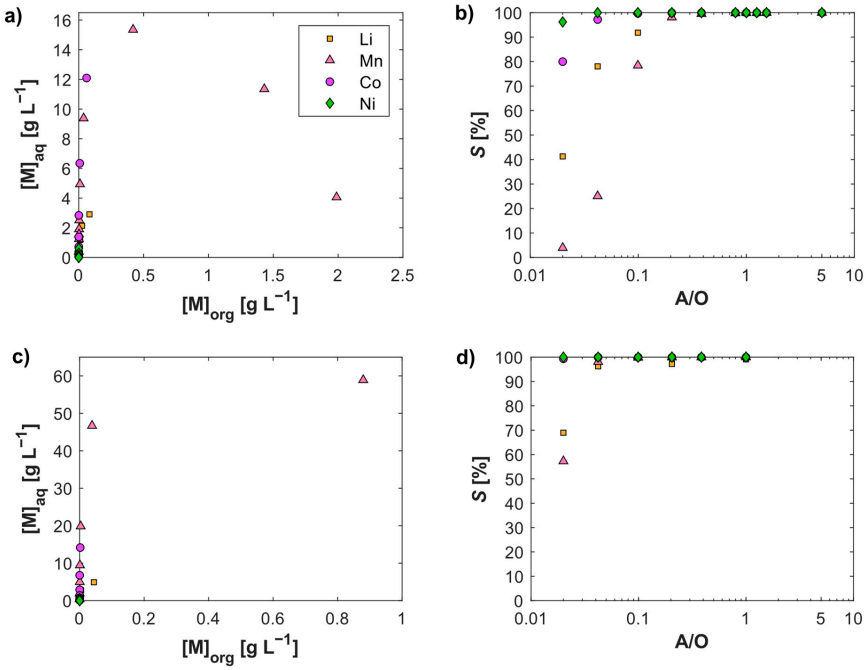

Figure 6. Backextraction of Li, Ni, Co, and Mn by H_2SO_4 from loaded 0.8 M D2EHPA (modified by 5 vol-% TBP and diluted in Exxsol D80). $T = 25 \pm 1$ °C; $t_{eq} = 15$ min. Initial concentrations in the organic phase [g L^{-1}]: Li: 0.15; Ni: 0.01; Co: 0.3; Mn: 2.02. Subfigures: (**a**) Distribution of metals in stripping with 0.5 M H_2SO_4; (**b**) Percentages of metals stripped with 0.5 M H_2SO_4; (**c**) Distribution of metals in stripping with 2 M H_2SO_4; (**d**) Percentages of metals stripped with 2 M H_2SO_4. Note the logarithmic A/O-axis in subfigures (**b**,**d**).

3.3. Separation of Co from Li and Ni by Cyanex 272

Since Mn can be completely extracted from the simulated leachate, the loading isotherm of Co with 0.8 M Cyanex 272 (Figure 7) was determined for a Mn-free solution at pH = 5.3, which was chosen based on the pH isotherms (Figure 3b). The highest $[Co]_{org}$ (14.5 g L^{-1}) (Figure 7a) corresponds to approximately 61.5% of the theoretical loading capacity of 0.8 M Cyanex 272. However, 0.8 M Cyanex 272 was highly selective for

Co at pH = 5.3 with O/A ratios between 0.04–1.5 (Figure 7c), meaning that $[Co]_{org}$ can be maintained somewhat lower than at 14 g L^{-1} to avoid problems related to high viscosity (see chapter 3.1). Although the concentrations of Li and Ni were low (<0.3 g L^{-1}) in the Cyanex 272 extracts (Figure 7b), their extraction became significant after the aqueous phase was practically free from Co (Figure 7c).

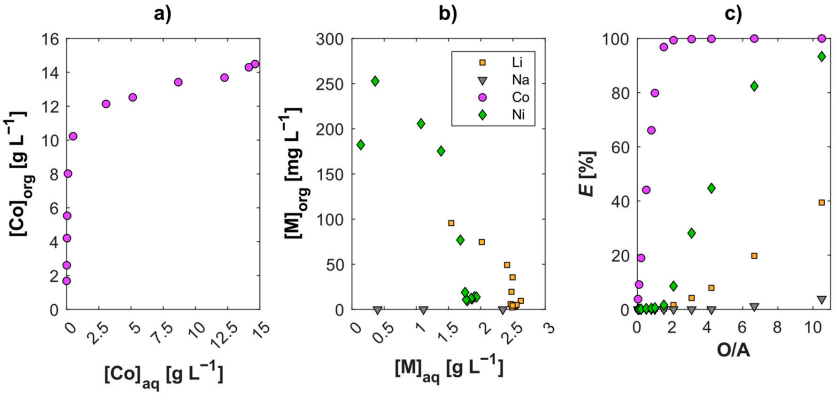

Figure 7. Distribution of Li, Ni, Co, and Na between 0.8 M Cyanex 272 (diluted in Exxsol D80) and Mn-free simulated LIB leachate: (**a**) Concentrations of cobalt in equilibrium; (**b**) Concentrations of Li, Ni, and Na in equilibrium; (**c**) Effect of O/A ratio on percentages of metals extracted. $T = 25 \pm 1$ °C; pH = 5.3; t_{eq} = 15 min. Initial aqueous concentrations [g L^{-1}]: Li: 2.70; Ni: 1.91; Co: 15.2.

Co was concentrated to over 100 g L^{-1} by stripping loaded Cyanex 272 with 2 M H_2SO_4 at O/A = 10–50 (Figure 8). The Cyanex 272 solution for the stripping experiments (Figure 8) was prepared by single extraction at pH = 4.95 and O/A = 1.5. Stripping the loaded Cyanex 272 once at O/A = 10 backextracted all Li and Ni, and 99.9% Co, resulting in 99.8 wt.% relative purity for Co. Scrubbing of Li and Ni can be applied before stripping to obtain the Co fraction at an even higher purity [10,33].

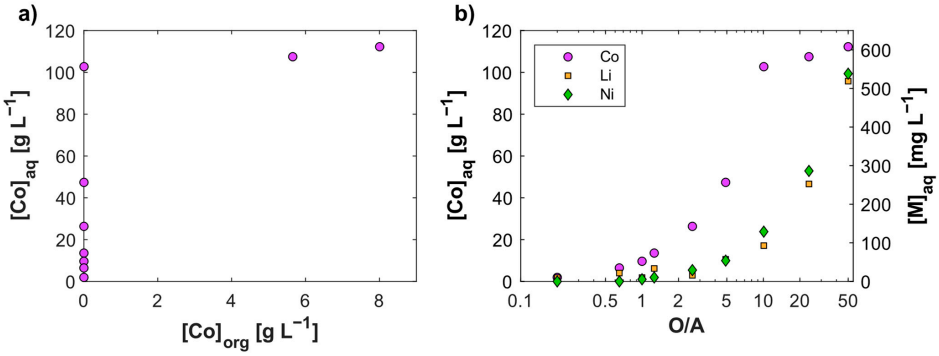

Figure 8. Backextraction of Co, Li, and Ni by 2 M H_2SO_4 from loaded 0.8 M Cyanex 272 (diluted in Exxsol D80): (**a**) Equilibrium distributions of Co; (**b**) Effect of O/A ratio on the metal concentrations in the stripping raffinate. $T = 25 \pm 1$ °C; t_{eq} = 15 min. Initial concentrations in the organic phase: 10.2 g L^{-1} Co, 10.5 mg L^{-1} Li, and 10.1 mg L^{-1} Ni. Note the logarithmic O/A-axis and secondary *y*-axis for Ni and Li in subfigure (**b**).

A total of 99.8% Co was extracted by 0.8 M Cyanex 272 in three countercurrent stages operating at S/F = 2.5, leaving approximately 30 mg L^{-1} Co in the raffinate (Table 3). The relative purity of Co in the extract was 99.2 wt.% (Table 3). A major benefit of the current process scheme is that complete removal of Co is not required when NCM synthesis mixtures are produced instead of pure Ni fractions because the remaining Co in the raffinate will eventually be extracted together with Ni by D2EHPA (Figure 1). Therefore, the production of NCM synthesis mixtures is more flexible than the production of purified Ni fractions. A solution containing 2 g L^{-1} Ni allows approximately 0.25 g L^{-1} Co to maintain the stoichiometric ratio of NCM811 and, respectively, 0.66 g L^{-1} Co can be allowed to produce NCM622 sulfate mixture (see Section 3.5). The tolerable amount of Co in the CoSX raffinate also depends on the level of Co in the Mn-D2EHPA (Figure 1). Comparable removal rate (98.8%) and relative purity of Co in the organic phase (99.4 wt.%) was obtained in a single extraction at O/A = 2 (Figure 7), meaning that additional extraction stages do not bring significant advantages with the process concept in Figure 1.

Table 3. Compositions of the extract and raffinate in three-stage countercurrent extraction of Co from the MnSX raffinate by 0.8 M Cyanex 272. S/F = 2.5; $T = 21 \pm 1$ °C; τ_{mix} = 5.7 min. Concentrations in [mg L^{-1}]. Numbering of the stages is started from the organic feed stage.

	[Li]	[Na]	[Mn]	[Co]	[Ni]	pH_{avg}
MnSX raffinate (aq. feed)	2180	8610	111	16,200	1990	Stage 1: 5.35 ± 0.43
Raffinate	1930	18,900	0	27.4	2390	Stage 2: 4.86 ± 0.31
Extract	3.89	0	46.0	6490	4.14	Stage 3: 3.68 ± 0.19

The unexpectedly high [Ni] in the raffinate (2.39 g L^{-1}; Table 3) was a temporary spike likely due to pH fluctuation. Once the pH stabilized, the excess Ni was backextracted and resulted in a higher analytical concentration. This might also explain the mass balance error in the Li concentrations. As to Mn and Co, the mass balance is closed because they are extracted at a significantly lower pH than Ni and Li. The small amount of Mn in the aqueous feed (0.11 g L^{-1}) had a negligible effect on the separation of Co from Li and Ni by 0.8 M Cyanex 272 because the extractant was not even near saturation (Table 3).

3.4. Separation of Ni and Li

Several extraction stages are required for nearly complete removal (≥99%) and preconcentration of Ni by 0.8 M D2EHPA at pH = 4.7 (Figure 9a). A high percentage of Ni (98.1%) was extracted in two countercurrent stages operating at S/F = 0.5 and pH = 7.0–7.7 (Table 4) but $[Ni]_{org}/[Li]_{org}$ remained relatively low. If Ni is extracted from a solution that contains a small amount of Co, the remaining Co is also extracted during the extraction of Ni with both D2EHPA and Cyanex 272 (see Section 3.1). Lowering of the O/A ratio did not result in a decrease in $[Li]_{org}$ (Figure 9b), which suggests that Ni^{2+} ions cannot displace Li^{+} from D2EHPA. The co-extracted Li can likely be recovered (see Section 3.5), so the extraction of Li does not need to be eliminated but it is recommended to maximize the $[Ni]_{org}/[Li]_{org}$ ratio during the extraction of Ni (see Section 3.5). Any residual Ni, Co, or Mn in the Li-rich raffinate can be precipitated as, e.g., mixed hydroxides, which can be recycled to the process feed. Li can be precipitated from the Ni-, Co-, and Mn-free raffinate as Li_2CO_3.

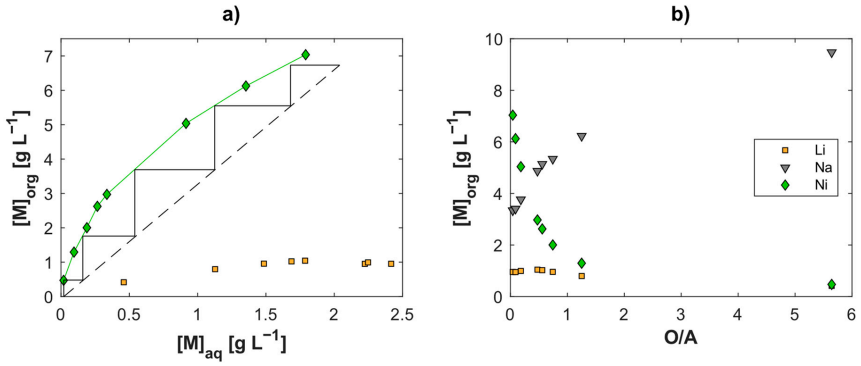

Figure 9. (**a**) A McCabe–Thiele analysis applied on the equilibrium distribution of Ni between 0.8 M D2EHPA (modified by 5 vol-% TBP and diluted in Exxsol D80) and a sulfate solution containing initially 2.41 g L^{-1} Li, 2.04 g L^{-1} Ni, and 20.8 g L^{-1} Na; and (**b**) metal concentrations in the organic phase at different O/A ratios. $T = 25 \pm 1$ °C; pH = 4.7; t_{eq} = 15 min. The operating line was calculated with S/F = 0.3 and 99% Ni removal.

Table 4. Compositions of the extract and raffinate in two-stage countercurrent extraction of Ni and Li from the CoSX raffinate by pre-neutralized 0.8 M D2EHPA. S/F = 0.5; $T = 21 \pm 1$ °C; τ_{mix} = 4 min. Concentrations in [mg L^{-1}]. Pre-neutralization: 81.5 mL 10 M NaOH in one liter of 0.8 M D2EHPA (modified by 5 vol-% TBP). Numbering of the stages is started from the organic feed stage.

	[Li]	[Na]	[Mn]	[Co]	[Ni]	pH_{avg}
CoSX raffinate (aq. feed)	2580	20,900	0	98.5	2000	Stage 1: 7.19 ± 0.12
Raffinate	1680	26,700	0	1.03	38.7	Stage 2: 7.66 ± 0.10
Extract	1770	9150	0	191	3830	

3.5. Production of the NCM Synthesis Mixture

Mixing the MnSX extract (Table 2) with the NiSX extract (Table 4) at 0.15:1 volumetric ratio yields NCM-D2EHPA where n(Ni):n(Mn) = 8.06 and n(Ni):n(Co) = 14.16. The Ni:Co:Mn stoichiometric ratio can be adjusted accurately to, for example, 8:1:1 by changing the mixing ratio of the D2EHPA extracts as well as through the addition of the concentrated $CoSO_4$ raffinate (Figure 8a) after complete stripping of the NCM-D2EHPA. However, the NCM-D2EHPA for the continuous stripping experiment (Table 5) was, for practical reasons, loaded with metals in a single contact instead of mixing two extracts from separate countercurrent extractions. Therefore, the initial $[Na]_{org}$ was unnecessarily high (Figure 9b).

Table 5. Compositions of the extract and raffinate in continuous stripping of Ni, Co, Mn, Li, and Na from 0.8 M NCM-D2EHPA with 3 M H_2SO_4. S/F = 10; $T = 21 \pm 1$ °C; τ_{mix} = 7.3 min. Concentrations in [mmol L^{-1}].

	[Li]	[Na]	[Mn]	[Co]	[Ni]	pH_{avg}
NCM-D2EHPA (org. feed)	55.2	391	11.2	11.1	89.9	
Raffinate	228	1770	30.1	49.2	399	1.62 ± 0.08
Extract	9.38	40.4	6.68	1.55	11.8	

Stripping of Ni, Co, and Mn from 0.8 M NCM-D2EHPA was incomplete with a substoichiometric amount of H_2SO_4, and the concentrations of Ni, Co, and Mn in the organic phase were not decreasing significantly until most (≈75%) of the Na was stripped

(Figure 10). Table 5 and Figure 11 show the raffinate composition in continuous stripping of NCM811-D2EHPA. The total concentration of Ni, Co, and Mn ([NCM]) was increased from 112 mmol L^{-1} to 478 mmol L^{-1}. Significantly higher [NCM] can be obtained from stripping of NCM-D2EHPA with optimized composition, sufficiently high stripping acid concentration, and S/F ratio (see Sections 3.2 and 3.3). In addition to the possibility of concentrating the NCM mixture to the level required for direct precursor precipitation, controlling the amount of Li and Na in NCM-D2EHPA is important because their back-extraction consumes the stripping acid and they have the lowest solubilities—as grams of metal per kg of H_2O—among the metal sulfates studied here (Figure 12). It is likely that Li can be recovered from the NCM synthesis mixture by carbonate precipitation after precipitating the NCM precursor because the solubility limit of LiOH in water enables 36 g Li per kilogram of water at 25 °C [34].

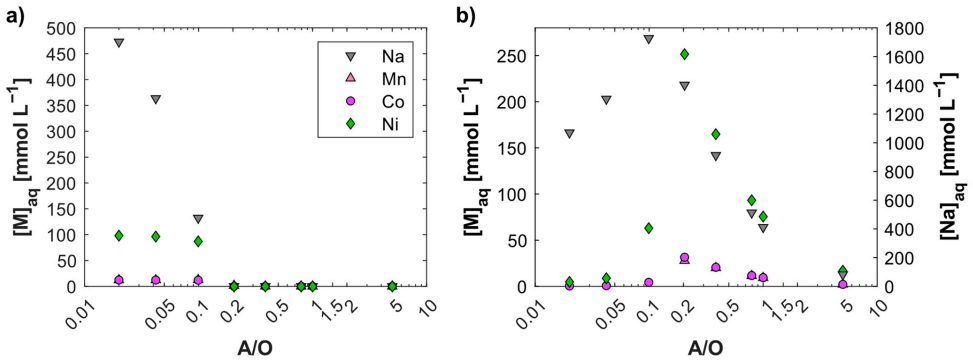

Figure 10. Equilibrium concentrations of metals in (**a**) the organic phase and (**b**) the aqueous phase in stripping of Ni, Co, Mn, and Na from 0.8 M NCM-D2EHPA with 2 M H_2SO_4. $T = 25 \pm 1$ °C; t_{eq} = 15 min. $[Ni]_{0,org}$ = 93.1 mmol L^{-1}, $[Co]_{0,org}$ = 11.7 mmol L^{-1}, $[Mn]_{0,org}$ = 11.5 mmol L^{-1}, $[Na]_{0,org}$ = 529 mmol L^{-1}.

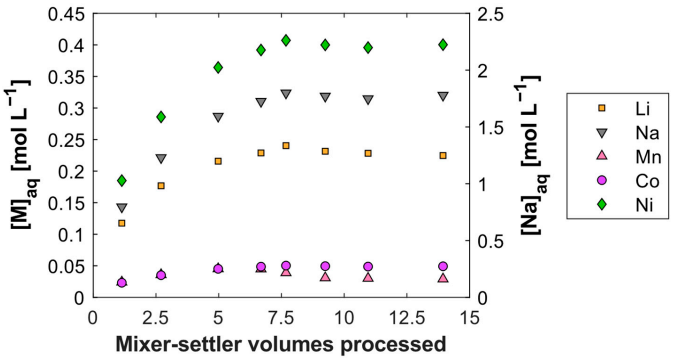

Figure 11. Metal concentrations in the raffinate during continuous stripping of 0.8 M NCM-D2EHPA with 3 M H_2SO_4. $T = 21 \pm 1$ °C, S/F = 10; τ_{mix} = 7.3 min. $[Li]_{0,org}$ = 55.2 mmol L^{-1}, $[Ni]_{0,org}$ = 89.9 mmol L^{-1}, $[Co]_{0,org}$ = 11.1 mmol L^{-1}, $[Mn]_{0,org}$ = 11.2 mmol L^{-1}, $[Na]_{0,org}$ = 391 mmol L^{-1}.

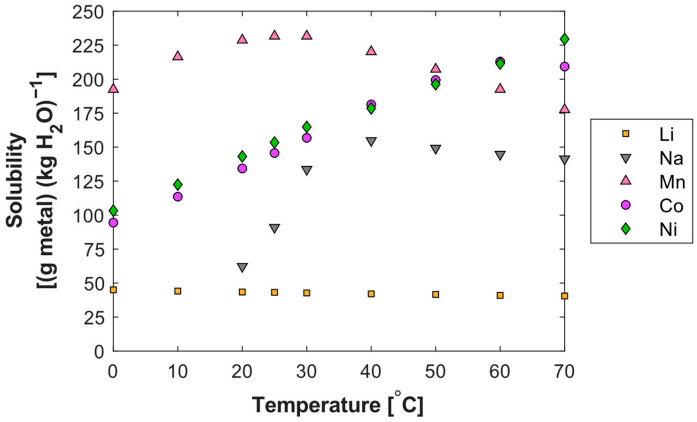

Figure 12. Solubilities of the metal sulfates in water (binary systems) at different temperatures given as grams of metal cations per kilogram of water. Data from [34,35].

The mass balance in Table 5 is not closed because the extract-to-raffinate volumetric flow ratio differed from S/F = 10. The change in volumetric phase ratio can easily be observed visually, especially in batch extraction. The changes in phase volumes are likely explained by the break-up of microemulsion or reversed micelle structures and by the release of hydrated water, and this must be considered in process optimization.

Preparing a Ni-rich sulfate solution from a Co-rich LIB leachate without additional input of transition metal salts is a task with increased complexity (Figure 1). When the molar ratios of Ni, Co, and Mn in the LIB leachate match with a commercial NCM cathode composition or when additional $NiSO_4$, $CoSO_4$, and $MnSO_4$ are used to adjust the solution composition [12–14], a more straightforward solvent extraction process than the concept in Figure 1 can be used. Adjusting the Ni:Co:Mn molar ratio in the Co-rich leachate (Table 1) to 8:1:1 using transition metal salts would require approximately 590 kg $NiSO_4 \cdot 6H_2O$ and 42 kg $MnSO_4 \cdot H_2O$ per 1.0 m^3 of leachate. The requirement for compensating the deficit is high since much more metals should be introduced into the process than is delivered into it from the 1.0 m^3 of leachate. Then, the solution should be diluted if 2 mol L^{-1} is the target total concentration, and 1.4–1.5 m^3 of NCM811 synthesis mixture would be obtained. The process concept in Figure 1 produces approximately 21 L of NCM811 synthesis mixture (at 2 mol L^{-1} total concentration of Ni, Co, and Mn) from 1 m^3 of leachate (Table 1), assuming 100% material recovery. The material loops of the transition metals are closed in the concept of Figure 1. In addition, purified Li_2SO_4, $CoSO_4$ and $MnSO_4$ fractions are obtained.

4. Conclusions

In this study, a solvent extraction process concept was developed and demonstrated experimentally for the processing of Co-rich LIB leachates into Ni-rich solutions that are suitable for producing, for example, NCM811 or NCM622 cathode precursors. Furthermore, it is possible to obtain Li and excess Mn and Co in high purity into their own fractions. The proposed process offers an alternative to producing NCM cathode precursors from pure $NiSO_4$, $CoSO_4$, and $MnSO_4$ salts. The process is robust because total separation of the metals is not required, and the compositions of the streams can be adjusted by internal recycling.

94.2% Mn was extracted by 0.8 M D2EHPA from the simulated LIB leachate in three countercurrent stages operating at pH 2.1–2.5, $T = 21 \pm 1$ °C, and S/F = 0.8. Part of the Mn-rich D2EHPA, which also contains Co, Li, and Ni, can be blended with Ni-rich D2EHPA from another stage of the process to form NCM-D2EHPA. The NCM-D2EHPA is stripped

using moderately concentrated H_2SO_4 at a high S/F ratio to obtain the NCM mixture, which can be used in the precursor synthesis. Co, Li, and Ni are scrubbed from the excess Mn-rich D2EHPA to enable the production of purified $MnSO_4$.

All of the remaining Mn and 99.8% Co was extracted by 0.8 M Cyanex 272 in three countercurrent stages operating at pH 3.7–5.4, $T = 21 \pm 1$ °C, and S/F = 2.5. The relative purity of Co in the extract was over 99 wt.%. Subsequently, 98.1% Ni was extracted from the Co-barren raffinate by pre-neutralized 0.8 M D2EHPA in two countercurrent stages operating at pH 7.2–7.7, $T = 21 \pm 1$ °C, and S/F = 0.5. The raffinate from continuous Ni extraction contained 1.68 g L^{-1} Li, 26.7 g L^{-1} Na, 1 mg L^{-1} Co, and 38.7 mg L^{-1} Ni. Continuous stripping of the NCM-D2EHPA increased the total concentration of Ni, Co, and Mn from 112 mmol L^{-1} to 478 mmol L^{-1}. The different steps of the process were not optimized.

Author Contributions: Conceptualization, N.J., S.V. and T.S.; data curation, N.J. and S.V.; formal analysis, N.J. and S.V.; funding acquisition, S.V. and T.S.; investigation, N.J.; methodology, N.J., S.V. and T.S.; project administration, S.V. and T.S.; resources, S.V. and T.S.; supervision, S.V. and T.S.; validation, N.J. and S.V.; visualization, N.J.; writing—original draft, N.J.; writing—review and editing, S.V. and T.S. All authors have read and agreed to the published version of the manuscript.

Funding: The research was funded by the BATCircle2.0 project (main funder Business Finland, grant number 44412/31/2020).

Institutional Review Board Statement: Not applicable.

Informed Consent Statement: Not applicable.

Data Availability Statement: The data presented in this study are available within the article.

Acknowledgments: The experimental assistance from Antti Tolvanen (LUT, Finland) and Siiri Närvänen (LUT, Finland) is gratefully acknowledged.

Conflicts of Interest: The authors declare no conflict of interest. The funders had no role in the design of the study; in the collection, analyses, or interpretation of data; in the writing of the manuscript; or in the decision to publish the results.

References

1. Chagnes, A.; Pospiech, B. A Brief Review on Hydrometallurgical Technologies for Recycling Spent Lithium-Ion Batteries. *J. Chem. Technol. Biotechnol.* **2013**, *88*, 1191–1199. [CrossRef]
2. Li, L.; Zhang, X.; Li, M.; Chen, R.; Wu, F.; Amine, K.; Lu, J. The Recycling of Spent Lithium-Ion Batteries: A Review of Current Processes and Technologies. *Electrochem. Energy Rev.* **2018**, *1*, 461–482. [CrossRef]
3. Meshram, P.; Pandey, B.D.; Mankhand, T.R. Extraction of Lithium from Primary and Secondary Sources by Pre-Treatment, Leaching and Separation: A Comprehensive Review. *Hydrometallurgy* **2014**, *150*, 192–208. [CrossRef]
4. Chen, W.S.; Ho, H.J. Recovery of Valuable Metals from Lithium-Ion Batteries NMC Cathode Waste Materials by Hydrometallurgical Methods. *Metals* **2018**, *8*, 321. [CrossRef]
5. Chen, X.; Chen, Y.; Zhou, T.; Liu, D.; Hu, H.; Fan, S. Hydrometallurgical Recovery of Metal Values from Sulfuric Acid Leaching Liquor of Spent Lithium-Ion Batteries. *Waste Manag.* **2015**, *38*, 349–356. [CrossRef]
6. Chen, X.; Zhou, T.; Kong, J.; Fang, H.; Chen, Y. Separation and Recovery of Metal Values from Leach Liquor of Waste Lithium Nickel Cobalt Manganese Oxide Based Cathodes. *Sep. Purif. Technol.* **2015**, *141*, 76–83. [CrossRef]
7. Liu, T.; Chen, J.; Li, H.; Li, K. An Integrated Process for the Separation and Recovery of Valuable Metals from the Spent $LiNi_{0.5}Co_{0.2}Mn_{0.3}O_2$ Cathode Materials. *Sep. Purif. Technol.* **2020**, *245*, 116869. [CrossRef]
8. Suzuki, T.; Nakamura, T.; Inoue, Y.; Niinae, M.; Shibata, J. A Hydrometallurgical Process for the Separation of Aluminum, Cobalt, Copper and Lithium in Acidic Sulfate Media. *Sep. Purif. Technol.* **2012**, *98*, 396–401. [CrossRef]
9. Tanong, K.; Tran, L.H.; Mercier, G.; Blais, J.F. Recovery of Zn (II), Mn (II), Cd (II) and Ni (II) from the Unsorted Spent Batteries Using Solvent Extraction, Electrodeposition and Precipitation Methods. *J. Clean. Prod.* **2017**, *148*, 233–244. [CrossRef]
10. Virolainen, S.; Fallah Fini, M.; Laitinen, A.; Sainio, T. Solvent Extraction Fractionation of Li-Ion Battery Leachate Containing Li, Ni, and Co. *Sep. Purif. Technol.* **2017**, *179*, 274–282. [CrossRef]
11. Wang, F.; He, F.; Zhao, J.; Sui, N.; Xu, L.; Liu, H. Extraction and Separation of Cobalt(II), Copper(II) and Manganese(II) by Cyanex272, PC-88A and Their Mixtures. *Sep. Purif. Technol.* **2012**, *93*, 8–14. [CrossRef]
12. Liu, T.; Chen, J.; Shen, X.; Li, H. Regulating and Regenerating the Valuable Metals from the Cathode Materials in Lithium-Ion Batteries by Nickel-Cobalt-Manganese Co-Extraction. *Sep. Purif. Technol.* **2021**, *259*, 118088. [CrossRef]

13. Shuya, L.; Yang, C.; Xuefeng, C.; Wei, S.; Yaqing, W.; Yue, Y. Separation of Lithium and Transition Metals from Leachate of Spent Lithium-Ion Batteries by Solvent Extraction Method with Versatic 10. *Sep. Purif. Technol.* **2020**, *250*, 117258. [CrossRef]
14. Yang, Y.; Xu, S.; He, Y. Lithium Recycling and Cathode Material Regeneration from Acid Leach Liquor of Spent Lithium-Ion Battery via Facile Co-Extraction and Co-Precipitation Processes. *Waste Manag.* **2017**, *64*, 219–227. [CrossRef] [PubMed]
15. Chen, L.; Tang, X.; Zhang, Y.; Li, L.; Zeng, Z.; Zhang, Y. Process for the Recovery of Cobalt Oxalate from Spent Lithium-Ion Batteries. *Hydrometallurgy* **2011**, *108*, 80–86. [CrossRef]
16. Porvali, A.; Chernyaev, A.; Shukla, S.; Lundström, M. Lithium Ion Battery Active Material Dissolution Kinetics in Fe(II)/Fe(III) Catalyzed Cu-H_2SO_4 Leaching System. *Sep. Purif. Technol.* **2020**, *236*, 116305. [CrossRef]
17. Joo, S.H.; Shin, D.J.; Oh, C.H.; Wang, J.P.; Senanayake, G.; Shin, S.M. Selective Extraction and Separation of Nickel from Cobalt, Manganese and Lithium in Pre-Treated Leach Liquors of Ternary Cathode Material of Spent Lithium-Ion Batteries Using Synergism Caused by Versatic 10 Acid and LIX 84-I. *Hydrometallurgy* **2016**, *159*, 65–74. [CrossRef]
18. Virolainen, S.; Wesselborg, T.; Kaukinen, A.; Sainio, T. Removal of Iron, Aluminium, Manganese and Copper from Leach Solutions of Lithium-Ion Battery Waste Using Ion Exchange. *Hydrometallurgy* **2021**, *202*, 105602. [CrossRef]
19. Nayl, A.A.; Hamed, M.M.; Rizk, S.E. Selective Extraction and Separation of Metal Values from Leach Liquor of Mixed Spent Li-Ion Batteries. *J. Taiwan Inst. Chem. Eng.* **2015**, *55*, 119–125. [CrossRef]
20. Peng, C.; Chang, C.; Wang, Z.; Wilson, B.P.; Liu, F.; Lundström, M. Recovery of High-Purity MnO_2 from the Acid Leaching Solution of Spent Li-Ion Batteries. *JOM* **2020**, *72*, 790–799. [CrossRef]
21. Cheng, C.Y. Purification of Synthetic Laterite Leach Solution by Solvent Extraction Using D2EHPA. *Hydrometallurgy* **2000**, *56*, 369–386. [CrossRef]
22. Sole, K.C. The Evolution of Cobalt–Nickel Separation and Purification Technologies: Fifty Years of Solvent Extraction and Ion Exchange. In *Extraction 2018*; Springer International Publishing: Cham, Switzerland, 2018; pp. 1167–1191. ISBN 978-3-319-95021-1. [CrossRef]
23. Flett, D.S. Solvent Extraction in Hydrometallurgy: The Role of Organophosphorus Extractants. *J. Organomet. Chem.* **2005**, *690*, 2426–2438. [CrossRef]
24. Yang, Y.; Lei, S.; Song, S.; Sun, W.; Wang, L. Stepwise Recycling of Valuable Metals from Ni-Rich Cathode Material of Spent Lithium-Ion Batteries. *Waste Manag.* **2020**, *102*, 131–138. [CrossRef] [PubMed]
25. Swain, B.; Jeong, J.; Lee, J.; Lee, G.H. Separation of Cobalt and Lithium from Mixed Sulphate Solution Using Na-Cyanex 272. *Hydrometallurgy* **2006**, *84*, 130–138. [CrossRef]
26. Porvali, A.; Aaltonen, M.; Ojanen, S.; Velazquez-Martinez, O.; Eronen, E.; Liu, F.; Wilson, B.P.; Serna-Guerrero, R.; Lundström, M. Mechanical and Hydrometallurgical Processes in HCl Media for the Recycling of Valuable Metals from Li-Ion Battery Waste. *Resour. Conserv. Recycl.* **2019**, *142*, 257–266. [CrossRef]
27. Paatero, E.; Sjöblom, J. Phase Behaviour in Metal Extraction Systems. *Hydrometallurgy* **1990**, *25*, 231–256. [CrossRef]
28. Cui, Y.; Liu, K.; Man, J.; Cui, J.; Zhang, H.; Zhao, W.; Sun, J. Preparation of Ultra-Stable $Li[Ni_{0.6}Co_{0.2}Mn_{0.2}]O_2$ Cathode Material with a Continuous Hydroxide Co-Precipitation Method. *J. Alloys Compd.* **2019**, *793*, 77–85. [CrossRef]
29. Eilers-Rethwisch, M.; Winter, M.; Schappacher, F.M. Synthesis, Electrochemical Investigation and Structural Analysis of Doped $Li[Ni_{0.6}Mn_{0.2}Co_{0.2}\text{-}XMx]O_2$ (x = 0, 0.05; M = Al, Fe, Sn) Cathode Materials. *J. Power Sources* **2018**, *387*, 101–107. [CrossRef]
30. Lee, M.H.; Kang, Y.J.; Myung, S.T.; Sun, Y.K. Synthetic Optimization of $Li[Ni_{1/3}Co_{1/3}Mn_{1/3}]O_2$ via Co-Precipitation. *Electrochim. Acta* **2004**, *50*, 939–948. [CrossRef]
31. Luo, X.; Wang, X.; Liao, L.; Gamboa, S.; Sebastian, P.J. Synthesis and Characterization of High Tap-Density Layered $Li[Ni_{1/3}Co_{1/3}Mn_{1/3}]O_2$ Cathode Material via Hydroxide Co-Precipitation. *J. Power Sources* **2006**, *158*, 654–658. [CrossRef]
32. Xun, F.; Golding, J.A. Solvent Extraction of Cobalt and Nickel in Bis(2,4,4-Trimethylpentyl) Phosphinic Acid, "Cyanex 272". *Solvent Extr. Ion Exch.* **1987**, *5*, 205–226. [CrossRef]
33. Vasilyev, F.; Virolainen, S.; Sainio, T. Numerical Simulation of Counter-Current Liquid–Liquid Extraction for Recovering Co, Ni and Li from Lithium-Ion Battery Leachates of Varying Composition. *Sep. Purif. Technol.* **2019**, *210*, 530–540. [CrossRef]
34. Söhnel, O.; Novotný, P. *Densities of Aqueous Solutions of Inorganic Substances*; Elsevier: Amsterdam, The Netherlands, 1985.
35. Potter, R.W., II; Clynne, M.A. Solubility of Highly Soluble Salts in Aqueous Media—Part 1, NaCl, KCl, $CaCl_2$, Na_2SO_4, and K_2SO_4 Solubilities to 100 °C. *J. Res. U.S. Geol. Surv.* **1978**, *6*, 701–705.

ACTA UNIVERSITATIS LAPPEENRANTAENSIS

1028. CHAUHAN, VARDAAN. Optimizing design and process parameters for recycled thermoplastic natural fiber composites in automotive applications. 2022. Diss.

1029. RAM, MANISH. Socioeconomic impacts of cost optimised and climate compliant energy transitions across the world. 2022. Diss.

1030. AMADI, MIRACLE. Hybrid modelling methods for epidemiological studies. 2022. Diss.

1031. RAMÍREZ ANGEL, YENDERY. Water-energy nexus for waste minimisation in the mining industry. 2022. Diss.

1032. ZOLOTAREV, FEDOR. Computer vision for virtual sawing and timber tracing. 2022. Diss.

1033. NEPOVINNYKH, EKATERINA. Automatic image-based re-identification of ringed seals. 2022. Diss.

1034. ARAYA GÓMEZ, Natalia Andrea. Sustainable management of water and tailings in the mining industry. 2022. Diss.

1035. YAHYA, MANAL. Augmented reality based on human needs. 2022. Diss.

1036. KARUPPANNAN GOPALRAJ, SANKAR. Impacts of recycling carbon fibre and glass fibre as sustainable raw materials for thermosetting composites. 2022. Diss.

1037. UDOKWU, CHIBUZOR JOSEPH. A modelling approach for building blockchain applications that enables trustable inter-organizational collaborations. 2022. Diss.

1038. INGMAN, JONNY. Evaluation of failure mechanisms in electronics using X-ray imaging. 2022. Diss.

1039. LIPIÄINEN, SATU. The role of the forest industry in mitigating global change: towards energy efficient and low-carbon operation. 2022. Diss.

1040. AFKHAMI, SHAHRIAR. Laser powder-bed fusion of steels: case studies on microstructures, mechanical properties, and notch-load interactions. 2022. Diss.

1041. SHEVELEVA, NADEZHDA. NMR studies of functionalized peptide dendrimers. 2022. Diss.

1042. SOUSA DE SENA, ARTHUR. Intelligent reflecting surfaces and advanced multiple access techniques for multi-antenna wireless communication systems. 2022. Diss.

1043. MOLINARI, ANDREA. Integration between eLearning platforms and information systems: a new generation of tools for virtual communities. 2022. Diss.

1044. AGHAJANIAN, SOHEIL. Reactive crystallisation studies of CaCO3 processing via a CO2 capture process: real-time crystallisation monitoring, fault detection, and hydrodynamic modelling. 2022. Diss.

1045. RYYNÄNEN, MARKO. A forecasting model of packaging costs: case plain packaging. 2022. Diss.

1046. MAILAGAHA KUMBURE, MAHINDA. Novel fuzzy k-nearest neighbor methods for effective classification and regression. 2022. Diss.

1047. RUMKY, JANNATUL. Valorization of sludge materials after chemical and electrochemical treatment. 2022. Diss.

1048. KARJUNEN, HANNU. Analysis and design of carbon dioxide utilization systems and infrastructures. 2022. Diss.

1049. VEHMAANPERÄ, PAULA. Dissolution of magnetite and hematite in acid mixtures. 2022. Diss.

1050. GOLOVLEVA, MARIA. Numerical simulations of defect modeling in semiconductor radiation detectors. 2022. Diss.

1051. TREVES, LUKE. A connected future: The influence of the Internet of Things on business models and their innovation. 2022. Diss.

1052. TSERING, TENZIN. Research advancements and future needs of microplastic analytics: microplastics in the shore sediment of the freshwater sources of the Indian Himalaya. 2022. Diss.

1053. HOSEINPUR, FARHOOD. Towards security and resource efficiency in fog computing networks. 2022. Diss.

1054. MAKSIMOV, PAVEL. Methanol synthesis via CO2 hydrogenation in a periodically operated multifunctional reactor. 2022. Diss.

1055. LIPIÄINEN, KALLE. Fatigue performance and the effect of manufacturing quality on uncoated and hot-dip galvanized ultra-high-strength steel laser cut edges. 2022. Diss.

1056. MONTONEN, JAN-HENRI. Modeling and system analysis of electrically driven mechatronic systems. 2022. Diss.

1057. HAVUKAINEN, MINNA. Global climate as a commons — from decision making to climate actions in least developed countries. 2022. Diss.

1058. KHAN, MUSHAROF. Environmental impacts of the utilisation of challenging plastic-containing waste. 2022. Diss.

1059. RINTALA, VILLE. Coupling Monte Carlo neutronics with thermal hydraulics and fuel thermo-mechanics. 2022. Diss.

1060. LÄHDEAHO, OSKARI. Competitiveness through sustainability: Drivers for logistics industry transformation. 2022. Diss.

1061. ESKOLA, ROOPE. Value creation in manufacturing industry based on the simulation. 2022. Diss.

1062. MAKARAVA, IRYNA. Electrochemical recovery of rare-earth elements from NdFeB magnets. 2022. Diss.

1063. LUHAS, JUKKA. The interconnections of lock-in mechanisms in the forest-based bioeconomy transition towards sustainability. 2022. Diss.

1064. QIN, GUODONG. Research on key technologies of snake arm maintainers in extreme environments. 2022. Diss.

1065. TAMMINEN, JUSSI. Fast contact copper extraction. 2022. Diss.

LUT University

ISBN 978-952-335-913-0
ISBN 978-952-335-914-7 (PDF)
ISSN 1456-4491 (Print)
ISSN 2814-5518 (Online)
Lappeenranta 2023